A Comparative Analytical Study on Low-Voltage Ride-Through Reference-Current-Generation (LVRT-RCG) Strategies in Converter-Interfaced DER Units

by

Masoud Mohammadalizadeh Shabestary

A thesis submitted in partial fulfillment of the requirements for the degree of

Master of Science
in
Energy Systems

Department of Electrical and Computer Engineering
University of Alberta

Abstract

Recently, riding through grid faults and supporting the grid voltage under faults have become major requirements in distributed energy resource (DER) units. There have been also extensive efforts in academia and industry to develop and implement control strategies to ride through voltage disturbances, and even to support the grid under such faulted conditions which can be named as low-voltage ride-through (LVRT) technology. Therefore, a comprehensive and comparative study seems to be very useful in order to analyze and discuss available LVRT reference-current-generation (LVRT-RCG) strategies in converter-interfaced DER units, compare their performances, and introduce their pros and cons. This thesis studies all existing (nine) LVRT-RCG strategies available in the literature. These strategies are categorized into two main groups. The analytical evaluations and mathematical assessments of all LVRT-RCG strategies are performed. For a comprehensive evaluation of these strategies, the following important parameters are used in this study: instantaneous active/reactive powers oscillation and maximum phase currents. Analytical expressions of these parameters are formulated, evaluated and used to conduct several evaluation and comparative studies on different strategies. Based on the obtained formulas for the maximum phase currents, the maximum allowable reactive power delivery (MARPD) equations are proposed specifically for each of the nine LVRT-RCG strategies. Proposed equations help each LVRT-RCG technique to provide their best voltage support under the specific maximum phase current restrictions imposed by DER owners. Using different test cases, the strategies are compared and the proposed equations are validated. This thesis can be helpful to evaluate the performance

of existing LVRT-RCG strategies, solve their existing drawbacks, exploit the best performance out of each, combine their individual capabilities, and improve them.

DEDICATED TO MY BELOVED WIFE, SHAHED.

Acknowledgments

I would like to express my gratitude to my supervisors, Prof. Wilsun Xu and Prof. Yasser A.-R. I. Mohamed, for their assistance and support. I am thankful to Prof Xu, who introduced me to this project, supported me financially, and instructed me about challenges involved in practical engineering projects. This assistance made my research more productive and pragmatic. I owe my greatest gratitude to Prof. Mohamed for his incredible support throughout this work and I am specially grateful for his consistent encouragement. Without his technical advices and faith in me, the achievements during my MSc research would have been impossible. I would also like to thank the examiners committee for their interests in my project and their valued feedback.

My sincere appreciation also goes to my parents, who have always inspired and supported me. I would like to dedicate this thesis to my beloved wife, Shahed, whose inspiration, fortitude, and genuine love cannot be conveyed in words. It was her patience and support which paved my way to complete my degree.

Contents

List of Tables

List of Figures

List of Bar Graphs

Abbreviations

Well-Known Abbreviations Extensively Used in the Literature

BESS	Battery Energy Storage Systems
CSA	Canadian Standards Association
DER	Distributed Energy Resource
DFIG	Doubly-Fed Induction Generator
DG	Distributed Generation
DS	Distributed Storage
HVRT	High-Voltage Ride-Through
IVGTF	Integration of Variable Generation Task Force
LVRT	Low Voltage Ride Through
NERC	North American Electric Reliability Corporation
PCC	Point of Common Coupling
PMSG	Permanent Magnet Synchronous Generators
PR	Proportional Resonant
PV	Photo-Voltaic
THD	Total Harmonic Distortion
TSO	Transmission System Operators
VSC	Voltage-Sourced-Converter
WECS	Wind Energy Conversion Systems
WPP	Wind Power Plants
WPPP	Wind Power Penetration Percentage
WT	Wind Turbine

Abbreviations Specifically Used in This Thesis

HWPP	High Wind-Power-Penetrated
LWPP	Low Wind-Power-Penetrated
CI-DER	Converter-Interfaced DER
RCG	Reference-Current Generation
UPD	Uninterrupted Power Delivery

Abbreviations for UPD Strategies

IARC	Instantaneous Active-Reactive Control
AARC	Average Active-Reactive Control
BPSC	Balanced Positive-Sequence Control
ICPS	Instantaneously-Controlled Positive Sequence
PNSC	Positive and Negative Sequence Control
ZSCI	Zero-Sequence Current Injection

FVS	Flexible Voltage Support

Abbreviations for FVS Strategies

FPNSC	Flexible Positive and Negative Sequence Control
FBSS	Flexible Balance of Symmetric Sequences
MFBSS	Modified Flexible Balance of Symmetric Sequences

MARPD	Maximum Allowable Reactive Power Delivery

Nomenclatures

General Terms Widely Used in the Thesis

V_p	Magnitude of the Positive-Sequence of the PCC Voltage
V_n	Magnitude of the Negative-Sequence of the PCC Voltage
g	Instantaneous Conductance
b	Instantaneous Susceptance
$v_\perp$	Orthogonal Voltage Vector (90° leading from v)
ω	Grid Frequency
P^*	Active Power Reference Command
Q^*	Reactive Power Reference Command
i_p^*	Active Current Reference Signal
i_q^*	Reactive Current Reference Signal
P	Average Value of the Active Power
Q	Average Value of the Reactive Power
$\tilde{p}$	Active Power Oscillations
$\tilde{q}$	Reactive Power Oscillations
$\tilde{p}_{s2}$	Active Power Oscillations Oscillating by sin (2ω)
$\tilde{p}_{c2}$	Active Power Oscillations Oscillating by cos (2ω)
$\tilde{q}_{s2}$	Reactive Power Oscillations Oscillating by sin (2ω)
$\tilde{q}_{c2}$	Reactive Power Oscillations Oscillating by cos (2ω)
P_{s2}	Magnitude of $\tilde{p}_{s2}$

P_{c2} Magnitude of $\tilde{p}_{c2}$

Q_{s2} Magnitude of $\tilde{q}_{s2}$

Q_{c2} Magnitude of $\tilde{q}_{c2}$

P^{0} Average Value of Active Power Generated by Zero-Sequence Voltage and Current

P_{s2}^{0} Oscillation Magnitude of the Active Power, Oscillating by sin (2ω), with-respect-to the Zero-Sequence Voltage and Current Contribution

P_{c2}^{0} Oscillation Magnitude of the Active Power, Oscillating by cos (2ω), with-respect-to the Zero-Sequence Voltage and Current Contribution

X System Reactance

R System Resistance

Terms Specifically Introduced in This Thesis

$\tilde{p}_{\max}$ Magnitude of the Overall Oscillations on the Active Power

$\tilde{q}_{\max}$ Magnitude of the Overall Oscillations on the Reactive Power

I_{max} Maximum amount among three fault current magnitudes of *abc* phases

I_{limit} Imposed Limitation for I_{max} by DG Owners (and/or System Operators)

I_{limit}^{*} Reference Command of Agreed I_{limit}

Q_{max} Maximum Allowable Reactive Power with-respect-to the Agreed I_{limit}

Chapter 1

Introduction

1.1 Background

Encouraging political and socioeconomic circumstances along with increasing fossil fuel prices have encouraged the development of renewable energy and distributed energy resource (DER) systems in recent years as reflected saliently in global energy statistics [1]-[2]. At the same time, the construction of wind farms is economically feasible and leads to relatively large amounts of wind-based power penetration into the grid [3]. Growing penetration of DERs (most notably wind power) into the distribution systems (medium-voltage level), an increasing portion of power is no longer generated by centralised synchronous generators, but rather from de-centralised converter based DER units that have severely dissimilar operating characteristics. For low wind-power-penetrated (LWPP) systems, such as China with wind power penetration percentage (WPPP) of 1.6% [4], these unique characteristics posture no concern to the network operator. In these grids, wind power plants (WPPs) are simply seen as negative loads (i.e., consume negative active power); and network voltage and frequency continue to be controlled by large scale conventional approaches [5]. As a result, ancillary services [6]-[9] or fault-ride-through (FRT) capabilities [10]-[13] are not mandatory for WPPs connection in LWPP systems (such as US with 3.5% WPPP in 2012 [2], [4] and Canada with 3.6% WPPP [4]) unlike in high wind-power-penetrated (HWPP) grids (such

as Denmark with 34.2% WPPP in 2012, Germany with 8.0% WPPP, and Spain with 17.5% WPPP [4]), where the fulfillment of FRT requirements are obligatory for WPPs connection.

In North American power systems and other LWPP systems, the conventional control philosophy is currently applied which allows WPPs to inject whole available power near unity power factor and quickly disconnect them in the presence of grid disturbances. However, with non-negligible WPPs portion in the generation field, the conventional simple control strategies will incur grid instability and unreliability issues in near future [5], [14]. Network operators have comprehended the approaching challenges and responded by releasing new grid codes that directly point the robust and safe connection of DERs such as photo-voltaic (PV), wind, fuel cells and micro-turbines into the grid [15]. Such codes has been firstly documented in parts of Europe, most remarkably Germany. Later, many utilities across North America have also begun to pose their own grid codes for the connections of DERs. These ascending codes are starting to impose expectations for ancillary services, grid support and low voltage ride through (LVRT) requirements [16]-[19]. In this regard, response of WPPs during grid faults and LVRT capabilities of wind turbine (WT) systems has been widely studied by industry and academia e.g. in [20]-[29]. Among the studies on the LVRT technology in WTs, most efforts target doubly-fed induction generators (DFIGs), as for instance in [30]-[37]. On the other hand, numerous research have been also carried out on the LVRT technology applied in converter-interfaced DER (CI-DER) units such as permanent magnet synchronous generators (PMSGs) [38]-[41] and PVs [42]. The main focus of this thesis is also the second group, LVRT strategies applied in the CI-DER units.

The electrical grid is a dynamical system, whose behavior depends upon many aspects such as constraints set by system operators, occurrence of grid faults, excitation of resonances, and existence of nonlinear loads. As a consequence, CI-DER units should be designed in a way that they guarantee a robust and safe operation under generic grid voltages, especially exposing best performance under abnormal grid conditions [43]. The tight requirements forced by system operators, mainly related to LVRT and grid support during and after faults, have inspired engineers and researchers to amend the conventional

control strategies. Occurrences of grid faults usually cause the appearance of unbalanced voltages at the point of common coupling (PCC). Under unbalanced voltages, the currents injected into the grid may become non-sinusoidal and/or unbalanced. Such currents and voltages may lead to undesired fluctuations in the active/reactive powers delivered to the grid leading to grid instability and power converter unreliability. The appropriate operation of CI-DER under such conditions is a critical issue. Subject to the aim of the control strategy used to generate the reference-currents under different faults, the general performance of the grid-connected CI-DER and its interaction with the network will significantly vary. Consequently, reference-current generation (RCG) of CI-DER units during faults is another challenging issue [25].

References [8], [23], [25], [38]-[39], [42]-[57] propose, study and apply numerous RCG methods for the LVRT capability enhancement of CI-DERs. However, there are only nine unique LVRT-RCG strategies proposed by [43]-[47]; whereas other researches just represent the same ideas in other manners. Therefore, this thesis presents a detailed comparative study and evaluation results all of these nine LVRT-RCG strategies; and then presents analytical expressions to characterize the performance of these strategies and enable effective LVRT design of CI-DER units.

1.2 Objectives and Scope

The objectives of this thesis are to:

1. Study and review all available LVRT-RCG strategies in CI-DERs based on reference current formulas proposed in [43]-[47] and group them in two main categories:
    - Uninterrupted power delivery (UPD) LVRT-RCG strategies, and
    - Flexible voltage support (FVS) LVRT-RCG strategies.
2. Develop analytical approaches to find expressions of the most important terms of each LVRT-RCG strategy. These terms are:

- Instantaneous active and reactive powers,
- Maximum oscillations on instantaneous active and reactive powers, and
- Maximum phase currents under a generic grid condition (i.e. different fault types, various system and controller parameters, etc.)

3. Propose a novel analytical method to find expressions of the maximum allowable reactive power delivery (MARPD) for each LVRT-RCG technique. This method aims to:
    - provide the best support for PCC voltage by injecting the maximum allowable reactive power;
    - and simultaneously; respect phase-current limits imposed by DER owners.

Consequently, the proposed method exploits the best conceivable performance out of each LVRT-RCG strategy proposed by [43]-[47]; and it will allow the CI-DER units to ride through different grid faults under predetermined limitations (e.g. phase-current and maximum allowable reactive power limits).

The contents of the LVRT techniques studied in this thesis are limited to reference current calculation strategies applied to CI-DER units, such as PMSG, PV, fuel cells, etc., with an emphasis on the power electronically interfaced DER units and application of the voltage-sourced-converter (VSC). Therefore, the LVRT techniques applied in other converter-based DER topologies (such as DFIG) are outside the thesis scope.

1.3 Layout

Chapter two provides the overview and literature review on renewable energies booming growth, the dominant requirements of new grid codes and interconnection standards relating to ancillary services and LVRT technologies in DERs (either CI-DER units or other DER topologies). Chapter three studies and reviews all available LVRT-RCG

strategies in CI-DERs based on reference current formulas proposed in [43]-[47] and divides them into two main groups (i.e. UPD and FVS). Chapter four and five mathematically and analytically find expressions of the aforementioned important terms for each LVRT-RCG strategy in UPD and FVS groups, respectively; and verifies the analytical results by simulation results. Lastly, Chapter six concludes the thesis work and highlights main contributions, notable outcomes, and future work.

Chapter 2

Literature Review

2.1 Distributed Energy Resources (DERs)

There are several kinds of (and various technologies for) energy sources and energy storage systems under the concept of DERs. Moreover, many methods exist in coordinating these energy sources and energy storage systems and connecting them to the grid such as direct connection, converter-interfaced connection, or a combination between these two. Commonly, a modular architecture for grouping of DER components is considered in the literature which permits the formation of distinct power generation units, each one a collection of DER elements suited for a particular study. In this section, a brief overview of DERs, their subsets and types is provided in order to establish the accurate scope of this thesis. In particular, the concepts of a DER unit and its main conceivable elements (i.e. energy storage system and energy source) are introduced. Later in subsection 2.1.3, a certain type of DER units is introduced under the label of converter-interfaced DER units (CI-DERs), which is the main concentration of this work.

2.1.1 Distributed storage

The term distributed storage (DS) systems denotes different forms of energy storage systems which are capable to be connected to the distribution network. The integration of

DSs is mainly developed with distributed generation (DG) units in order to provide a dispatchable energy rather than a non-dispatchable stochastic energy (which is the nature of many renewable energy sources like solar, wind, wave, etc.). The use of DSs is specifically beneficial in micro-grid applications where the balance between generation and loads must be met within the micro-grid in an islanded operation [5]. There are several forms of energy storage technologies such as [58]:

- Battery energy storage systems (BESS)s (most common technology)
- Super-capacitors
- Flywheels
- Pumped hydro-electric storage systems
- Compressed air storage systems

2.1.2 Distributed generation

It is generally accepted to refer any source of electric power of limited capacity, directly connected to the distribution network as a DG unit [58]. A typical DG unit can have any capacity from a few kilowatts to several megawatts [59]. There are similarly several forms of DG technologies [58]:

- Renewable energies: wind, solar, biomass, hydro, geothermal and solar-thermal
- Reciprocating engines: gas or diesel
- Gas turbines: micro-turbine or combustion-turbine
- Fuel cells

2.1.3 DER unit

Generally, a DER unit contains a DG source with or without a DS connected to the distribution network, including all necessary interconnection equipment, at the point of common coupling (PCC). An illustration of a DER unit is provided in Fig. 2.1. Typically DER units use power electronics to convert the power output of the DG (or DS), which can be DC or AC with varying frequencies, to the grid compatible ac power. To obtain this goal, there are various converter topologies and connection schemes, with a final option dependent on different parameters like desired system operating characteristics, technical requirements, system constraints, and cost. In most cases, the final power conversion stage at the grid interface will require one or more dc-ac converters. As a result, the interaction or behaviour of a DER unit with the network is primarily characterized by this converter topology rather than the actual energy source. Therefore, these DER units are often referred to as inverter based generation. These inverter based DERs have operating characteristics that are completely different from conventional power generation units, and comprise the following [5]:

- Electrical decoupling of energy source from the grid
- Absence of source inertia
- Relatively low short circuit fault current capability
- Capability for fast dynamics

The scope of this work is constrained to converter-interfaced DER (CI-DER) units which interface to the distribution network utilising DC/AC converters. In particular, a stress is placed on the application of VSCs. The energy source(s) for each DER unit is (are) inclusive of all DS and DG as stated earlier in section 2.2.1 and section 2.2.2, respectively. However, the LVRT in other DER connection technologies is important, as for instance in DFIGs. Due to their importance, different LVRT technologies in DFIGs is briefly addressed in section 2.3.

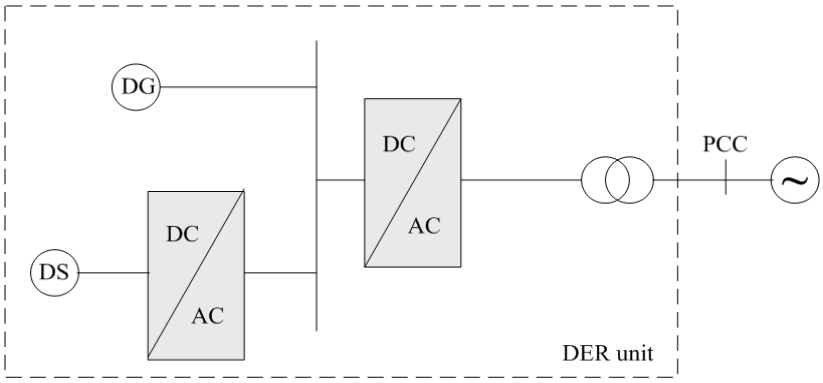

Fig. 2.1. An example of a DER unit [5]

2.2 Grid Code Requirements

According to International Energy Agency, in the last decade wind power had one of the highest average annual growth rates among renewable sources [60]. Spanish grid is a good example, where the average wind power penetration has been 11%, 13.8%, and 16% in 2008, 2009, and 2010, respectively [61]-[63], although the wind energy penetration can temporarily reach a much higher value, e.g. the 64% on September 24, 2012 [64]. A study from European Wind Energy Association [65] estimates that wind is capable of delivering 12% from the electricity consumption by 2020 and in excess of 20% by 2030. On the same time in the last decade, the wind turbines become bigger and bigger and currently single units up to 5 MW are commercially available. The future development of wind power is also expected in Canada, Australia and Japan. Modern up to 5 MW wind turbines currently replace a large number of small wind turbines [66]. Therefore some countries have issued dedicated grid codes for connecting the wind turbines/farms to the electrical network addressed to transmission and/or distributed system. The grid code requirements are established by power system operators to ensure the reliability and safe operation of the utility [67]. These requirements can be divided into two categories [66]:

- Steady-state or quasi-stationary operation requirements (such as reactive and active power regulation to support the utility voltage and frequency)

- LVRT requirements

Some general and useful reviews of the grid code requirements of several countries are presented in [5], [67], [69], which is also briefly discussed in section 2.2.2 and section 2.2.3. Under grid disturbances, the traditional grid code requirements allowed the disconnection of the WECSs to prevent large over-currents. However, with the increasing growth in the wind energy penetration, the sudden disconnection of WECSs can cause instability of the entire power system, even leading to global blackouts [66]. Accordingly, the power system operators have updated their grid code requirements, and engineers and researches try to find novel control methods to comply with updated requirements. For instances, [68] addresses LVRT control with high-order filters and advanced voltage control to mitigate fast voltage disturbances; whereas LVRT applications in microgrids is studied in [70] to enhance microgrids reliability.

With new grid code requirements, the LVRT requirement demands wind power plants to remain connected when a grid-voltage disturbance occurs, thus continuing to deliver active and reactive power to the grid, with a specific profile depending on the grid-voltage dip depth, in order to have network voltage and frequency stability. Therefore, LVRT is the most challenging requirement among the new grid codes, at least from the point of view of the WECS [66]. LVRT requirements, extracted from the new grid codes of the utility operator E-ON [72], are shown in Fig. 2.2 and Fig. 2.3. Similar curves are presented in the LVRT requirements of other power systems operators [67]-[69], also presented in section 2.2.2. Moreover, during the voltage disturbances, the WECS has to deliver a reactive current to aid the utility in holding the grid voltage, illustrated in Fig. 2.3 and discussed in details in [5]. The reactive power to be delivered depends on grid voltage reduction, the system rated current, and the reactive current delivery before the disturbance occurrence.

In most of the grid codes, e.g. Denmark and Ireland, these new requirements have focus on power controllability, power quality, and fault ride-through capability. Moreover, some grid codes require grid support during network disturbances e.g. Germany and Spain. Denmark has the most demanding requirements regarding the controllability of the produced power. Wind farms connected at the transmission level

should act as a conventional power plant providing a wide range of controlling the output power based on transmission system operators (TSOs) demands. The power quality requirements are very demanding in respect with flicker emission as well as the harmonic compatibilities especially at distribution systems [69].

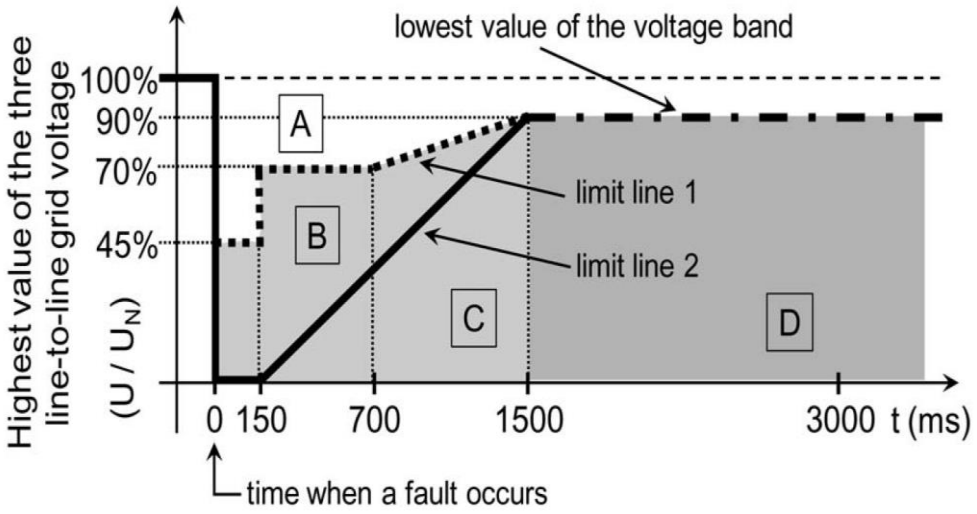

Fig. 2.2. Voltage limit curve to allow generator disconnection.

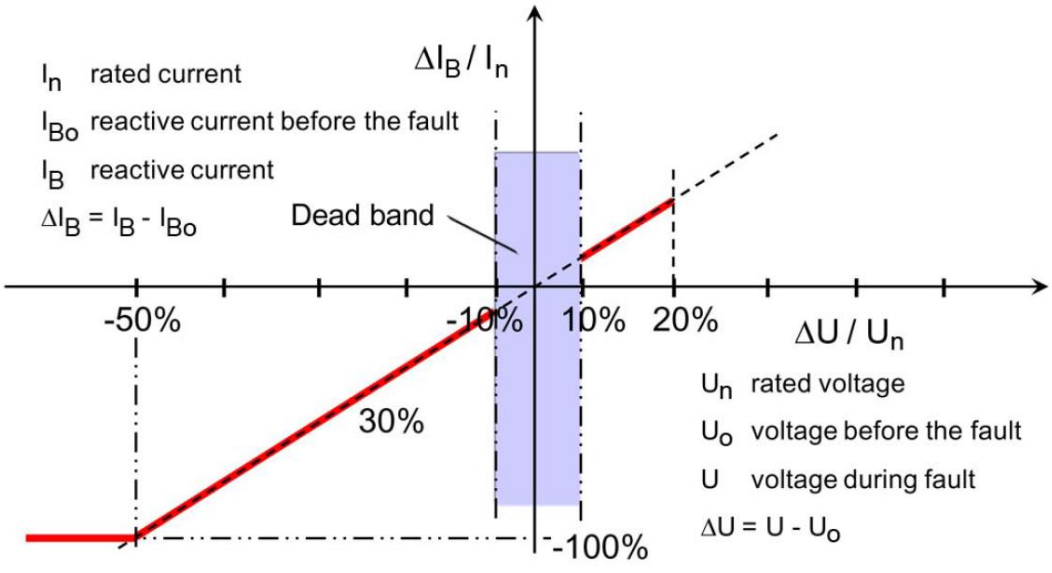

Fig. 2.3. Reactive current to be delivered to the grid under a voltage dip.

2.2.1 Grid Voltage Disturbances

Within the context of FRT, many grid codes and technical standards frequently use various terms such as under-voltage, low-voltage, dips and sags in order to quantify similar disturbances in the grid voltage [5]. For an instance, "according to [73] the voltage sags are short duration reductions in RMS values of the voltage, caused by short circuits, overloads and starting of large motors" [69]. As another example, "a voltage dip is a drop in voltage with duration between one half-cycle and one minute [74], which is, in most cases, caused by a short-circuit fault" [75]. Hence, to maintain consistency when discussing voltage deviations from steady-state values the term voltage sag is used throughout this work to indicate a temporary decrease in voltage magnitude from its nominal value (at fundamental frequency), regardless of the disturbance duration and depth. On the other hand, the term voltage swell indicates a temporary increase in voltage magnitude from the nominal value. However, it should be noted that there are several different sub-categories under which voltage deviations are classified depending on their relative magnitude, duration and frequency content [5]. Since voltage sags are caused by faults located at hundreds of kilometres away in the transmission system these events are more global problems than an interruption [73]. The magnitude of the voltage sags are determined by the following factors [69], [73]:

- Distance to fault
- Connection type of transformers between the location of fault and the recording point
- Cross section of the lines and cables
- Type of the grid (radial or meshed)
- Short-circuit impedance of the network, etc.

On the other hand, the common causes for voltage swells include [5]:

- A line-to-ground fault can increase the voltages on the healthy phases
- Switching in capacitor banks onto the network
- Sudden and severe reduction in system load (e.g., large loads switched off-line)

For the system, symmetrical disturbances, particularly the deep voltage sags, are more stressing than asymmetrical disturbances since all phases are lost. However, most of the disturbances are asymmetrical; and their analysis is more complex due to the appearance of negative-sequence components in voltages and currents. Only 12% of grid voltage sags are symmetrical [73], [76]-[77]. Furthermore, based on the presented survey in [69] studying different faults on the electrical network other useful conclusions can be drawn:

- Most of the faults are located on overhead lines, and in 132 kV networks.

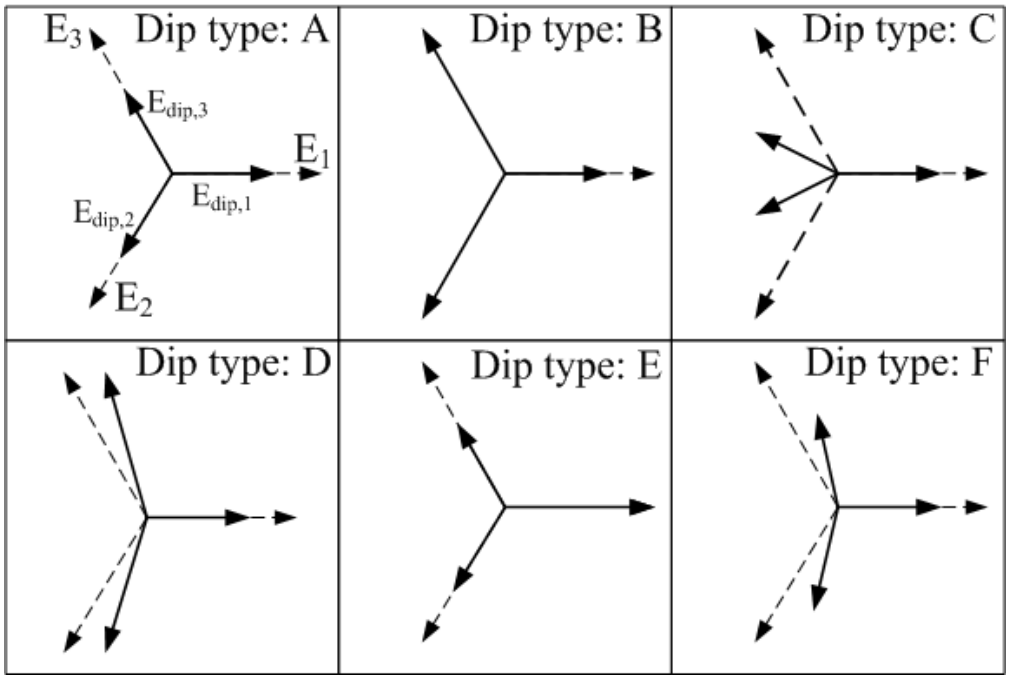

Fig. 2.4. Voltage dip classification "A" to "F." Phasors of three-phase voltage before (dotted) and during fault (solid) are displayed.

- The single phase fault has the highest probability to occur.
- Most of the voltage sags down to 0.75 pu have a duration of several cycles; while most of the voltage sags down to 0.25 pu have the duration of several seconds up to minutes.

Finally, according to interesting fault analysis carried out in [75]-[76], six distinct fault types in power electric networks are identified as illustrated in Fig. 2.4.

2.2.2 LVRT Requirements in National Grid Codes

In [69], an overview of the LVRT requirements in some of the national grid codes (as for instance in Denmark [78], Ireland [79]-[80], Germany [72], England [81], Spain [82], Italy [83]-[84], USA [85], Hydro-Quebec [86], AESO-Alberta [87]) for wind turbines is presented. Some national grid codes e.g. Denmark and Ireland have specific fault ride-through requirements for distribution networks as well as for transmission ones while other national grid codes have focus only on the transmission level, e.g. Germany and Spain. All considered grid codes in [69] require FRT capabilities for wind turbines. A summary of these requirements is given in Table 2.1. Voltage values are provided to specify the depth of the voltage sag and the clearance time. The voltage value for LVRT capabilities in different countries can be summarized as shown in Fig. 2.5.

Irish grid code is very demanding regarding the fault duration while Denmark has the lowest voltage sag time duration with only 100 msec. However, Danish grid code mandates the wind turbine to remain connected to the electrical network during consecutive faults. The German grid code necessitates wind energy conversion systems (WECSs) to remain connected during most severe voltage sags even down to 0% for a duration of 150 msec. In addition, during the fault a reactive current injection (up to 100%) is mandatory in German code as well as in Spanish grid code.

TABLE 2.1. Summary of LVRT codes for wind turbines/farms in different national grid codes [69].

Country	Voltage Level	Fault ride-through capability				
		Fault duration	Voltage drop level	Recovery time	Voltage profile	Reactive current injection
Denmark	DS	100 msec	25%U_r	1 sec	2, 3-ph	no
	TS	100 msec	25%U_r	1 sec	1, 2, 3-ph	no
Ireland	DS/TS	625 msec	15%U_r	3 sec	1, 2, 3- ph	no
Germany	DS/TS	150 msec	0%U_r	1.5 sec	generic	Up to 100%
Great Britain	DS/TS	140 msec	15%U_r	1.2 sec	generic	no
Spain	TS	500 msec	20%U_r	1 sec	generic	Up to 100%
Italy	> 35 kV	500 msec	20%U_r	0.3 sec	generic	no
USA	TS	625 msec	15%U_r	2.3 sec	generic	no
Ontario	TS	625 msec	15%Ur	-	-	no
Quebec	TS	150 msec	0%U_r	0.18 sec	Positive-sequence	no

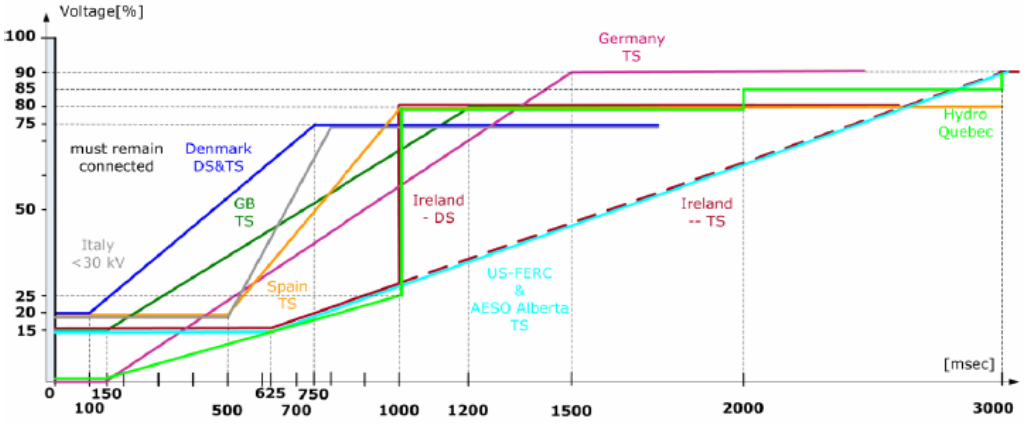

Fig. 2.5. Summary regarding LVRT capability of WESs in national grid codes [67].

2.2.3 Technical Standards for DER Interconnection

These standards encompass a broad set of topics such as power quality, response to network disturbances and system operating limits. Utilities commonly use these standards as guidelines for developing their respective grid codes. Reference [5] identifies the key standards governing the interconnection of DERs and summarizes their requirements.

However, the scope of standards is limited to North America. It reviews different technical standards:

- IEEE Std. 929 [88] is presented in 1988 for the PV interconnection. This standard focuses on smaller capacity systems, 10 kW or less, which is the characteristic of single phase residential installations. There are no explicit FRT requirements in this standard.

- IEEE Std. 1547 [16], published in 2003, is well adopted by utilities and system manufacturers throughout North America as a technical guide for integrating DERs within the electrical network. Unlike IEEE Std. 929, which targeted only PV systems, IEEE Std. 1547 was designed to be inclusive of all DG technologies. In conjunction with this standard, application guide IEEE Std. 1547.2 [89] was released in 2008. The scope of IEEE Std. 1547 covers installations of any DG technology with a capacity up to 10 MVA. A lower capacity limit of 30 kW is presented in [89] to distinguish DER systems that have a minimal impact on power system operations. One of the most prominent recommendations in IEEE Std. 1547 is that DER systems should quickly stop to energize the distribution network once a fault is detected. There is no mention of FRT capabilities to aid maintaining grid stability, even though this standard provides recommendations for system capacities up to 10 MVA. This philosophy evidently implies that there is no footprint of LVRT requirements in this standard.

- CSA Std. C22.3 No.9-08 - Canadian electrical code part III: interconnection of distributed resources and electricity supply systems [90]: The Canadian Standards Association (CSA) prepared Std. C22.3 No.9-08 in 2008 to address the need for standardized connection practices. CSA Std. C22.3 No.9-08 covers the interconnection of DERs and distribution systems with voltages less than 50 kV and applies to any DG technology, with an aggregate system capacity up to 10 MW. This standard focuses on inverter based systems

connected to the distribution system where the PCC is at the medium-voltage level (defined as 0.75 kV through 50 kV). A power factor operating range of ±0.9 is recommended.

- UL1741 standard for safety - Standard for inverters, converters, controllers and interconnection system equipment for use with distributed energy resources [91]: this is a well-known and commonly utilized standard that covers the construction, safe operation and performance testing of inverters, converters, charge controllers and interconnection system equipment associated with DERs. In contrast to the previously discussed standards that provide technical recommendations, most utilities require inverters obtain UL1741 certification as a prerequisite for grid connection.

- Finally, IEEE Std. 519 [92] is studied and reviewed in [5] which includes recommended practices and requirements for harmonic control in electrical power systems.

2.2.4 Grid code requirements for DER Interconnection

The objective of this section is to briefly introduce some main grid requirements for the connections of DER systems. A detailed study in this regard is provided in [5] which has considered:

- Anticipated developments in North American grid requirements for DERs,

- Requirements for a practically safe interconnections.

- Dominant features and common trends of emerging grid codes.

2.2.4.1 Agreed active power

Agreed active power denotes the maximum active power injection permitted by a DER system for delivery into the distribution system and is contractually agreed by both the utility and DER owner. In this thesis, the agreed active power is defined as a fixed maximum amount of active power that can be delivered to the distribution system by the DER system at the PCC. This limitation bounds the contractually obliged reactive power requirements of the DER system at the PCC. The agreed active power is determined by:

- Sum of the maximum active power outputs of each on-site DER unit,
- Aggregate load demands of the DER system, and
- DER system objectives such as micro-grid capability or dedicated feed-in-tariff operation [5].

2.2.4.2 FRT requirements

These requirements specify an expected system response or behavior, both during and immediately following the faults, where the DER system is disallowed from disconnecting. The enforcement of FRT requirements have two advantages [93]:

- A large DER system will not disconnect due to the short-term faults and it does not lead to a sudden significant loss of generation that could further result in grid instability.
- There will be the voltage and frequency support for the network both during and immediately after the fault.

Depending on the network configuration and type of fault, a voltage sag neighboring the fault propagates differently through system impedances [75], resulting in voltage sags at the DER system PCC with differing possible severities. These voltage conditions can be tackled by grid connected inverters in order to ride through the faults and thus maintain

synchronous connection of the DER system. This obligatory resistance to temporary voltage sags during grid faults is commonly referred to as low-voltage ride-through (LVRT). LVRT requirements are expressed by a voltage versus time curve similar to the example presented in Fig. 2.2 or Fig. 2.5. When the PCC voltage is above the pre-specified line in Fig. 2.2, the DER system is obliged to maintain a synchronous grid connection. However, when the voltage is under the determined line, the DER is allowed to disconnect.

Similar to LVRT, requirements to tolerate temporary voltage swells is referred to as high-voltage ride-through (HVRT). HVRT requirements are the complement to LVRT as they identify voltage swells that a DER system must remain synchronously connected. Voltage swells occur less frequently than voltage sags. It is possible to define HVRT constraints by a voltage versus time curve similar to LVRT curves; however, it is most frequently established in the literature with a simple table of voltage ranges and corresponding trip times [5]. The common causes for voltage swells were mentioned in section 2.2.1.

2.2.4.3 Ancillary services

Ancillary services were traditionally provided only by synchronous generators to support and ensure that the power system operates in a safe, robust and reliable manner [94]. They required a certain additional network reserve of active and reactive power to help maintaining system frequency and voltage within expected limits. However, with recent growth of DERs, some burdens of these important roles are on the shoulders of various de-centralized sources. Ancillary services from DERs can provide even progressive functions such as [5]:

- Assist in supporting local voltage
- Assist in regulating the frequency
- Black start capability

- Harmonic compensation
- Contribution to grid spinning reserve

Therefore, state of the art power electronics provide advanced schemes for DER systems to emulate most ancillary services traditionally provided by centralized synchronous generators. In this thesis, ancillary services are defined as functions accomplished by grid interfacing inverters.

2.2.5 WECS specific codes

Due to the significant growth and increased penetration of grid connected WECSs in recent years, many countries have released their own wind specific grid codes, usually at the sub-transmission and transmission systems. These codes enforce technical requirements on grid connected operation of WECSs [5]. The main reasons for the development of these grid codes are to [67]:

- Provide WECSs performances similar to those of synchronous generators
- Lower the amount of wind power lost in the case of short-term disturbances
- Improve and stabilize wind turbine systems operations

Interesting discussions and comparisons of existing WECS grid codes across Europe and North America are available in [67], [69], [95]. Denmark and Germany were the first countries to have WECSs, connected into their high voltage networks, meeting the LVRT requirements associated with their new grid codes [96] and are often considered as leaders in this field. Other European nations have also adapted their own grid codes subsequently. Transmission system operators in Canada and the USA have followed the path of their European counterparts, and published their own WECS specific grid codes. Notably, the WECS grid codes of Hydro-Quebec [86] and the Alberta Electric System Operator [87] are often referred to as successful Canadian standards, as they are well established and

moderately progressive. Each code has its individual set of requirements due to the respective grid operating characteristics. Good examples are Germany, Spain, Great Britain and Ireland grids where an injection of reactive current during grid faults is necessary while other codes do not impose this requirement [69]. As another example, Hydro-Quebec imposes a wide range of frequencies which the WECS must ride-through due to the lack of synchronous links with neighboring grids [97]. Although each WECS grid code may have some unique sets of requirements, they all normally have common characteristics. These common requirements can be listed as:

- FRT capabilities - namely LVRT and HVRT specifications
- Voltage regulation capabilities and associated reactive power injection
- Frequency regulation capabilities and associated active power injection
- Power quality enhancements
- Voltage and frequency operational limits

It is also important to put an emphasize on dissimilarity (non-harmonization) in WECS grid codes as this is repeatedly deliberated in literature and has caused major challenges for the wind industry in designing systems for compliance with multiple rules. This contrast between codes is best clarified with curves depicting LVRT requirements from several different WES grid codes, shown Fig. 2.5 [69]. On the other hand, existing WECS grid codes still experience revisions because of increasing penetration levels. To tackle these issues, the power system operators, engineers and researchers should aim to move toward grid code harmonization. Despite aforementioned challenges, most wind turbine manufacturers are now able to supply WECSs that are compliant with target codes [5].

2.2.6 DERs specific codes

Similar to grid connected WECSs which have changed sub-transmission and transmission grid codes, the unprecedented growth of other DGs is contributing to the

formulation of new medium-voltage grid codes governing the operation of DERs. Mainly these medium-voltage grid codes specify interconnection restrictions for DER systems including various DG technologies. Due to strong growth of DERs, particularly PV, Germany has advanced technical rules for interconnections of DERs [98]. They have released their technical guidelines for generating plants connected to their medium-voltage network [99] in 2008, which commands both LVRT requirements and ancillary services. A detailed discussion of this code is provided in [100]. Although existing medium-voltage codes are less developed in North America compared to those in Europe, various North American organizations are introducing task forces/working groups to assess the impact of large scale DERs interconnected into the power grid [5]. As a notable effort, the North American Electric Reliability Corporation (NERC) originated the integration of variable generation task force (IVGTF) in 2007. In 2009, the IVGTF released a preliminary report [101] which summaries several recommended actions for both the NERC and industry. In 2011, an update on the IVGTF activities was reported in [14] where initial suggestions exposed an updated set of requirements that include LVRT. These IVGTF recommendations seem to be running in parallel with the developments in order to adapt to increasing DER penetration. If realized, these recommendations and code requirements will provide North American grids a robust and safe operation with a high penetration level of DERs.

2.2.7 Requirements from DER owner point of view

First and foremost, DER owners need to have regulated maximum phase currents under any fault in order to protect their devices. Furthermore, oscillations on the active and reactive powers are important for DER owners, since they have serious impacts on the controllers design (such as DC-voltage regulation) and devices sizing (e.g. DC-link capacitor sizing). These important terms (i.e. maximum phase currents and active/reactive power oscillations) along with their expressions and analysis will be thoroughly studied in next chapters.

2.3 Example of LVRT Technology I: LVRT in DFIGs

2.3.1 Why DFIG?

Two of the most common types of wind turbine systems are DFIG (which occupies close to 50% of the wind energy market [102]) and PMSG (with market share of almost 20% [103]). In [104], three generators suitable for wind energy applications are studied: a direct-drive synchronous generator (offered by Enercon [105]), a direct-drive PMSG (marketed by different companies, e.g., Vestas [106] and Clipper [107]), and a DFIG (manufactured by several companies such as Vestas [106] and Gamesa [108]). The results in terms of weight, cost, size, and losses are available in [66], [104]. From these results, it is concluded that the total costs are almost the same. The total weight of a WECS based on a direct-drive PMSG is about 4 times higher than that of a WECS based on a DFIG [104]. The stator diameter of a direct-drive PMSG is about six times that of a DFIG of similar power. However, the power losses in PMSG is almost half of the total power losses in a DFIG.

2.3.2 Systems and Controls in DFIG under Grid Faults

Behaviour of the DFIG under the grid voltage disturbances is studied in [66] in details. It is stated that the grid disturbances cause rotor over-currents and over-voltages with a dc-link over-voltage which can lead to converter failure if no protection is involved [71], [109]. Different protection tools are depicted in Fig. 2.6. Their operation and some control methods to fulfil with the LVRT requirements is discussed in [66].

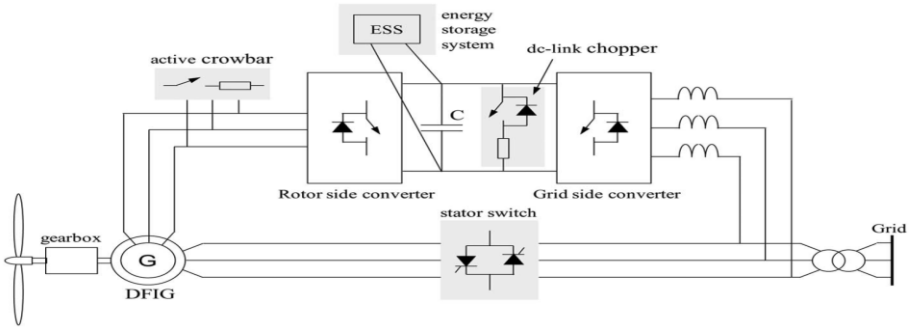

Fig. 2.6. Rotor and converter protection devices of a typical DFIG: crowbar, dc-link chopper, ESS, and ac switch [120].

The primary solution implemented by manufacturers to protect the rotor and the converter was to short-circuit the rotor windings with the so-called crowbar and to disconnect the turbine from the grid [110]. This solution is not permissible with the LVRT requirements because the WECSs do not support the utility to continue normal operation. If the rotor side converter is sized to generate a voltage equal to the rotor over-voltages, it will be able to fully control the rotor currents and avoid the crowbar operation [71], [111]. This is the simplest solution to take care of rotor over-voltages because it provides full control of the DFIG at all times. A technique to determine the rotor side converter size based on the maximum rotor over-voltage and over-current is presented in [112]. One of the most comprehensive analysis of the operation limits for the rotor side converter under grid disturbance is presented in [113], which takes the impact of limited ratings for the DFIG converters into account under grid disturbances. Oversized converters provide more controllability, but the DFIG topology loses its advantages of the low-size power converter [71]. It is well-recognized that the DFIG converters ratings are around 30% of the total DFIG power [66] and is not normally sized to generate a voltage equal to the rotor over-voltages [71]. It is also noted in [66] that for deep voltage sags the rotor side converter over-sizing is far beyond the converter steady-state ratings. Converter sizing is thus a tradeoff between the LVRT requirements and the cost, together with other protection devices such as the crowbar and the dc-link chopper.

In [114], it is proposed to connect the grid-side and rotor-side converters in parallel, using appropriate ac switches, to provide more reactive power to the grid. If the DFIG is not able to provide the reactive power support required by the gird code requirements,

dynamic and static VAR compensators [115], or static synchronous compensators [116]–[117] can be installed at DFIG terminals to support it. Other equipment, such as the dynamic voltage restorer, can also be used [118].

The dc-link chopper is not essential for fault ride-through operation, but it increases the range of DFIG operation [119]. The energy storage systems [120], connected to the dc-link absorbs the extra energy supplied to the dc link during the fault, and returns it to the DFIG in normal operation. However, it dramatically increases the cost and complexity of the WECS. An interesting performance comparison between using a crowbar, a dc-link chopper, and an energy storage system is presented in [120]. The stator switch proposed by [121] is another device to meet the LVRT requirements.

2.3.3 Control Methods for LVRT in DFIG

To control rotor voltages and currents, reduce the rotor over-voltages and/or over-currents, and avoid the crowbar activation in order to keep full DFIG control at all times to meet the LVRT requirements are some of the hottest research directions in recent efforts in academia and industry [122]-[132]. However, in many cases, the crowbar activation cannot be avoided, and the crowbar mode contemporarily operates with control methods. Some control approaches regulate the currents of the rotor and the grid-side converter in the positive and negative *d–q* reference frames [112], [122] based on a positive- and negative-sequence models of DFIG [123]. The main goals are the DFIG active and reactive power controls to meet the LVRT requirements. As it will be discussed in section 2.4, each power converter has four degrees of freedom, allowing including additional control goals, as for instance the regulation of the dc-link voltage, stator current balancing, and cancelation of the oscillations in the active power, rotor current, and torque [66]. Although crowbar activation cannot be avoided in the case of severe asymmetrical faults [112], non-crowbar methods to lower the rotor over-voltages based on injecting demagnetizing flux currents from the rotor-side converter is proposed by [124]-[125]. Full DFIG control is reported; but a large rotor current capacity is needed, and there is limited capability in the case of severe asymmetrical faults. If the crowbar is activated,

the use of the demagnetizing current lowers the crowbar mode time [126]. A robust controller in the α–β stationary frame is offered in [127], claiming full control in all LVRT cases. However, the results have been attained with oversized converters that can accommodate rotor over-voltages and full rotor current control. With normal converter ratings, this control method may have some limitations.

Another control approach presents a virtual resistance in the rotor to reduce rotor over-currents [128]. A combination of demagnetization and virtual resistance control is also presented in [128]. For symmetrical dips, reduced rotor currents (in comparison with the results of [124]) are also reported in [128]. However, operation under asymmetrical faults is beyond the scope of [128]. PI controllers with resonant compensators are addressed in [129]-[130] for operation under grid voltage disturbances. In [131], the conventional controller used in normal operation is switched to the proposed vector-based hysteresis current controller during voltage disturbances. Appropriate system performance is reported; however, the operation limits are not specified, and there are drawbacks to the hysteresis control. Last but now least, sliding-mode control has been effectively applied to DFIG in [132] under asymmetrical faults and harmonically distorted grid conditions. Future application of sliding-mode control method in the DFIG to meet the LVRT requirements can be expected.

2.4 Example of LVRT Technology II: LVRT in CI-DERs

As stated earlier, most of the DER units interconnect to the grid by power electronic devices and converter interfaces; which are also the main scope of this thesis, and they are called CI-DERs and referred to consistently throughout this thesis. A typical CI-DER unit connected to the grid is shown in Fig. 2.7. Far away from operating in perfect steady-state, balanced and stable conditions, the electrical grid behaves as an ‘alive’ system, with its specific dynamical performance, that is affected by resonances, overloads, faults, etc. Therefore, the control of grid-connected CI-DERs should be carefully considered in order

to guarantee a proper performance under countless operating conditions. Recently, the operation of CI-DERs under abnormal grid conditions, mainly under voltage sags, has become a great challenge for the DG industry due to the increasing demands of the new grid code requirements LVRT and ancillary services such as reactive power injection during grid faults. Despite the fact that the initial developments were predominantly oriented to tackled balanced grid faults, the attention of engineers and researchers has lately moved towards controlling the current injection of CI-DERs under unbalanced grid voltage conditions. Under generic grid conditions, the voltage at the point of connection of this active rectifier can be expressed as [43]:

$$v=\sum_{n=1}^{\infty}(\mathrm{v}^{+n}+\mathrm{v}^{-n}+\mathrm{v}^{0n})= \\ =\sum_{n=1}^{\infty}\left\{V^{+n}\begin{bmatrix}\cos(\mathrm{n}\,\omega\mathrm{t}+\phi^{+n})\\ \cos(\mathrm{n}\,\omega\mathrm{t}+\phi^{+n}-\frac{2\pi}{3})\\ \cos(\mathrm{n}\,\omega\mathrm{t}+\phi^{+n}+\frac{2\pi}{3})\end{bmatrix}+V^{-n}\begin{bmatrix}\cos(\mathrm{n}\,\omega\mathrm{t}+\phi^{-n})\\ \cos(\mathrm{n}\,\omega\mathrm{t}+\phi^{-n}+\frac{2\pi}{3})\\ \cos(\mathrm{n}\,\omega\mathrm{t}+\phi^{-n}-\frac{2\pi}{3})\end{bmatrix}+V^{0n}\begin{bmatrix}\cos(\mathrm{n}\,\omega\mathrm{t}+\phi^{0n})\\ \cos(\mathrm{n}\,\omega\mathrm{t}+\phi^{0n})\\ \cos(\mathrm{n}\,\omega\mathrm{t}+\phi^{0n})\end{bmatrix}\right\} \tag{2.1}$$

where superscripts $+n$, $-n$ and $0n$ represent respectively the positive, negative and zero sequence components of the n-th harmonic of the voltage vector v. Similarly, the current injected by the CI-DER can be generically written as:

$$i=\sum_{n=1}^{\infty}\left\{I^{+n}\begin{bmatrix}\sin(\mathrm{n}\,\omega\mathrm{t}+\delta^{+n})\\ \sin(\mathrm{n}\,\omega\mathrm{t}+\delta^{+n}-\frac{2\pi}{3})\\ \sin(\mathrm{n}\,\omega\mathrm{t}+\delta^{+n}+\frac{2\pi}{3})\end{bmatrix}+I^{-n}\begin{bmatrix}\sin(\mathrm{n}\,\omega\mathrm{t}+\delta^{-n})\\ \sin(\mathrm{n}\,\omega\mathrm{t}+\delta^{-n}+\frac{2\pi}{3})\\ \sin(\mathrm{n}\,\omega\mathrm{t}+\delta^{-n}-\frac{2\pi}{3})\end{bmatrix}\right\} \tag{2.2}$$

According to the instantaneous power theory [133]-[134], the instantaneous active and reactive powers resulting from the interaction of these voltages and currents can be obtained by respectively calculating their inner and cross product, as follows:

$$p=v.i \quad ; \quad q=|\,\mathrm{v}\times\mathrm{i}\,| \tag{2.3}$$

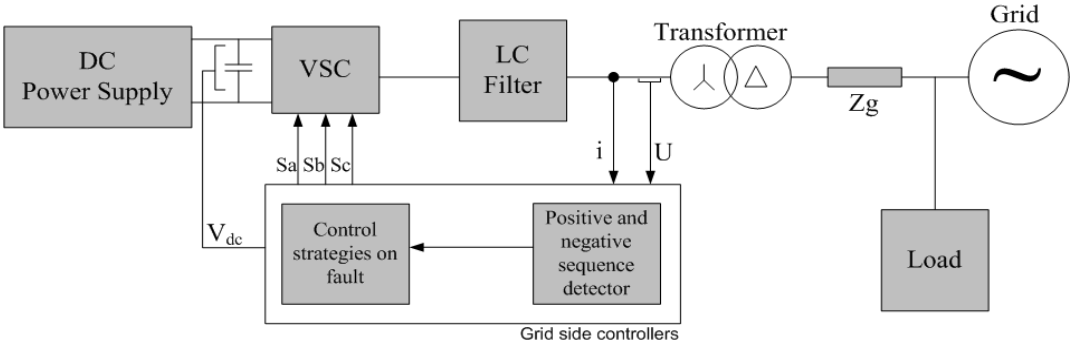

Fig. 2.7. A typical CI-DER connected to the grid [44].

As stated in references [43] and [133], average values in the instantaneous active and reactive powers, P and Q, result from the interaction of voltage and current components with the same frequency and sequence, while oscillations in these instantaneous powers, $\tilde{p}$ and $\tilde{q}$, result from the interaction of voltage and current components with either different frequencies or sequences. Considering only the fundamental frequency in voltage and current expressions, i.e. making n = 1, the generic instantaneous active and reactive powers expressions under unbalanced grid conditions can be expressed in the form of following expressions [135]:

$$p = P + P_{c2}\cos(2\omega t) + P_{s2}\sin(2\omega t) \tag{2.4}$$

$$q = Q + Q_{c2}\cos(2\omega t) + Q_{s2}\sin(2\omega t) \tag{2.5}$$

where P and Q are the average values of the instantaneous active and reactive powers respectively, whereas P_{c2}, P_{s2}, Q_{c2} and Q_{s2} represent the magnitude of the oscillating terms in the instantaneous active and reactive powers [136]. In most of the existing studies dealing with power flow in power converters under unbalanced grid conditions [38]-[57], the voltages and the currents to calculate these power magnitudes are expressed on synchronous reference frames. Therefore, the amplitude of these power magnitudes can be obtained as:

$$P = \frac{3}{2}(v_d^+ i_d^+ + v_q^+ i_q^+ + v_d^- i_d^- + v_q^- i_q^-) \tag{2.6}$$

$$P_{c2} = \frac{3}{2}(v_d^- i_d^+ + v_q^- i_q^+ + v_d^+ i_d^- + v_q^+ i_q^-) \tag{2.7}$$

$$P_{s2} = \frac{3}{2}(v_q^- i_d^+ - v_d^- i_q^+ - v_q^+ i_d^- + v_d^+ i_q^-) \tag{2.8}$$

$$Q = \frac{3}{2}(v_q^+ i_d^+ - v_d^+ i_q^+ + v_q^- i_d^- - v_d^- i_q^-) \tag{2.9}$$

$$Q_{c2} = \frac{3}{2}(v_q^- i_d^+ - v_d^- i_q^+ + v_q^+ i_d^- - v_d^+ i_q^-) \tag{2.10}$$

$$Q_{s2} = \frac{3}{2}(-v_d^- i_d^+ - v_d^- i_q^+ + v_d^+ i_d^- + v_q^+ i_q^-) \tag{2.11}$$

where v_d^+ , v_q^+ and i_d^+ , i_q^+ are calculated by Park transform [137] and represent the *dq* components of the positive-sequences of voltage and current vectors represented on a synchronous reference frame rotating at the fundamental grid frequency ω, whereas v_d^- , v_q^- and i_d^- , i_q^- are the components of the negative-sequences of the voltage and current vectors lying on a synchronous reference frame rotating at –ω, respectively [43]-[44]. Many of the studies on the control of CI-DERs under unbalanced grid voltages have rewritten power terms of (2.6)-(2.11) in the form of following matrix expression [38], [43], [45], [52]-[53]:

$$\begin{bmatrix} P \\ Q \\ P_{c2} \\ P_{s2} \end{bmatrix} = \underbrace{\frac{3}{2}\begin{bmatrix} v_d^+ & v_q^+ & v_d^- & v_q^- \\ v_q^+ & -v_d^+ & v_q^- & -v_d^- \\ v_d^- & v_q^- & v_d^+ & v_q^+ \\ v_q^- & -v_d^- & -v_q^+ & v_d^+ \end{bmatrix}}_{M_{4\times4}} \begin{bmatrix} i_d^+ \\ i_q^+ \\ i_d^- \\ i_q^- \end{bmatrix} \tag{2.12}$$

By inverting the matrix $M_{4\times4}$, it is possible to find the current set-points that gives a certain value of the active and reactive power components for given grid voltage conditions, as:

$$\begin{bmatrix} i_d^{+*} \\ i_q^{+*} \\ i_d^{-*} \\ i_q^{-*} \end{bmatrix} = M_{4\times4}^{-1} \times \frac{2}{3} \begin{bmatrix} P^* \\ Q^* \\ P_{c2}^* \\ P_{s2}^* \end{bmatrix} \tag{2.13}$$

Therefore, from (2.13) it is possible to calculate the currents to be injected by the converter that give a certain value of P and Q, while also cancelling out the active power oscillations terms, P_{c2} and P_{s2}, under unbalanced grid voltages. These power references can be fulfilled by calculating the current references as shown in (2.14):

$$\begin{bmatrix} i_d^{+*} \\ i_q^{+*} \\ i_d^{-*} \\ i_q^{-*} \end{bmatrix} = M_{4\times4}^{-1} \times \frac{2}{3} \begin{bmatrix} P^* \\ Q^* \\ 0 \\ 0 \end{bmatrix} \tag{2.14}$$

The expression shown in (2.14) for setting the current references has been extensively used in the literature [43]-[45], [52], [138]. However, other alternative approaches have been presented more recently, as for instance in [45], [139]. In other studies, the power losses associated with the filter between the converter and grid are considered in the calculation of the reference currents [140]. Nevertheless, all these efforts mainly target to attenuate active power oscillations; but the reactive power oscillations is normally beyond their scope. In parallel with the studies related to the regulation of the currents to be delivered by grid connected CI-DERs in order to preserve the active power constant during unbalanced voltages, several studies started to emphasize the importance of proposing new operation states in order to realize additional characteristics. For an example, [45] tries to cancel out oscillations on either active or reactive powers and simultaneously have balanced currents. As other examples, [46]-[47] deal with not only the LVRT requirements, but also with other ancillary services such as flexible voltage supports under voltage disturbances. Actually, there exist infinite combinations for the currents to be delivered to the grid by a three-phase grid-connected power converter in order to acquire certain values for the average active and reactive powers, P and Q, under

given grid voltage conditions. Therefore, depending on the control objective, e.g. perfect control of the instantaneous active and reactive powers, cancellation of active and reactive power oscillations, having sinusoidal and balanced currents, flexibly supporting the grid voltage, etc., different expressions can be proposed to calculate the reference currents to be delivered by the grid-connected power converter in order to exchange given averaged values of active and reactive powers [44]-[57], [141]. The specific methods to find these reference current expressions to meet the LVRT requirements are referred to in this thesis as LVRT reference current generation (LVRT-RCG) techniques. This thesis reviews, studies, analyzes, and expands nine previously introduced LVRT-RCG strategies [43]-[47] in the following chapters.

Once the reference currents to exchange given active and reactive powers with the grid under generic voltage conditions are properly determined, it is necessary to have a proper current controller that is able to inject such currents into the grid. The current control loop structures proposed for tracking the reference currents have been extensively improved throughout the years [43]. Firstly, back in the 1990s, [140] proposed the implementation of a single PI current controller on the positive-sequence synchronous reference frame for tracking both positive- and negative-sequence reference currents. Later, by the end of the 1990s, other authors introduced two control loops, one for the positive-sequence and another one for the negative-sequence currents [142]. Song et al. proposed PI controllers which contain notch filters tuned at twice the fundamental frequency to attenuate associated oscillations (these oscillations at twice the fundamental frequency in the reference currents *dq* signals come from the interactions between current vectors and reference frames with different sequences [43], [142]).

As an alternative to the current controllers based on the double synchronous reference frame, resonant controllers operating on the stationary reference frame have been demonstrated to have appropriate performances in order to track the calculated reference currents under unbalanced and distorted grid voltages [143]-[144]. These controllers are based on frequency adaptive filters, which show the same performance for both positive and negative frequencies. Other solutions based on hysteresis current controllers [145] (offer fast dynamic response and robust performance), direct power control methods

[146]-[147] and model-based predictive control [148], can also be used to regulate the currents under generic distorted voltages. It is necessary to mention that the appropriate performance of any of these current controllers under generic grid conditions significantly depends on the accuracy of the grid synchronization system [149]. In the case of three-phase systems, the grid synchronization effects get more severe, since the symmetrical components of the grid voltage in positive and negative sequences should be perfectly calculated in order to acquire a proper control of the positive- and negative-sequence currents.

Last point to be mentioned is that the reference currents during unbalanced grid faults may be balanced, unbalanced or even distorted (non-sinusoidal). As a consequence, the current injected by the grid-connected power converter is likely to be different from one phase to another phase. Therefore, one additional crucial issue is taking the maximum instantaneous phase currents into account in order to avoid any undesired overcurrent tripping. This last point will be addressed thoroughly in Chapter 4 and Chapter 5.

2.5 Summary

In this chapter, the DERs were presented and discussed with their fundamental components (i.e. distributed energy storage systems and distributed generation systems). Also, a well-known category of DERs with the label of converter-interfaced DERs (CI-DERs) is introduced. Furthermore, newly developed grid codes and their strict requirements were categorized and studied from different points of views (such as LVRT requirements in national grid codes, technical standards for DER interconnection, wind energy conversion systems specific codes, etc.). Finally, two examples of the LVRT technologies were studied in twofold DERs, i.e. directly connected DFIGs and CI-DERs. As the scope of this thesis, the other three chapters will specifically focus on LVRT technologies in CI-DERs.

Chapter 3

A Generic Comparative Study on Available LVRT-RCG strategies in CI-DER Units

3.1 Introduction

Subject to the aim of the control strategy used to generate the reference currents under different faults, the general performance of the power converter and its interaction with the electrical network will vary significantly. Additionally, the grid codes impose specific requirements related to the injection of active and reactive currents during grid faults. Consequently, reference current generation during faults is a challenging issue in the control of power converters [25]. [43]-[47] have proposed different reference current generation methods under grid faults (mostly under asymmetrical faults). The tight requirements forced by the grid operators, mainly related to low-voltage ride-through and grid support during grid faults, has inspired engineers and researchers to amend the conventional control strategies for grid-connected DG converters [43]. Occurrences of grid faults usually cause the appearance of unbalanced voltages at PCC. Under unbalanced voltages, the currents injected into the grid may become non-sinusoidal and/or unbalanced. Such currents and the unbalanced grid voltages may lead to undesired fluctuations in the active and reactive power injected into the grid. The appropriate operation of the power converter under such conditions is another critical issue.

In 2007, Rodriguez et al. [44] proposed a flexible active power control under the grid faults based on a reference current selector. In [44], using experimental results, five strategies to generate the proper reference current were studied and compared during an asymmetrical fault. Another interesting contribution in the field of reference current generation is recently proposed by Ma et al. in [45]. In this work a new control strategy which uses the zero sequence components is proposed to improve the power controllability under grid faults. By injecting appropriate zero sequence current and relevant circuit configurations, the DG converter can have more flexible control objectives, e.g. achieving better performances in the delivered power, having non-oscillatory active and reactive power injection and injecting more enhanced load currents when suffering from unbalanced AC voltage.

In balanced voltage sags, the DG inverter should inject reactive current in order to boost the voltage in all phases. However, in asymmetrical faults, the main concern of the DG inverter is to equalize three-phase voltages by decreasing the negative sequence of the voltage in order to reduce the phase jump [46]. Due to system restrictions, a balance between these two severe policies is required. In 2013, a flexible control scheme for grid-connected DG inverters was proposed by Camacho et al. [46] in order to have more flexibility to either boost the three-phase voltages or reduce the negative sequence voltage based on system requirements. In [46], the grid equivalent impedance is assumed to contain only the inductive part. However, a modified control strategy of grid-connected DG inverters for the positive sequence voltage recovery and negative sequence voltage reduction under asymmetrical grid faults is presented very recently by Guo et al. [47]. Unlike the control strategy of [46], which was based on an assumption that the grid impedance is just inductive, the proposed control strategy in [47] considers the impact of the resistive part of the grid impedance, which is of great importance especially in low-voltage networks. The presented control strategy is examined in a low-voltage grid where the grid impedance just contains the resistive part.

A comprehensive and comparative study on available LVRT-RCG strategies in terms of their merits and demerits under a generic voltage sag condition is the main focus of this chapter as reported in the following sections. This chapter collects two categories of

LVRT-RCG methods. The first group aims to control power under grid voltage disturbances and imbalances which are introduced in section 3.2; whereas, the second group, presented in section 3.3, targets to flexibly support the voltage under the grid faults.

3.2 Uninterrupted Power Delivery Control Strategies under Unbalanced Grid Voltages

The control of the delivered instantaneous active/reactive powers of a three-phase grid-connected power converter under unbalanced and faulted grid voltages needs the determination of proper reference-currents. In this section, six strategies to calculate the reference-currents introduced in [43]-[45] will be studied. The aim of control strategies of this group is uninterrupted power delivery (UPD) under the grid faults. Each of these strategies intends to demonstrate a specific performance for the delivered active/reactive powers and/or injected currents. The energy source of power converters usually have slow dynamics and consequently the delivered power can be assumed constant during a grid-fault. Also, the dc-side of the converter in all following strategies can be assumed to be a constant dc source [43]-[45].

3.2.1 Instantaneous Active-Reactive Control (IARC)

According to instantaneous power theories [133], any current vector aligned with the voltage vector, v, will produce the active power, P, while any current vector aligned with the orthogonal voltage vector, $v_{\perp}$ (90° leading from v), will produce the reactive power, Q. Therefore, one can obtain the reference active/reactive currents i_p^* and i_q^* given by (3.1) in order to deliver P and Q:

$$i_p^* = g\, v \quad , \quad i_q^* = b\, v_\perp \tag{3.1}$$

where g and b can be considered as instantaneous conductance and instantaneous susceptance obtained by [43]:

$$P^* = i_p^*.\, v = g\, v.\, v = g\,|v|^2 \Rightarrow g = \frac{P^*}{|v|^2} \tag{3.2}$$

$$Q^* = i_q^*.\, v = b\, v_\perp.\, v = b\,|v|^2 \Rightarrow b = \frac{Q^*}{|v|^2} \tag{3.3}$$

The total reference-current is obtained by:

$$i^* = i_p^* + i_q^* \tag{3.4}$$

Two points worth mentioning related to the IARC strategy. First, the IARC is the most effective reference-current determination method in the sense of delivering the exact instantaneous active/reactive powers under general grid voltages. Second, under balanced sinusoidal grid voltages, the reference-currents obtained from (3.1)-(3.4) are sinusoidal. However, under unbalanced voltages, the module $|v|^2$ contains oscillations at twice the fundamental frequency (ω)

$$|v|^2 = |v^+|^2 + |v^-|^2 + 2\,|v^+|\,|v^-|\cos(2\omega t + \phi^+ - \phi^-) \tag{3.5}$$

Therefore, the obtained reference-currents are not sinusoidal and include harmonics. These distorted currents have several drawbacks. First, they need more complicated control systems in order to track the harmonic components of the currents. Second, harmonic components of the currents may cause overcurrent problems, excitation of resonances and extra deterioration of PCC voltage.

3.2.2 Average Active-Reactive Control (AARC)

In order to omit the oscillations at twice the fundamental frequency in (3.5), average active-reactive control (AARC) strategy intends to use average conductance, *G*, and average susceptance, *B*, using (3.6) [43]:

$$G = \frac{P^*}{V^2} \quad , \quad B = \frac{Q^*}{V^2} \quad , \quad V^2 = |\,\mathrm{v}^+\,|^2 + |\,\mathrm{v}^-\,|^2 \tag{3.6}$$

Then, the reference-currents are

$$i_p^* = G\,v \quad , \quad i_q^* = B\,v_\perp \tag{3.7}$$

Also, the instantaneous active/reactive powers can be given by

$$p = i_p^*.\,v = \frac{|\,\mathrm{v}\,|^2}{V^2}P^* = P^* + \underbrace{\left[\frac{2\,|\,v^+\,||\,v^-\,|\cos\left(2\omega\mathrm{t}+\phi^+-\phi^-\right)}{|\,v^+\,|^2+|\,v^-\,|^2}\right]P^*}_{\tilde{p}} \tag{3.8}$$

$$q = i_q^*.\,v_\perp = \frac{|\,\mathrm{v}\,|^2}{V^2}Q^* = Q^* + \underbrace{\left[\frac{2\,|\,v^+\,||\,v^-\,|\cos\left(2\omega\mathrm{t}+\phi^+-\phi^-\right)}{|\,v^+\,|^2+|\,v^-\,|^2}\right]Q^*}_{\tilde{q}} \tag{3.9}$$

where $\tilde{p}$ and $\tilde{q}$ are active/reactive powers oscillations. Therefore, the injected currents by the AARC strategy will be perfectly sinusoidal at the cost of oscillations in active and reactive powers at twice the fundamental frequency.

3.2.3 Balanced Positive-Sequence Control (BPSC)

If the quality of the injected currents is important or the current controllers should be simple proportional-integrator compensators, then the reference-currents should be not only sinusoidal, but also balanced. Therefore, the value of the conductance and

susceptance can be modified in order to realize this objective by using balanced positive-sequence control (BPSC) strategy [43]-[44]:

$$i_p^* = G^+ v^+ \quad , \quad G^+ = \frac{P^*}{|v^+|^2} \tag{3.10}$$

$$i_q^* = B^+ v_\perp^+ \quad , \quad B^+ = \frac{Q^*}{|v^+|^2} \tag{3.11}$$

Using (3.10) and (3.11), the reference-currents become sinusoidal and balanced; and they only follow the positive sequence. Therefore, the current amplitudes will be relatively lower. The instantaneous active/reactive powers will be

$$p = v.i = (v^+ + v^-).(G^+ v^+ + B^+ v_\perp^+) = P^* + \underbrace{P^* \frac{v^+.v^-}{|v^+|^2} + Q^* \frac{v_\perp^+.v^-}{|v^+|^2}}_{\tilde{p}} \tag{3.12}$$

$$q = v_\perp.i = (v_\perp^+ + v_\perp^-).(G^+ v^+ + B^+ v_\perp^+) = Q^* + \underbrace{Q^* \frac{v^+.v^-}{|v^+|^2} + P^* \frac{v^+.v_\perp^-}{|v^+|^2}}_{\tilde{q}} \tag{3.13}$$

3.2.4 Instantaneously-Controlled Positive Sequence (ICPS)

Reference [44] introduces the instantaneously-controlled positive sequence (ICPS) strategy which delivers P and Q by imposing the following constraints:

$$i_p^{*-} = i_q^{*-} = 0 \quad , \quad i_p^{*+} = g^+ v^+ \quad , \quad i_q^{*+} = b^+ v_\perp^+ \tag{3.14}$$

$$i_p^{*+}.v = i_p^{*+}.(v^+ + v^-) = P^* \quad , \quad i_q^{*+}.v_\perp = i_q^{*+}.(v_\perp^+ + v_\perp^-) = Q^* \tag{3.15}$$

Then, the instantaneous positive conductance and susceptance can be obtained as:

$$g^{+}=\frac{P^{*}}{|v^{+}|^{2}+v^{+}.v^{-}} \quad , \quad b^{+}=\frac{Q^{*}}{|v^{+}|^{2}+v^{+}.v^{-}} \tag{3.16}$$

Using this strategy, non-sinusoidal and unbalanced reference-currents are generated under unbalanced conditions since g^{+} and b^{+} calculated by (3.16) have oscillations in their denominators at twice the fundamental frequency. Unbalances and harmonics in the currents may lead to the over current issues, etc. The instantaneous active and reactive powers using the ICPS method can be calculated as

$$p=v\,.\,i^{*}=(v^{+}+v^{-}).(i_{p}^{*+}+i_{q}^{*+})=P^{*}+\underbrace{Q^{*}\frac{v^{-}.v_{\perp}^{+}}{|v^{+}|^{2}+v^{+}.v^{-}}}_{\tilde{p}} \tag{3.17}$$

$$q=v_{\perp}\,.\,i^{*}=(v_{\perp}^{+}+v_{\perp}^{-}).(i_{p}^{*+}+i_{q}^{*+})=Q^{*}+\underbrace{P^{*}\frac{v_{\perp}^{-}.v^{+}}{|v^{+}|^{2}+v^{+}.v^{-}}}_{\tilde{q}} \tag{3.18}$$

where p and q contain oscillations at 2ω.

3.2.5 Positive and Negative Sequence Control (PNSC)

As another approach, the positive- and negative-sequence control (PNSC) strategy calculates a reference-current vector which contains a proper set of positive- and negative-sequence components and aims to remove some oscillation terms in the instantaneous active and reactive powers [43]-[44]:

$$i^{*}=i^{*+}+i^{*-}=i_{p}^{*+}+i_{q}^{*+}+i_{p}^{*-}+i_{q}^{*-} \tag{3.19}$$

Then, according to instantaneous power theories [133]-[134], the instantaneous active/reactive powers are as follows:

$$p = \underbrace{v^+.i_p^{*+} + v^-.i_p^{*-}}_{P} + \underbrace{v^+.i_q^{*+} + v^-.i_q^{*-}}_{0} + \underbrace{v^+.i_p^{*-} + v^-.i_p^{*+}}_{\tilde{p}_{c2}} + \underbrace{v^+.i_q^{*-} + v^-.i_q^{*+}}_{\tilde{p}_{s2}} \tag{3.20}$$

$$q = \underbrace{v_\perp^+.i_q^{*+} + v_\perp^-.i_q^{*-}}_{Q} + \underbrace{v_\perp^+.i_p^{*+} + v_\perp^-.i_p^{*-}}_{0} + \underbrace{v_\perp^+.i_q^{*-} + v_\perp^-.i_q^{*+}}_{\tilde{q}_{c2}} + \underbrace{v_\perp^+.i_p^{*-} + v_\perp^-.i_p^{*+}}_{\tilde{q}_{s2}} \tag{3.21}$$

Reference [43] proposes to cancel out the summation of fifth and sixth terms of both active and reactive powers presented in (3.20) and (3.21), respectively. So, the reference-currents can be obtained as

$$\begin{cases} P^* = v^+.i_p^{*+} + v^-.i_p^{*-} \\ \tilde{p}_{c2} = v^+.i_p^{*-} + v^-.i_p^{*+} = 0 \end{cases} \Rightarrow \begin{cases} i_p^{*+} = \dfrac{P^*\, v^+}{|\,\mathrm{v}^+\,|^2 - |\,\mathrm{v}^-\,|^2} \\ i_p^{*-} = \dfrac{-P^*\, v^-}{|\,\mathrm{v}^+\,|^2 - |\,\mathrm{v}^-\,|^2} \end{cases} \tag{3.22}$$

$$\begin{cases} Q^* = v_\perp^+.i_q^{*+} + v_\perp^-.i_q^{*-} \\ \tilde{q}_{c2} = v_\perp^+.i_q^{*-} + v_\perp^-.i_q^{*+} = 0 \end{cases} \Rightarrow \begin{cases} i_q^{*+} = \dfrac{Q^*\, v_\perp^+}{|\,\mathrm{v}^+\,|^2 - |\,\mathrm{v}^-\,|^2} \\ i_q^{*-} = \dfrac{-Q^*\, v_\perp^-}{|\,\mathrm{v}^+\,|^2 - |\,\mathrm{v}^-\,|^2} \end{cases} \tag{3.23}$$

3.2.6 Zero-Sequence Current Injection (ZSCI)

In previous strategies where the system has three-wire structure, there were six distinct terms for active and reactive powers as indicated in (3.20)-(3.21) and repeated here:

$$p = P + \tilde{p}_{s2} + \tilde{p}_{c2} = P + P_{s2}\sin(2\omega t) + P_{c2}\cos(2\omega t) \tag{3.24}$$

$$q = Q + \tilde{q}_{s2} + \tilde{q}_{c2} = Q + Q_{s2}\sin(2\omega t) + Q_{c2}\cos(2\omega t) \tag{3.25}$$

However, there were just four degree of freedom in generating reference-currents, i.e. i_p^{*+}, i_q^{*+}, i_p^{*-}, and i_q^{*-} as indicated in (3.19). Thus, the five previously mentioned strategies

suffer from unsatisfactory performances under unbalanced conditions such as high power oscillations or over-loaded/distorted currents. Thus, using four-wire structure and injecting proper zero-sequence currents, extra current control freedoms can be achieved, i.e. i_{Re}^{*0} and i_{Im}^{*0} [45]. Then, the instantaneous active power formula of (3.24) is changed to

$$p = P + \tilde{p}_{s2} + \tilde{p}_{c2} = \left[P + P^{0}\right] + \left[P_{s2} + P_{s2}^{0}\right]\sin(2\omega t) + \left[P_{c2} + P_{c2}^{0}\right]\cos(2\omega t) \tag{3.26}$$

It is worth mentioning that the zero-sequence voltage and current only contribute in the active power. One can use synchronous *dq*-frame in order to write six distinct terms of power with respect to six reference-currents as (3.27) [45]. Due to the lack of enough current control freedom in all five previously mentioned strategies, none of them can provide completely non-oscillatory active and reactive power delivery with sinusoidal current injection. However, by applying the ZSCI strategy and using (3.27), a power converter can easily accomplish non-oscillatory active and reactive powers (i.e. $P_{c2} + P_{c2}^{0} = P_{s2} + P_{s2}^{0} = Q_{c2} = Q_{s2} = 0$) without low-order harmonic content in currents [45].

$$\begin{bmatrix} P + P^{0} \\ P_{c2} + P_{c2}^{0} \\ P_{s2} + P_{s2}^{0} \\ Q \\ Q_{c2} \\ Q_{s2} \end{bmatrix} = \frac{3}{2}\begin{bmatrix} v_d^{+} & v_q^{+} & v_d^{-} & v_q^{-} & v_{\mathrm{Re}}^{0} & v_{\mathrm{Im}}^{0} \\ v_d^{-} & v_q^{-} & v_d^{+} & v_q^{+} & v_{\mathrm{Re}}^{0} & -v_{\mathrm{Im}}^{0} \\ v_q^{-} & -v_d^{-} & -v_q^{+} & v_d^{+} & -v_{\mathrm{Im}}^{0} & -v_{\mathrm{Re}}^{0} \\ v_q^{+} & -v_d^{+} & v_q^{-} & -v_d^{-} & 0 & 0 \\ v_q^{-} & -v_d^{-} & v_q^{+} & -v_d^{+} & 0 & 0 \\ -v_d^{-} & -v_q^{-} & v_d^{+} & v_q^{+} & 0 & 0 \end{bmatrix}\begin{bmatrix} i_d^{+} \\ i_q^{+} \\ i_d^{-} \\ i_q^{-} \\ i_{\mathrm{Re}}^{0} \\ i_{\mathrm{Im}}^{0} \end{bmatrix} \tag{3.27}$$

$$\begin{bmatrix} i_d^{+} \\ i_q^{+} \\ i_d^{-} \\ i_q^{-} \\ i_{\mathrm{Re}}^{0} \\ i_{\mathrm{Im}}^{0} \end{bmatrix} = \frac{2}{3}\begin{bmatrix} (P^{*}v_d^{+})/(v_d^{+} + v_d^{-})^{2} \\ (Q^{*}v_d^{+})/\left[(v_d^{-})^{2} - (v_d^{+})^{2}\right] \\ (P^{*}v_d^{-})/(v_d^{+} + v_d^{-})^{2} \\ -(Q^{*}v_d^{-})/\left[(v_d^{-})^{2} - (v_d^{+})^{2}\right] \\ (2P^{*}v_d^{+}.v_d^{-})/\left[v_{\mathrm{Re}}^{0}.(v_d^{+} + v_d^{-})^{2}\right] \\ (2Q^{*}v_d^{+}.v_d^{-})/\left[v_{\mathrm{Re}}^{0}.((v_d^{-})^{2} - (v_d^{+})^{2})\right] \end{bmatrix} \tag{3.28}$$

3.3 Flexible Voltage Support Control Strategies under Unbalanced Grid Faults

This section introduces another group of control strategies under unbalanced grid faults where the objective is flexible voltage support (FVS). The voltage support under unbalanced faults can be accomplished by either boosting the positive-sequence voltage (V^+) or reducing the negative-sequence voltage (V^-).

3.3.1 Flexible Positive and Negative Sequence Control (FPNSC)

Along with power control strategies under unbalanced grid voltages introduced in 2011 [43] and listed in previous section, Teodorescu et al. propose one flexible voltage support strategy named flexible positive and negative sequence control (FPNSC). In order to generate the reference-currents, the FPNSC strategy defines the positive- and negative-sequence values for conductance, g, and susceptance, b, (i.e. G^+, G^-, B^+, and B^-). Using these values, the active and reactive reference-currents can be calculated as:

$$i_p^* = k_1\, G^+\, v^+ + (1-k_1)\, G^-\, v^- \tag{3.29}$$

$$i_q^* = k_2\, B^+\, v_\perp^+ + (1-k_2)\, B^-\, v_\perp^- \tag{3.30}$$

where G^+, G^-, B^+, and B^- are as follows:

$$G^+ = \frac{P^*}{|\mathrm{v}^+|^2} \quad , \quad G^- = \frac{P^*}{|\mathrm{v}^-|^2}$$
$$B^+ = \frac{Q^*}{|\mathrm{v}^+|^2} \quad , \quad B^- = \frac{Q^*}{|\mathrm{v}^-|^2} \tag{3.31}$$

Using (3.24)-(3.25) and (3.29)-(3.30), the instantaneous active and reactive powers can be achieved as:

$$p = \underbrace{k_1 G^+ v^+.v^+ + (1-k_1) G^- v^-.v^-}_{P} + \underbrace{\left[k_1 G^+ + (1-\mathrm{k}_1) G^-\right] v^+.v^- + \left[k_2 B^+ - (1-\mathrm{k}_2) B^-\right] v_\perp^+.v^-}_{\tilde{p}} \tag{3.32}$$

$$q = \underbrace{k_2 B^+ v^+.v^+ + (1-k_2) B^- v^-.v^-}_{Q} + \underbrace{\left[k_2 B^+ + (1-\mathrm{k}_2) B^-\right] v^+.v^- + \left[-k_1 G^+ + (1-\mathrm{k}_1) G^-\right] v_\perp^+.v^-}_{\tilde{q}} \tag{3.33}$$

The proportion between positive- and negative-sequence current components in both the active and the reactive currents can be flexibly controlled by applying different values of k_1 and k_2 in (3.29)-(3.30). The interaction between the power converter and the grid during faults can be also controlled by this flexible strategy. For example, the positive-sequence reactive current injection ($k_2 \approx 1$) will boost the positive voltage component at the PCC in an inductive line. On the other hand, the negative-sequence reactive current injection ($k_2 \approx 0$) will decrease the negative voltage component in such line.

3.3.2 Flexible Balance of Symmetric Sequences (FBSS)

Another flexible voltage support strategy proposed in the literature is offered by Camacho et al. in 2013 [46] named flexible balance of symmetric sequences (FBSS). As presented earlier, different voltage support objectives can be obtained when the reference reactive currents (in inductive grids) contain a specific amount of both positive- and negative-sequence voltages [43], [46]. Therefore, another possibility for balancing the positive- and negative-sequence components can be obtained with the reactive current references proposed by [46] in the $\alpha\beta$ reference-frame:

$$i_{\alpha(\mathrm{q})}^* = \frac{2}{3} Q^* \frac{k^+ v_\beta^+ + k^- v_\beta^-}{k^+ \left[\left(v_\alpha^+\right)^2 + \left(v_\beta^+\right)^2\right] + k^- \left[\left(v_\alpha^-\right)^2 + \left(v_\beta^-\right)^2\right]} \tag{3.34}$$

$$i^*_{\beta(q)} = \frac{2}{3}Q^* \frac{-k^+ v^+_\alpha - k^- v^-_\alpha}{k^+\left[\left(v^+_\alpha\right)^2 + \left(v^+_\beta\right)^2\right] + k^-\left[\left(v^-_\alpha\right)^2 + \left(v^-_\beta\right)^2\right]} \tag{3.35}$$

where $k+$ and $k-$ are the complementary control parameters to balance the positive- and negative-sequence voltages and the relation "$k^-=1-k^+$" is imposed between them in order to normalize these control parameters. Using (3.34)-(3.35), flexible reactive references are obtained to raise or equalize voltages in an inductive grid. Different settings of control parameter $k+$ result in different voltage support levels. The power control strategies listed in previous section are fixed for different voltage sags and unbalance conditions. However, FBSS strategy is able to balance positive and negative sequences depending on sag conditions. To attain the preferred voltage support, a suitable setting of $k+$ is needed. By tuning $k+$ to be 0, reference-currents will follow negative-sequence voltages and the maximum voltage equalization is achieved at the cost of minimum voltage increment. This strategy is well fitted for unbalanced faults, supplying a significant negative sequence support. On the other hand, by setting $k+$ to be 1, the positive-sequence voltage will be increased leading to an increase in each phase rms voltage while no voltage equalization is obtained. This setting is suitable for three-phase balanced faults with negligible negative-sequence voltage. Between these two settings, a flexible combination of positive- and negative sequence voltages can be adopted with a combination of raising and equalizing objectives. In [46], the conventional strategy for active reference currents is applied in which the reference currents in active component only follow the positive components of the voltage like the BPSC strategy in Eq. (3.10). In inductive grids, the active current injection have negligible effect on the voltage support. However, as it will be discussed in the next part of this section, active current injection has considerable effect on the voltage support in grids with lower X/R ratios. Applying (3.24)-(3.25) in the FBSS strategy, one can write the instantaneous active and reactive power in $\alpha\beta$ frame as follows:

$$p=\underbrace{\frac{3}{2}(v_\alpha^+ i_\alpha^+ + v_\beta^+ i_\beta^+)}_{p^+=P}+\underbrace{\frac{3}{2}(v_\alpha^- i_\alpha^- + v_\beta^- i_\beta^-)}_{p^-=0}+\underbrace{\frac{3}{2}(v_\alpha^- i_\alpha^+ + v_\beta^- i_\beta^+ + v_\alpha^+ i_\alpha^- + v_\beta^+ i_\beta^-)}_{\tilde{p}=n\,P\cos(2\omega t)+\frac{k^+-k^-}{k^++n^2k^-}\,n\,Q\sin(2\omega t)} \tag{3.36}$$

$$q=\underbrace{\frac{3}{2}(-v_\alpha^+ i_\beta^+ + v_\beta^+ i_\alpha^+)}_{q^+=\frac{k^+}{k^++n^2k^-}\,Q}+\underbrace{\frac{3}{2}(-v_\alpha^- i_\beta^- + v_\beta^- i_\alpha^-)}_{q^-=\frac{n^2k^-}{k^++n^2k^-}\,Q}+\underbrace{\frac{3}{2}(-v_\alpha^- i_\beta^+ + v_\beta^- i_\alpha^+ - v_\alpha^+ i_\beta^- + v_\beta^+ i_\alpha^-)}_{\tilde{q}=-n\,P\,sin(2\omega t)+\frac{1}{k^++n^2k^-}\,n\,Q\,cos(2\omega t)} \tag{3.37}$$

where n is defined as "$n=V^-/V^+$".

3.3.3 Modified Flexible Balance of Symmetric Sequences (MFBSS)

One of the biggest drawbacks of FBSS strategy [46] is that it assumes that the grid is totally inductive which is not a true assumption in general. Therefore, [47] has recently proposed a modified version of FBSS strategy (named MFBSS in this Thesis) which takes into account the *X/R* ratios for different grids. [47] simply adds two terms related to the network impedance (i.e. $R/\sqrt{R^2+X^2}$ and $X/\sqrt{R^2+X^2}$) to (3.34)-(3.35). It is worth mentioning that [47] proposes MFBSS formula for the active reference current unlike FBSS [46] which applies the conventional active reference current formula of (3.10).

The active and reactive components of the reference currents in $\alpha\beta$ frame are as follows:

$$i_{\alpha(p)}^*=\frac{2}{3}P^*\frac{k^+v_\alpha^+ + \frac{R}{\sqrt{R^2+X^2}}k^-v_\alpha^-}{k^+\left[\left(v_\alpha^+\right)^2+\left(v_\beta^+\right)^2\right]+\frac{R}{\sqrt{R^2+X^2}}k^-\left[\left(v_\alpha^-\right)^2+\left(v_\beta^-\right)^2\right]} \tag{3.38}$$

$$i^{*}_{\beta\,(p)} = \frac{2}{3}P^{*}\frac{k^{+}v^{+}_{\beta} + \dfrac{R}{\sqrt{R^{2}+X^{2}}}k^{-}v^{-}_{\beta}}{k^{+}\left[\left(v^{+}_{\alpha}\right)^{2}+\left(v^{+}_{\beta}\right)^{2}\right]+\dfrac{R}{\sqrt{R^{2}+X^{2}}}k^{-}\left[\left(v^{-}_{\alpha}\right)^{2}+\left(v^{-}_{\beta}\right)^{2}\right]} \tag{3.39}$$

$$i^{*}_{\alpha\,(q)} = \frac{2}{3}Q^{*}\frac{k^{+}v^{+}_{\beta} + \dfrac{X}{\sqrt{R^{2}+X^{2}}}k^{-}v^{-}_{\beta}}{k^{+}\left[\left(v^{+}_{\alpha}\right)^{2}+\left(v^{+}_{\beta}\right)^{2}\right]+\dfrac{X}{\sqrt{R^{2}+X^{2}}}k^{-}\left[\left(v^{-}_{\alpha}\right)^{2}+\left(v^{-}_{\beta}\right)^{2}\right]} \tag{3.40}$$

$$i^{*}_{\beta\,(q)} = \frac{2}{3}Q^{*}\frac{-\,k^{+}v^{+}_{\alpha} - \dfrac{X}{\sqrt{R^{2}+X^{2}}}k^{-}v^{-}_{\alpha}}{k^{+}\left[\left(v^{+}_{\alpha}\right)^{2}+\left(v^{+}_{\beta}\right)^{2}\right]+\dfrac{X}{\sqrt{R^{2}+X^{2}}}k^{-}\left[\left(v^{-}_{\alpha}\right)^{2}+\left(v^{-}_{\beta}\right)^{2}\right]} \tag{3.41}$$

Using reference currents of (3.38)-(3.41) and performing mathematical calculations, one can obtain the instantaneous active and reactive powers as:

$$\begin{aligned} p = P^{*} + P^{*}\left\{\frac{k^{+}+k^{-}\dfrac{R}{\sqrt{R^{2}+X^{2}}}}{k^{+}+\dfrac{R}{\sqrt{R^{2}+X^{2}}}k^{-}\,n^{2}}\right\}n\times\cos(2\omega t) + \\ + Q^{*}\left\{\frac{k^{+}-k^{-}\dfrac{X}{\sqrt{R^{2}+X^{2}}}}{k^{+}+\dfrac{X}{\sqrt{R^{2}+X^{2}}}k^{-}n^{2}}\right\}n\times\sin(2\omega t) \end{aligned} \tag{3.42}$$

$$\begin{aligned} q = Q^{*} + Q^{*}\left\{\frac{k^{+}+k^{-}\dfrac{X}{\sqrt{R^{2}+X^{2}}}}{k^{+}+\dfrac{X}{\sqrt{R^{2}+X^{2}}}k^{-}\,n^{2}}\right\}n\times\cos(2\omega t) + \\ + P^{*}\left\{\frac{-k^{+}+k^{-}\dfrac{R}{\sqrt{R^{2}+X^{2}}}}{k^{+}+\dfrac{R}{\sqrt{R^{2}+X^{2}}}k^{-}n^{2}}\right\}n\times\sin(2\omega t) \end{aligned} \tag{3.43}$$

3.4 Simulation Results

Fig. 3.1 illustrates the block diagram of a grid-connected 1.0 MVA inverter where the gird voltage becomes deteriorated as indicated in Fig. 3.2. V^+ and V^- are calculated with MCCF-PLL (A detailed discussion of MCCF-PLL is provided in [150]). In order to ride through temporary faults, inverter should withstand during the fault and inject power into the grid. A dc power supply is used to emulate the renewable energy resources and storage in the dc link [151] which is widely used in most of the studies related to LVRT techniques [43]-[47]. It is assumed that a type B fault (A-to-G) [75] occurs with significant voltage dip. The typical system of Fig 1 is the fundamental test system which has been widely used in evaluation and assessment of different LVRT-RCG strategies in the literature [43]-[53]. System parameters are listed in Table 3.1.

3.4.1 Uninterrupted Power Delivery Control Strategies

This section presents the performance of each UPD strategy under grid fault in the HV grid, where the line impedance is mainly inductive. A single-phase-to-ground fault is emulated between 0.3s and 0.4s. The proportional resonant (PR) control is used in the $\alpha\beta$ reference frame for the converter current regulation which is studied in details in [43].

TABLE 3.1. Test system parameters

Z_L (Ω)	$j\omega\times(90\times10^{-6})$	Q^* (MVAR)	0
Z_g (mΩ)	1	V_{DC} (V)	2000
Z_f (mΩ)	1	$V_{L\text{-}L,\,RMS}$ (V)	690
P^* (MW)	1	f (Hz)	60

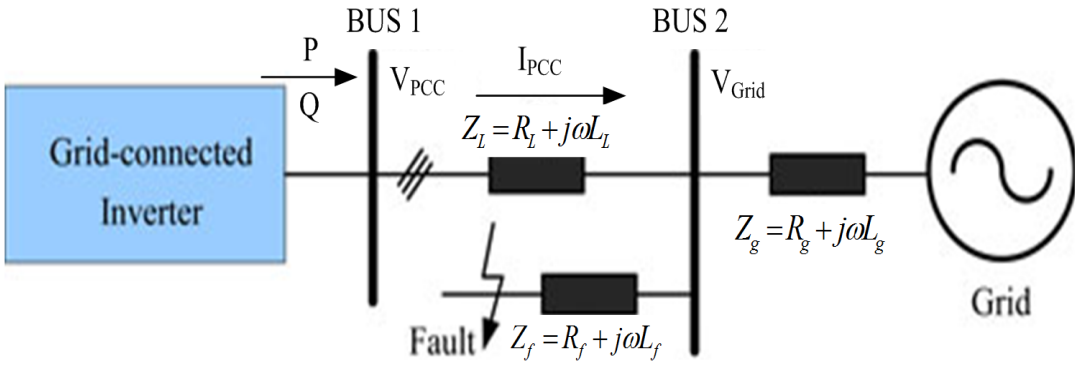

Fig. 3.1. Block diagram of grid-connected inverter.

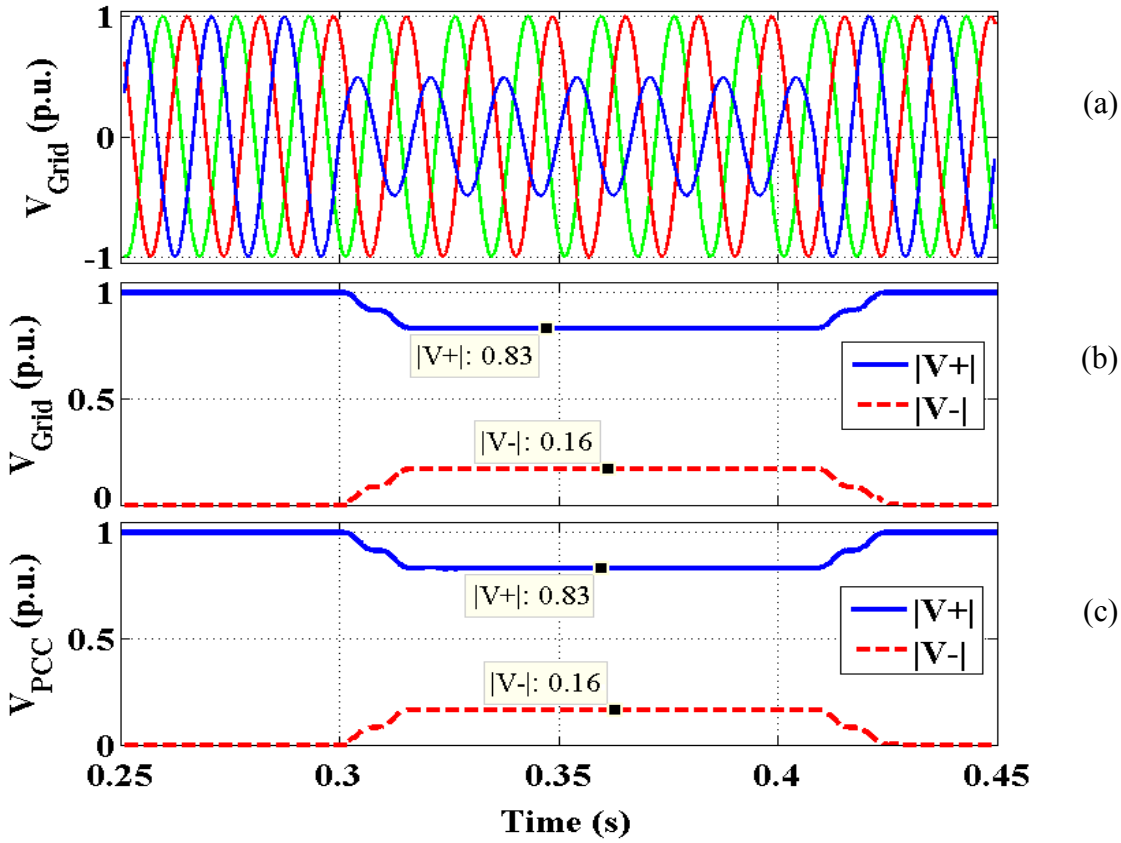

Fig. 3.2. Emulated fault: (a) voltage waveforms of the grid, (b) positive- and negative- sequences of the grid voltage, and (c) positive- and negative- sequences of the PCC voltage.

Simulation results of IARC strategy are shown in Fig. 3.3. In Fig. 3.3(a), the generated currents by IARC strategy are shown. As it is illustrated in Fig. 3.3(a), the currents are non-sinusoidal and unbalanced in agreement with the explanations of Section 3.2.1 and

(3.5). Since the effect of the injected currents on PCC voltage is also of interest in this particular example, the short-circuit power of the PCC is not assumed to be much higher than the reactive power injected by the inverter. Therefore, the PCC voltage is practically deteriorated by the injected harmonic currents as (as Fig. 3.3(b) shows). The instantaneous active and reactive powers are depicted in Fig. 3.3(c). Since the currents are not sinusoidal, the current control fails to perfectly track reference-currents.

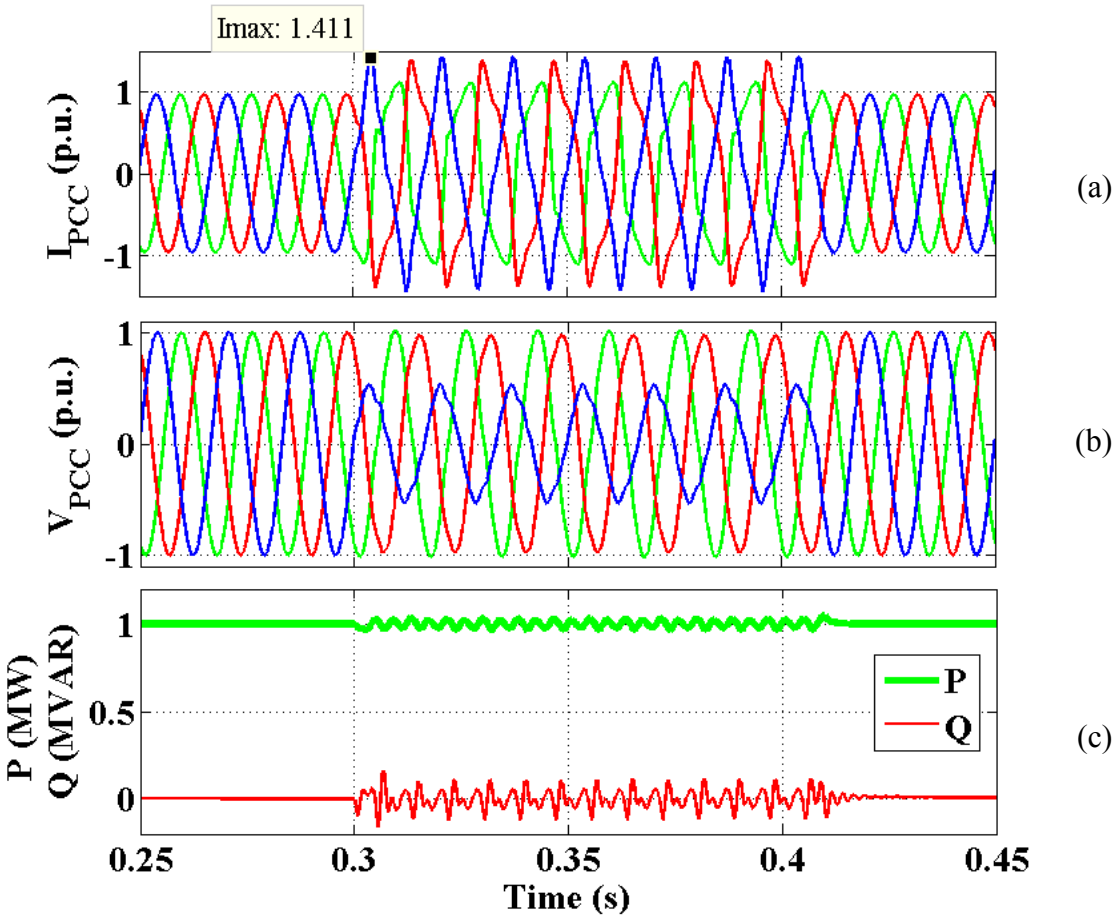

Fig. 3.3. Simulation results of IARC strategy: (a) currents injected by the inverter, (b) PCC voltage, and (c) instantaneous active and reactive powers delivered by the inverter.

Therefore, small oscillations on active and reactive powers are realistically unavoidable. Another negative point worth mentioning is high currents generated by IARC strategy (see Fig. 3.3(a)) which may cause overcurrent relays tripping. The simulation results of AARC strategy are demonstrated in Fig. 3.4. As it is indicated in Fig. 3.4(a), the currents are sinusoidal but unbalanced in agreement with the Section 3.2.2 and

(3.6). Since the injected currents do not contain harmonics, the PCC voltage remains sinusoidal as it is depicted in Fig. 3.4(b). The active/reactive powers are depicted in Fig. 3.4(c). According to (3.8) and (3.9), when Q is zero, the oscillation at 2ω appears only in the active power, and does not appear in the reactive power.

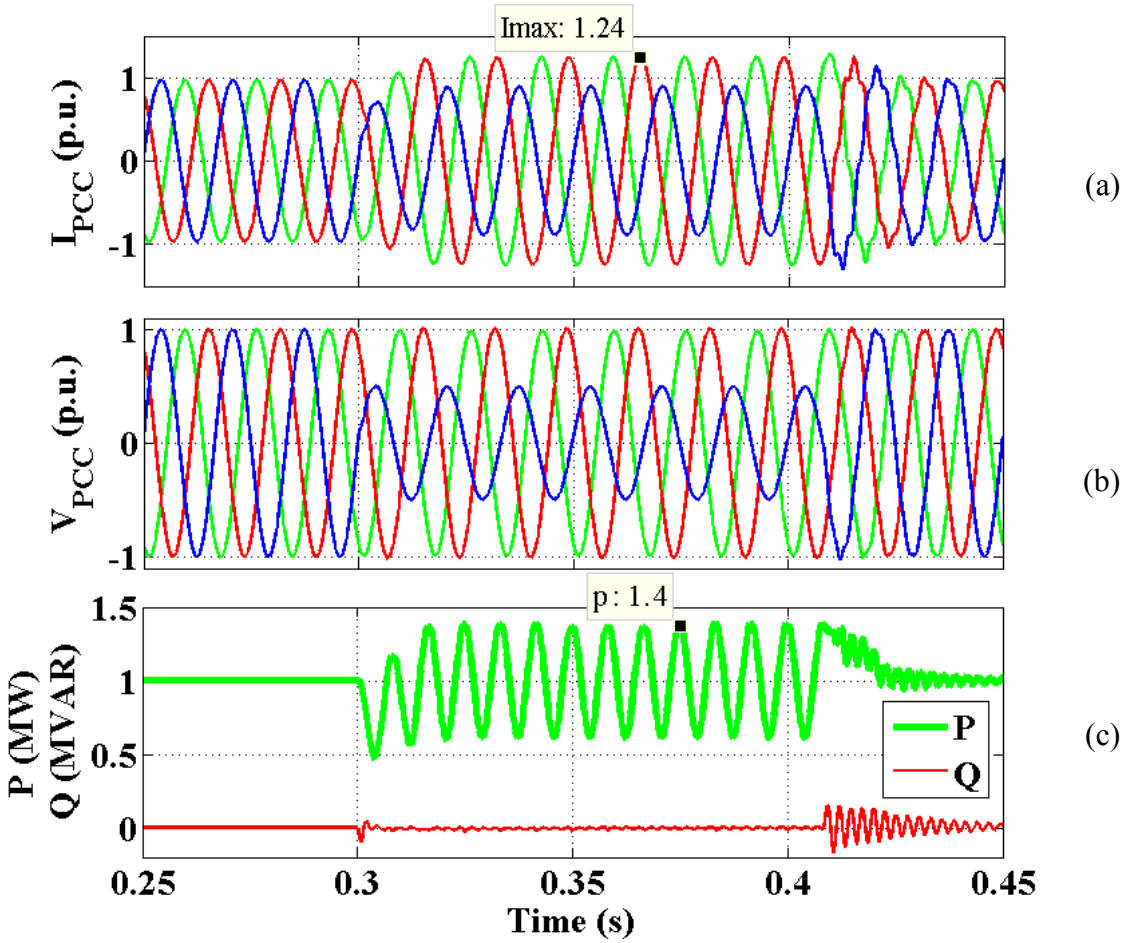

Fig. 3.4. Simulation results of AARC strategy: (a) currents injected by the inverter, (b) PCC voltage, and (c) instantaneous active and reactive powers delivered by the inverter.

The simulation results of the BPSC are illustrated in Fig. 3.5. As Fig. 3.5(a) shows, the currents are sinusoidal and balanced with relatively lower magnitudes under the fault which is an important advantage of this strategy as discussed in Section 3.2.3. The active/reactive powers are depicted in Fig. 3.5(b). According to (3.12) and (3.13), even if one of P or Q is non-zero, both instantaneous active and reactive powers will contain the oscillation at 2ω.

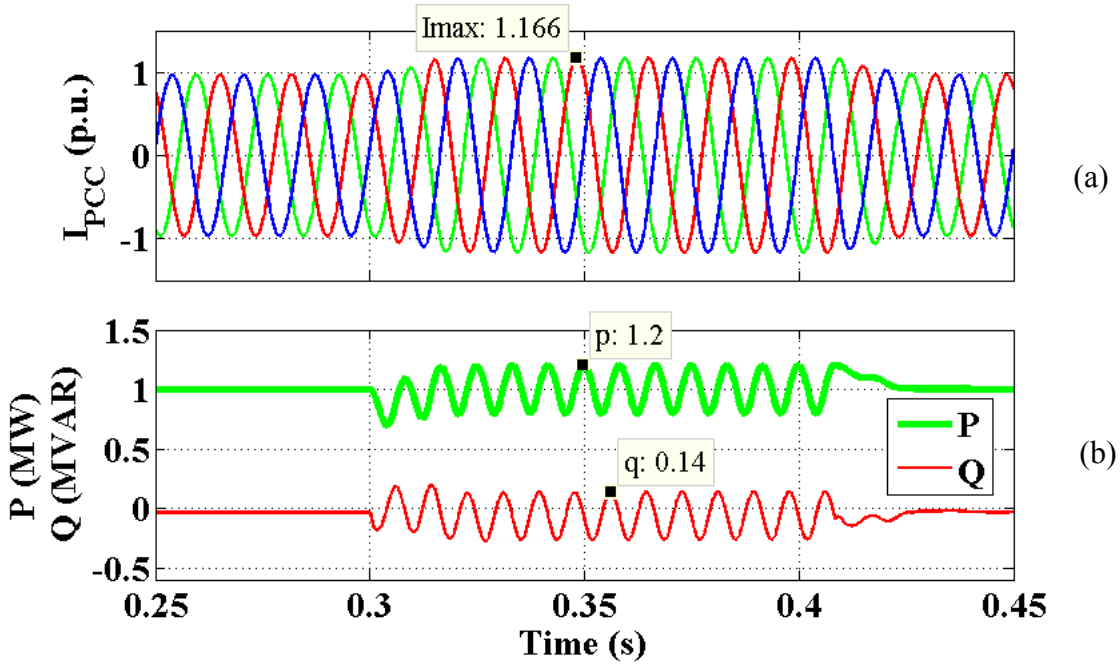

Fig. 3.5. Simulation results of BPSC strategy: (a) currents injected by the inverter, and (b) instantaneous active and reactive powers delivered by the inverter.

Fig. 3.6 demonstrates the simulation results of the ICPS. As it is indicated in Fig. 3.6(a), the currents are non-sinusoidal and unbalanced with a high magnitude in the faulted phase as explained in Section 3.2.4, which is a drawback of this strategy. The active/reactive powers are shown in Fig. 3.6(b). According to (3.17), when P is zero, then the instantaneous active power is non-oscillatory. The simulation results of the PNSC are shown in Fig. 3.7. As it is depicted in Fig. 3.7(a), the currents are sinusoidal but unbalanced with almost high magnitude in the faulted phase. The active/reactive powers are illustrated in Fig. 3.7(b). According to (3.20)-(3.21), when P is non-zero and Q is zero, the oscillation at 2ω only appears in the reactive power. Fig. 3.8 shows the simulation results of the ZSCI. As Fig. 3.8(a) demonstrates, the currents are sinusoidal but unbalanced with considerably high currents and high zero-sequence component. Using the proper zero-sequence current injection, the constant instantaneous active/reactive power (shown in Fig. 3.8(c)) can be achieved without harmonics in the currents unlike the IARC strategy.

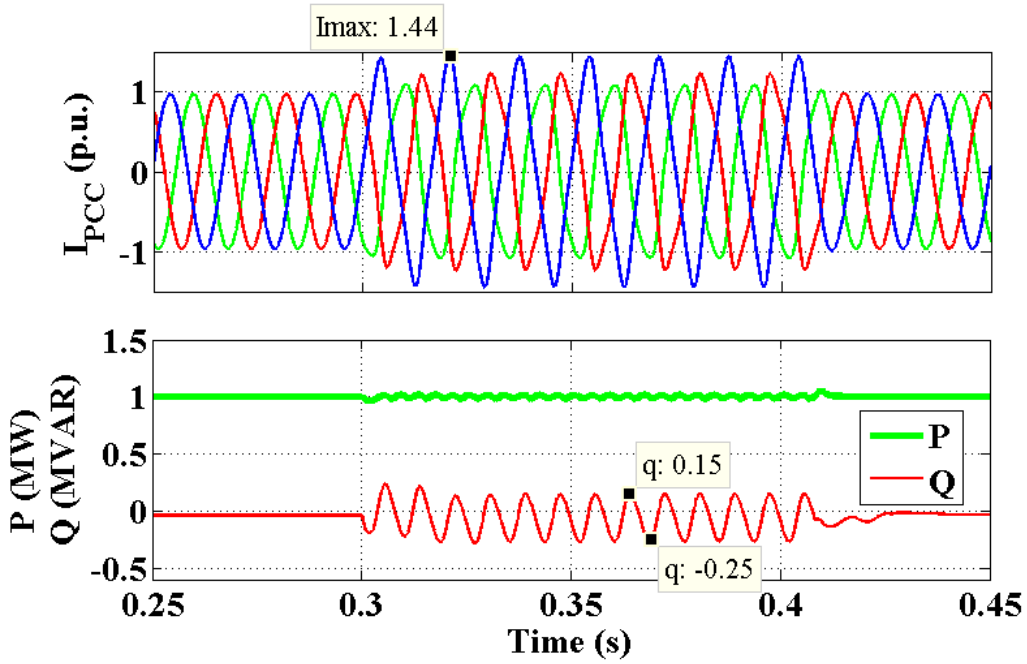

Fig. 3.6. Simulation results of ICPS strategy: (a) currents injected by the inverter, and (b) instantaneous active and reactive powers delivered by the inverter.

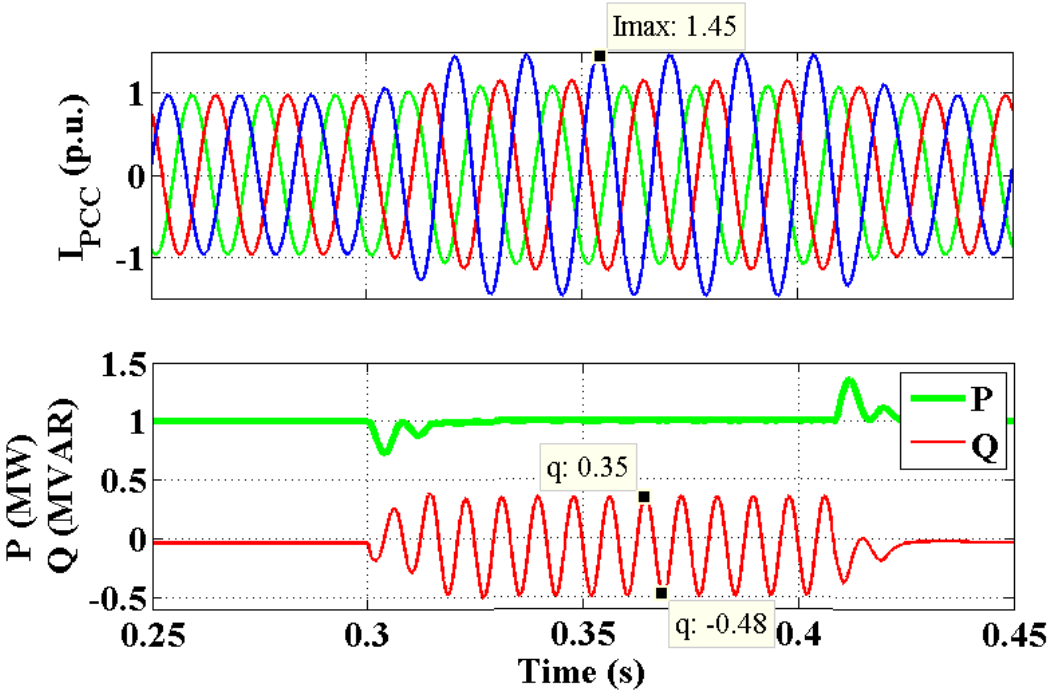

Fig. 3.7. Simulation results of PNSC strategy: (a) currents injected by the inverter, and (b) instantaneous active and reactive powers delivered by the inverter.

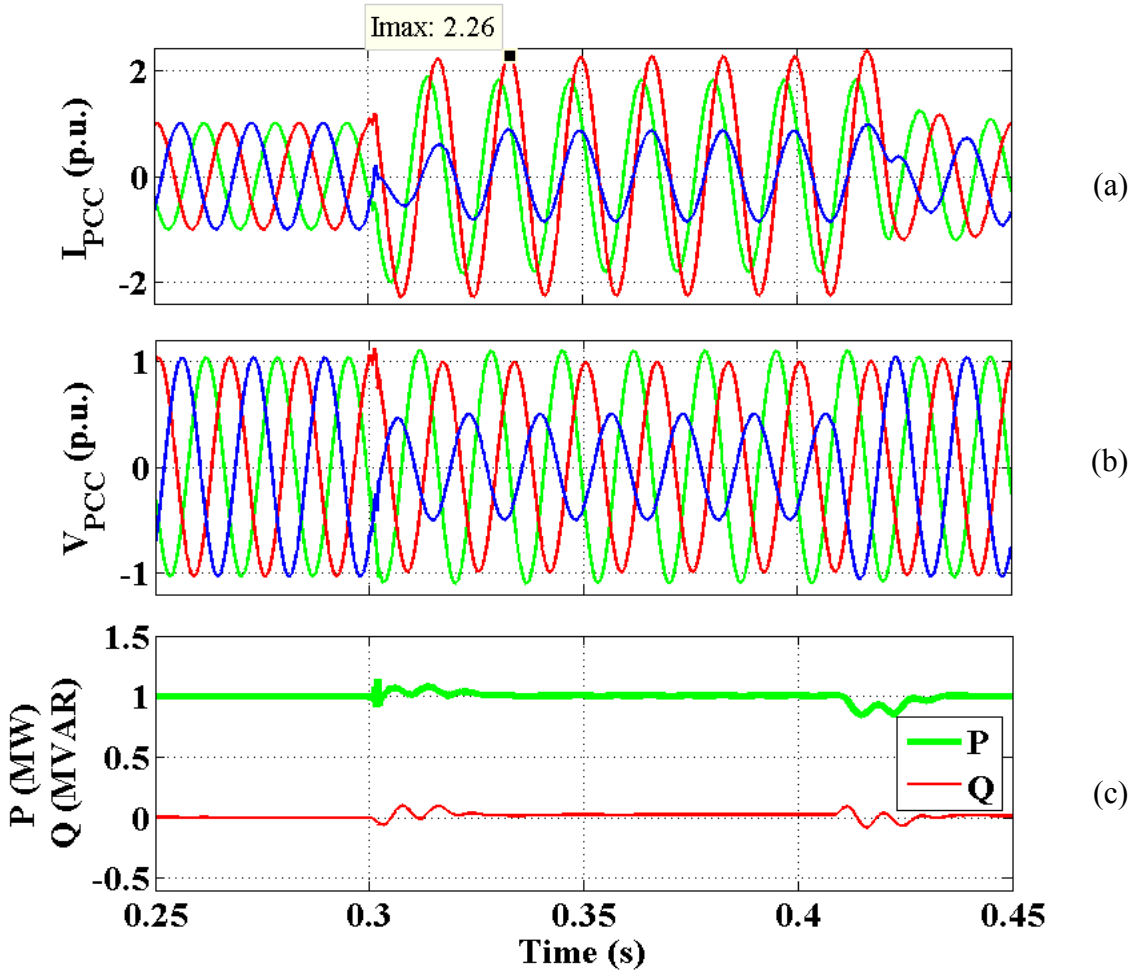

Fig. 3.8. Simulation results of ZSCI strategy: (a) currents injected by the inverter, (b) PCC voltage, and (c) instantaneous active and reactive powers delivered by the inverter.

Table 3.2 illustrates important characteristics of each of the UPD strategies e.g. oscillation amount on instantaneous powers, maximum current magnitudes, etc. In this test case, the ZSCI and IARC have the best performance from the point of view of non-oscillatory instantaneous active/reactive powers. In addition, the ICPS and BPSC have relatively good performances, since they yield less oscillation in the instantaneous powers. However, the AARC has the worst performance from the perspective of instantaneous power, since the oscillation on each power component depends on the average value of the same component. So, one cannot mitigate the oscillation on active power by setting the reactive power to zero. From the perspective of lower current amplitudes, the BPSC strategy is the best, and the ZSCI strategy is the worst according

to Table 3.2. IARC and ICPS have non-sinusoidal harmonic current injection which is a major drawback. Table 3.2 indicates their THD values in this test case. All in all, the BPSC seems to be the best strategy, since it has relatively lower oscillations on powers and lower current magnitudes, along with the sinusoidal and balanced currents. These features simplify the controller implementation.

TABLE 3.2. Characteristics of each UPD strategies in the simulated test case

	$\tilde{p}_{\max}$	$\tilde{q}_{\max}$	I_{max}	THD	sinusoidal	Balanced
IARC			1.41	21%		
AARC	0.4		1.24		✓	
BPSC	0.2	0.2	1.17		✓	✓
ICPS		0.2	1.44	10%		
PNSC		0.4	1.45		✓	
ZSCI			2.26		✓	

3.4.2 Flexible Voltage Support Control Strategies

This section presents the performance of each FVS reference-current generator strategy under a grid fault, where the line impedance includes both resistance and inductance. A type-B fault [75] (phase A to ground) is emulated from $t_0 = 0.2$ s, and V_{Grid} becomes deteriorated as shown in Fig. 3.9.

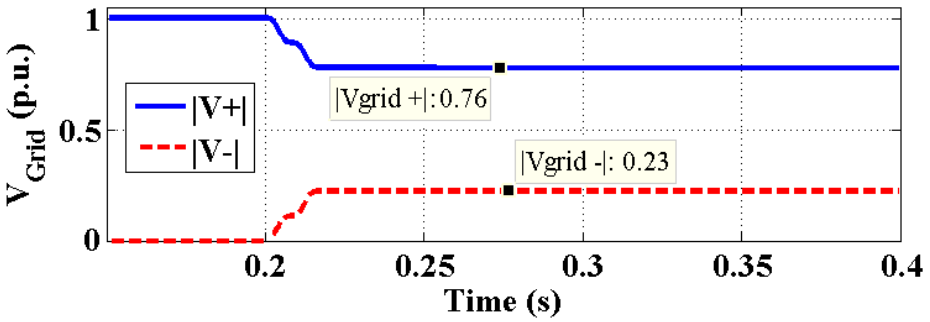

Fig. 3.9. Positive- and negative- sequences of the grid voltage under the fault

The simulation results of FPNSC are shown in Fig. 3.10. After t_1= 0.25s, P goes to zero and Q is configured to either boost V^+ or decrease V^-. Reference [43] presents an analytical approach to find the maximum current value, I_{max}, in each phase based on the delivered P and Q, k_1, k_2, and voltage dip. Therefore, I_{max} limitation can be applied in the process of reference-current generation which enables calculation of the maximum allowable Q. For example, 1.5p.u. is set as I_{max} limitation (shown in Fig. 3.10(c)) in the test case of the FPNSC strategy which leads to limit the average value of the reference reactive power as shown in Fig. 3.10(d). In the simulation study of the FPNSC strategy, three cases with three k_2 values in (3.30) are simulated and studied. The first value of k_2 is set to 0.9 between t_1 and t_2= 0.3s in order to inject mostly the positive reference-currents. Due to the positive current injection between t_1 and t_2, V^+ is boosted from 0.76p.u. to 0.9 p.u. as shown in Fig. 3.10(a) and Fig. 3.10(b). The second value of k_2 is 0.5, between t_2 and t_3= 0.35s, in order to inject both positive- and negative-sequence currents. As a result, V^+ is increased to 0.79p.u. and V^- is simultaneously decreased to 0.04p.u. Finally, k_2 is set to be 0.1 between t_3 and t_4= 0.4s, which leads to inject mostly the negative sequence currents. Therefore, V^- is decreased from 0.23p.u. to 0.03p.u. as shown in Fig. 3.10(a). The active/reactive powers are depicted in Fig. 3.10(d). According to (3.32) and (3.33), both active and reactive powers contain the oscillation at 2ω.

The simulation results of the FBSS are shown in Fig. 3.11. After t_1, P goes to zero and the reactive power is enabled to flexibly support the PCC voltage. The value of k^+ in (3.34) and (3.35) is set to 0.9 between t_1 and t_2 to generate mostly the positive currents. Due to the dominant positive current injection, V^+ is boosted from 0.76p.u. to 0.92p.u. as shown in Fig. 3.11(a) and Fig. 3.11(b). Between t_2 and t_3, k^+ is 0.5 which leads to inject half-negative and half-positive currents. Therefore, V^- is decreased from 0.23p.u. to 0.19p.u in addition to V^+ boost from 0.76p.u. to 0.91p.u. Between t_3 and t_4, k^+ is set to 0.1 to inject mostly negative-sequence currents. As a result, V^- is considerably decreased to 0.09p.u. Although, the portion of the positive current (and k^+) in the last case (i.e. k^+=0.1) is lower than the second case (i.e. k^+=0.5), V^+ value is still boosted to the same value (0.91p.u).

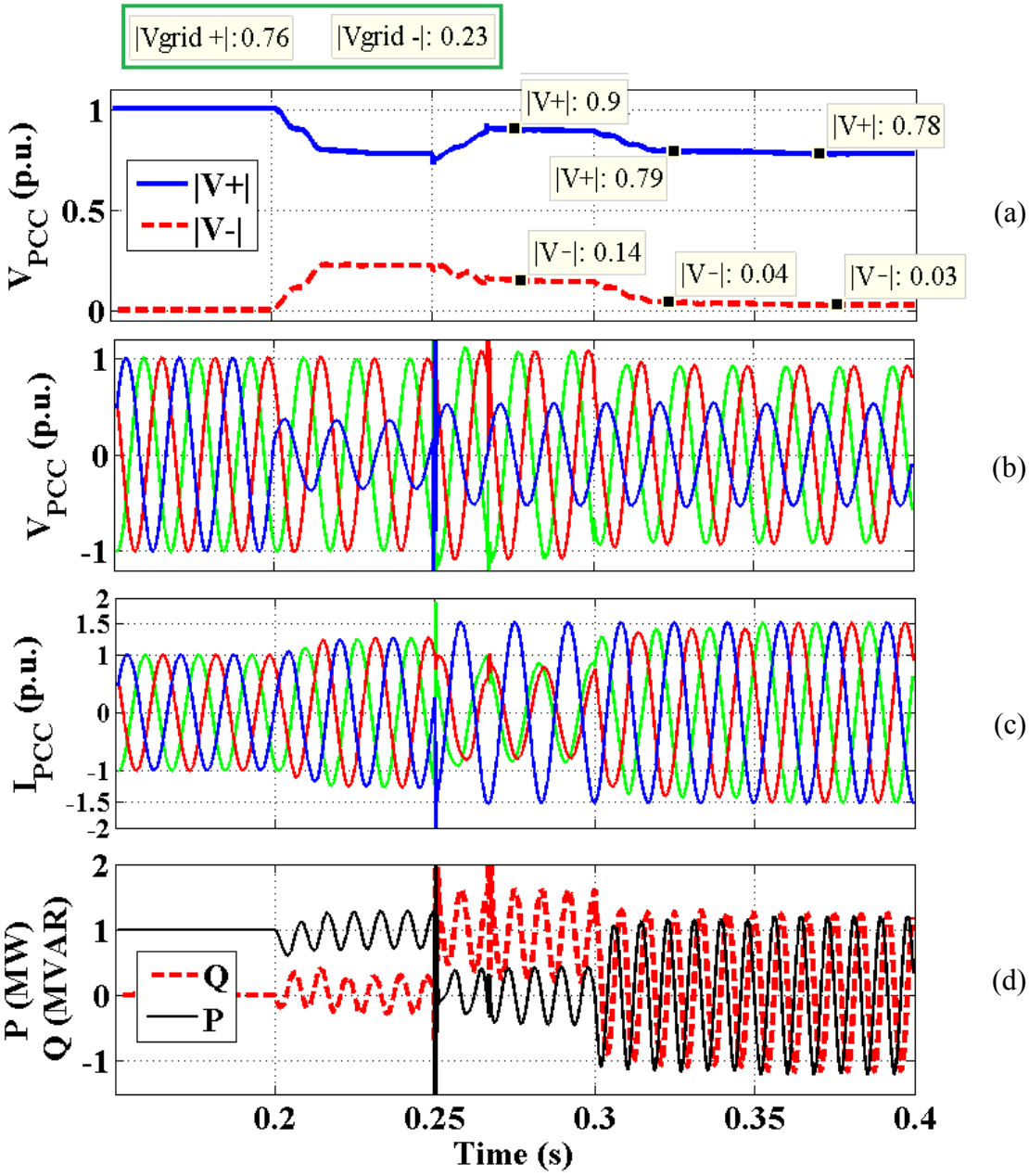

Fig. 3.10. Simulation results of FPNSC strategy: (a) positive and negative sequences of the PCC voltage, (b) currents injected by the inverter, (c) PCC voltage, and (d) instantaneous active and reactive powers delivered by the inverter.

This high V^+ boost and high V^- drop in the last case is at the cost of higher I_{max} in the faulted phase as it is seen between t_3 and t_4 in Fig. 3.11(c). The active/reactive powers are depicted in Fig. 3.11(d). According to (3.36), when P is zero and k^+ is 0.5, the active

power is constant and non-oscillatory as it is seen in Fig. 3.11(d) between t_2 and t_3. This can be a useful criteria to select proper k^+ values.

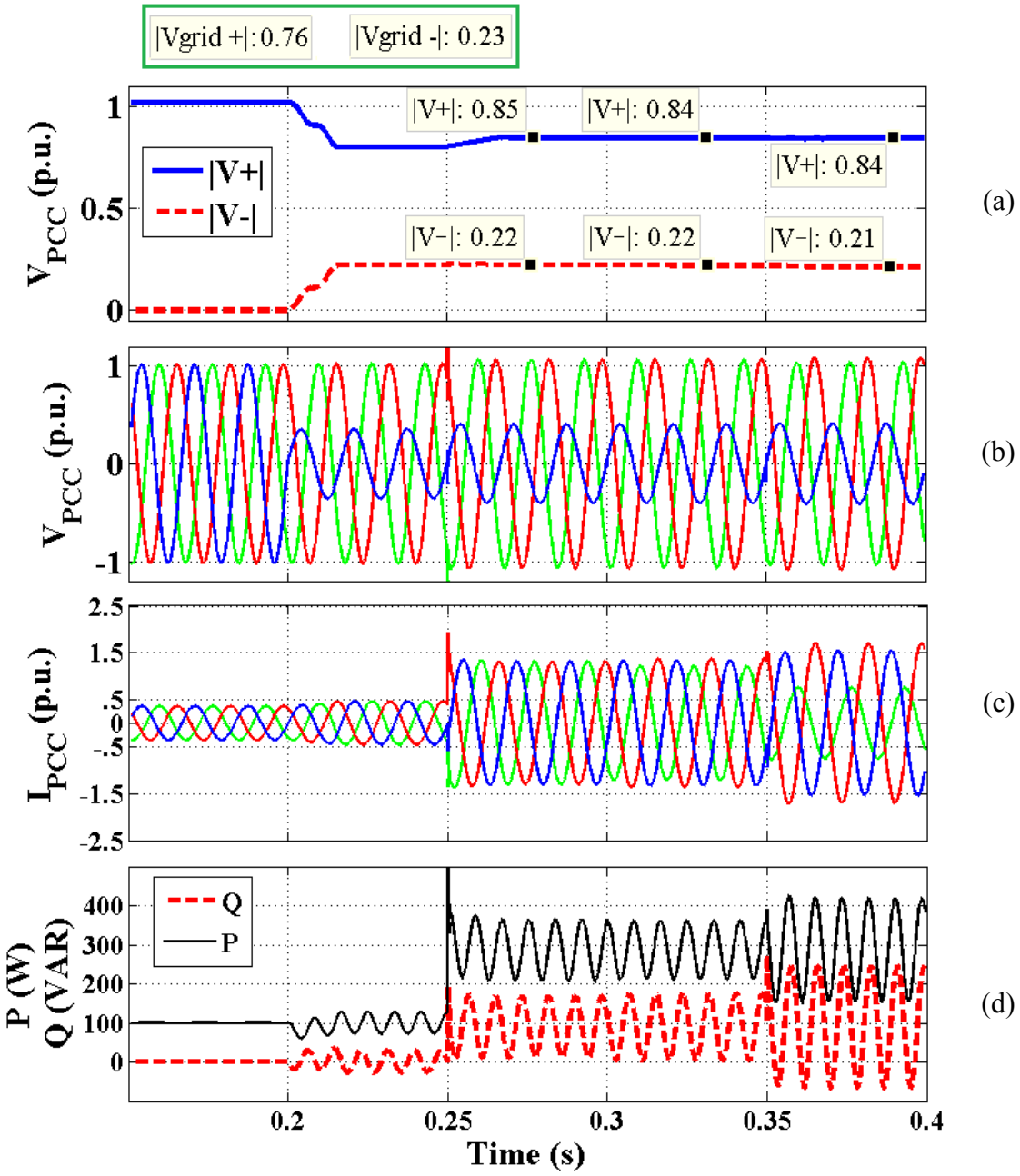

Fig. 3.11. Simulation results of FBSS strategy: (a) positive and negative sequences of the PCC voltage, (b) currents injected by the inverter, (c) PCC voltage, and (d) instantaneous active and reactive powers delivered by the inverter.

For the comparison between the performance of the FBSS and MFBSS in the case of a resistive line impedance, a test case in a LV grid is implemented with the same faulted

voltage values (i.e. V^+ is 0.76p.u. and V^- is 0.23p.u.). The resistance of the line is 1Ω and the inductance is 0.8 mH ($X/R \approx 0.3$ which is low). Therefore, for a flexible voltage support, P should be mostly delivered to the grid instead of Q. In both strategies, after t_1, 300MVA apparent power is available. The reference active/reactive powers in both strategies under the fault can be reasonably calculated as:

$$P^* = \left(R \Big/ \sqrt{R^2 + X^2} \right) \times S = 287\,W \tag{3.44}$$

$$Q^* = \left(X \Big/ \sqrt{R^2 + X^2} \right) \times S = 87\,VAR \tag{3.45}$$

The simulation results of FBSS and MFBSS are shown in Fig. 3.12 and Fig. 3.13, respectively. The value of k^+ in (3.34)-(3.35) (for FBSS) and in (3.38)-(3.41) (for MFBSS) is set to 0.9 between t_1 and t_2. Due to the positive-sequence current injection, V^+ is boosted from 0.76 p.u. to 0.85 p.u. in both strategies as shown in Fig. 3.12(a) and Fig. 3.13(a). The performance of both strategies is similar for high k^+ values. However, for k^+=0.5 (between t_2 and t_3), V^- is decreased to 0.22p.u. and 0.20p.u. in the FBSS and MFBSS, respectively. In addition, for k^+=0.1(between t_3 and t_4), V^- is decreased to 0.21 p.u. and 0.13p.u. in the

FBSS and MFBSS strategies, respectively. Therefore, one can conclude that in the grids with lower X/R ratios, the FBSS loses its flexibility to support the grid and fails to reduce V^- and unbalances. So, in resistive grids, the FBSS strategy with any k^+ value will result in the same V^+ boost and the negligible reduction in V^-. However, the MFBSS strategy is capable of flexibly support the voltage with different k^+ values even in different X/R ratios. The instantaneous active/reactive powers in the FBSS and MFBSS strategies are respectively depicted in Fig. 3.12(d) and Fig. 3.13(d).

Table 3.3 and Table 3.4 summarize the pros and cons of each reference-current generation strategy. Studying and analyzing Tables 3.2 and 3.3, and taking the simulation results into account, it can be generally concluded that the BPSC strategy [43] is the best strategy in the first group due to its considerable advantages such as low current

amplitudes, sinusoidal and balanced currents, and low power oscillations. Furthermore, the AARC [44] and ZSCI [45] strategies are good candidates in the first group despite their own drawbacks. For example, the AARC strategy causes low-amplitude and sinusoidal currents, but it results in high oscillations on the active power.

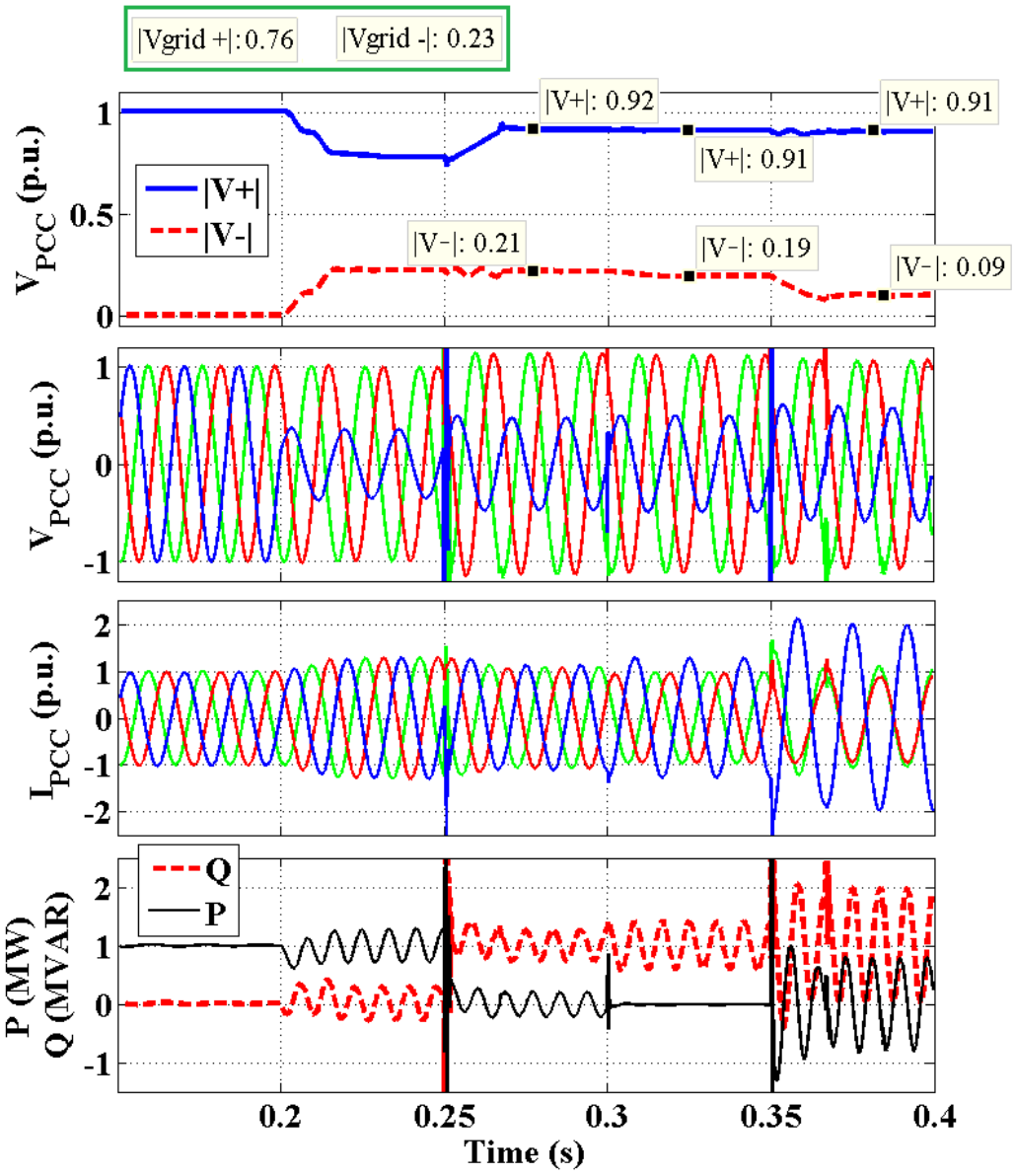

Fig. 3.12. Simulation results of FBSS strategy: (a) positive and negative sequences of the PCC voltage, (b) currents injected by the inverter, (c) PCC voltage, and (d) instantaneous active and reactive powers delivered by the inverter.

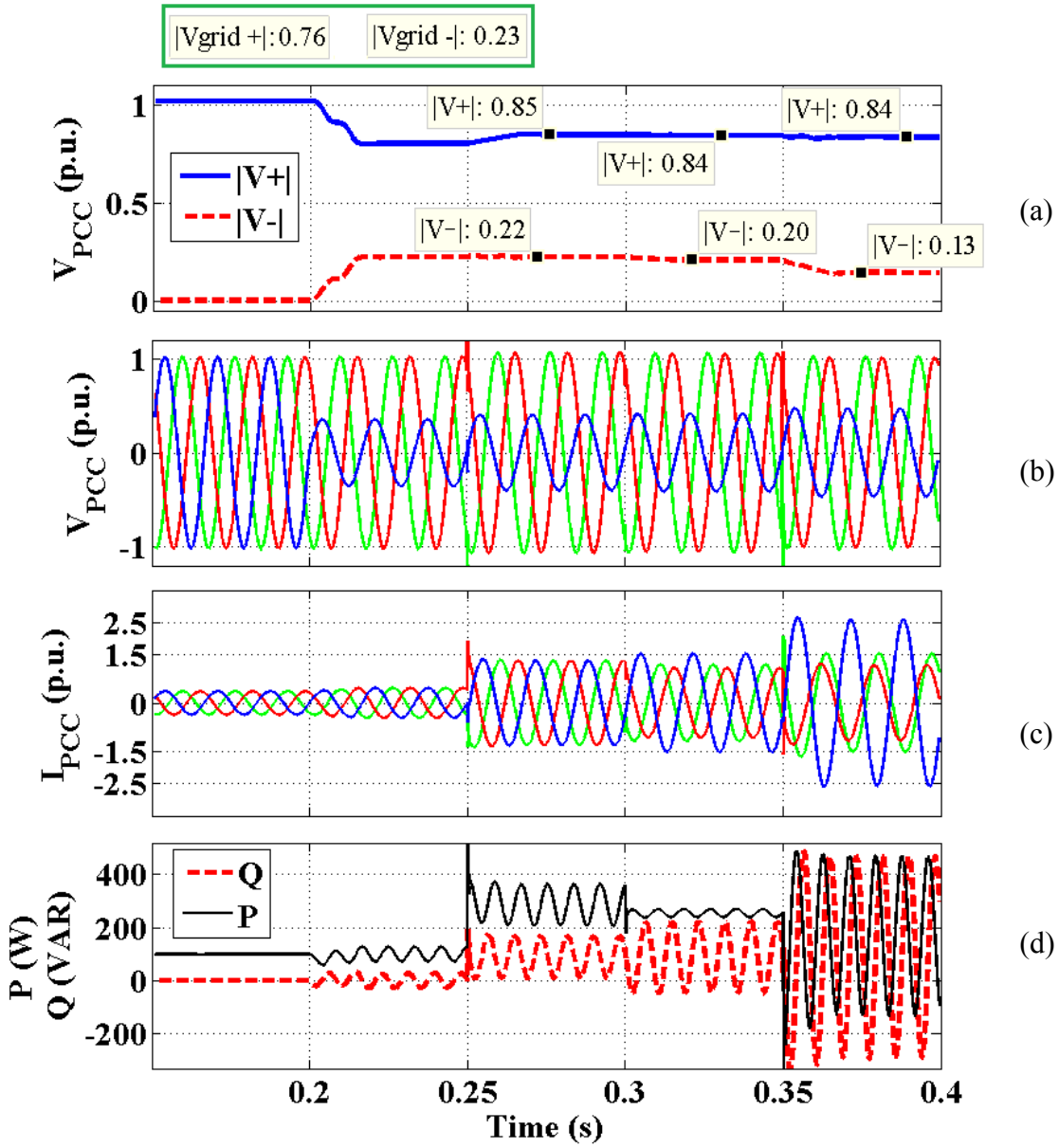

Fig. 3.13. Simulation results of MFBSS strategy: (a) positive and negative sequences of the PCC voltage, (b) currents injected by the inverter, (c) PCC voltage, and (d) instantaneous active and reactive powers delivered by the inverter.

Also, the ZSCI is very advantageous from the point of view of yielding constant instantaneous active and reactive power and simultaneously having sinusoidal currents. However, the high current amplitudes in the ZSCI strategy is its worst drawback. Finally, the ICPS strategy seems to be the worst strategy due to its listed drawbacks.

TABLE 3.3. Advantages and disadvantages of each reference current generation strategy

		Advantages	Disadvantages
UPD reference current generation strategies	IARC	- Instantaneously constant active and reactive powers. - Simple DC link controller.	- Harmonic currents. - PCC voltage harmonics. - Unbalanced currents. - High current amplitudes. - Complicated current controllers.
	AARC	- Sinusoidal currents.	- Power oscillations. - Oscillations in active power depends on the average value of active power itself. It is not desired; since, it cause ripple in the DC link.
	BPSC	- Sinusoidal and balanced currents. - Simple synchronous current controllers can be used. - Low current amplitudes. - Lower oscillations on each power component (although, oscillations exist on both active and reactive powers).	- Oscillations on both active and reactive powers even when one of them is zero.
	ICPS	- Lower power oscillation. - Oscillation on the active power depends on the average value of the reactive power. So, one can mitigate active power oscillation by zero reactive power injection.	- Harmonic currents. - PCC voltage harmonics. - Unbalanced currents. - High current amplitudes. - Complicated current controllers. - Power oscillations.
	PNSC	- Sinusoidal currents. - Oscillation on the active power depends on the average value of the reactive power. So, one can mitigate active power oscillation by zero reactive power injection.	- Power oscillations. - High current amplitude in the faulted phase.
	ZSCI	- Sinusoidal non-harmonic currents. - Instantaneously constant active and reactive powers. - Simple DC link controller.	- Unbalanced currents. - High current amplitudes. - It needs 4-wire or 6-wire structures.

Strategies of the second group have almost similar performances, summarized in Table IV. However, the FPNSC strategy [43] seems to be the best, due to its better flexibility and controlled current limitations. Finally, one can easily conclude that the strategies of the second group [43], [46]-[47] are generally better than the first one from the grid support perspective, and they are more useful for future grid requirements.

TABLE 3.4. Advantages and disadvantages of each reference current generation strategy

FVS reference current generation strategies	FPNSC	- Flexibly support the voltage: either by boosting the positive sequence or reducing the negative sequence. - Controlled current amplitudes. - More controlling parameters and more flexibility.	- Power oscillations.
	FBSS	- Flexibly support the voltage: either by boosting the positive sequence or reducing the negative sequence. - Controlled current amplitudes.	- Only flexible in the grids with high X/R ratio. - Power oscillations.
	MFBSS	- Flexibly support the voltage: either by boosting the positive sequence or reducing the negative sequence. - Applicable in the grids with any X/R ratio	- Power oscillations.

3.5 Conclusion

This chapter compares the performance of reference-current generating strategies for LVRT in converter-based DER units. These strategies aim to provide a proper set of reference-currents under different faults, low voltage and unbalanced voltage conditions. This chapter categorizes these strategies into two main groups. The first group aims to deliver the required active and reactive powers with a suitable performance under different faults or voltage sag conditions. On the other hand, strategies in the second group target to not only stand under faults (and deliver the power), but also support the grid

voltage by injecting a proper set of active and reactive currents. This chapter studied these strategies by analytical calculations, simulations and comparisons. Pros and cons of each strategy were addressed and summarized in Table 3.3 and Table 3.4. This chapter can be helpful to find appropriate LVRT strategies, solve their existing drawbacks, combine their individual capabilities and strengths, and propose other innovative and more enhanced LVRT strategies.

Chapter 4

Mathematical Assessment, Performance Evaluation, and MARPD Method I: UPD-LVRT-RCG Techniques

4.1 Introduction

A comparative study was conducted in Chapter 3 in order to collect all well-known and newly introduced LVRT-RCG strategies in gird connected CI-DER units [43]-[47], analyze them, compare their performances, and introduce their pros and cons under various conditions. These strategies have been categorized into two main groups. The first group of method (six LVRT-RCG strategies introduced by [43]-[45]) aims to control power under unbalanced grid conditions; while, the second group (three LVRT-RCG strategies proposed by [43], [46] and [47]) targets to not only control the power; but also, flexibly support the voltage under the grid faults.

This chapter presents the analytical evaluations and mathematical assessments of strategies of the first group, introduced in section 3.2 and named as UPD-LVRT-RCG strategies. These six strategies are studied, simulated and generally compared in the previous chapter. They aim to provide a proper set of reference-currents under different

faults, low voltage and unbalanced voltage conditions. In terms of practical applications of LVRT-RCG strategies, their thorough analytical evaluation and precise mathematical assessment are extremely necessary. This chapter introduces three most important terms for comprehensive analytical evaluations and reasonable comparisons of available LVRT-RCG techniques. Oscillation values on instantaneous active/reactive powers ($\tilde{p}$ and $\tilde{q}$, respectively) and the maximum phase currents (I_{max}) are three most important terms of each LVRT-RCG strategy. Afterward, the maximum allowable reactive power delivery is proposed. The maximum allowable reactive power delivery (MARPD) method aims to provide the best support for the PCC voltage (either boost the positive voltage or reduce the negative voltage component) and simultaneously respect the maximum limit of the phase currents imposed by DG owners. Simulation results for different fault conditions and reference values are performed in order to verify the accuracy and effectiveness of the proposed formulas.

The accurate mathematical equations of $\tilde{p}$ and $\tilde{q}$ for four UPD-LVRT-RCG strategies are currently available in [43]-[45], which have been collected and reported in Section 4.2. Moreover, the mathematical equations of $\tilde{p}$ and $\tilde{q}$ for the other two strategies are calculated based on the instantaneous power theories]311[-]311[, and presented also in Section 4.2. In addition, the precise mathematical equation of I_{max} is not available for none of 6 UPD-LVRT-RCG strategies in the literature. However, the equations of I_{max} for all six strategies are calculated and presented in Section 4.3. Using the equations of Section 4.3, it is very useful to obtain the maximum allowable reactive power, Q_{max}, which the converter can deliver to the grid under the grid faults (in order to support the grid voltage) without passing the maximum allowable instantaneous phase current limit, I_{limit}. The mathematical equations of Q_{max} under various conditions (i.e. different fault types, various voltage dip characteristics, several system parameters, different operating points, etc.) for all six strategies are obtained and presented in Section 4.4. Simulation results in various conditions, presented in Section 4.5, verify the accuracy and effectiveness of the obtained expressions.

4.2 Mathematical Equations of Instantaneous Active/Reactive Power Oscillation Terms

The control of the delivered instantaneous active and reactive powers of a three-phase grid-connected power converter under unbalanced and faulted grid voltages needs the determination of proper reference-currents. In this section, the equations of $\tilde{p}$ and $\tilde{q}$ for all six UPD-LVRT-RCG strategies will be presented using the instantaneous power theories [133]-[134].

The total reference-current can be written as:

$$i = i_p + i_q \tag{4.1}$$

Also, active and reactive reference currents can be divided into the positive and negative terms as:

$$i = i_p + i_q = i_p^+ + i_p^- + i_q^+ + i_q^- = i^+ + i^- \tag{4.2}$$

According to [43], the recognized equations of the instantaneous active/reactive powers can be thoroughly represented as:

$$p = v.i = (v^+ + v^-).(i^+ + i^-) = \underbrace{v^+.i^+ + v^-.i^-}_{P} + \underbrace{v^+.i^- + v^-.i^+}_{\tilde{p}} = P + \tilde{p} \tag{4.3}$$

$$q = |v \times i| = v_\perp.i = (v_\perp^+ + v_\perp^-).(i^+ + i^-) = \underbrace{v_\perp^+.i^+ + v_\perp^-.i^-}_{Q} + \underbrace{v_\perp^+.i^- + v_\perp^-.i^+}_{\tilde{q}} = Q + \tilde{q} \tag{4.4}$$

Also, according to [135]-[136], instantaneous active/reactive powers can be divided into its oscillatory terms as:

$$p = P + \underbrace{\tilde{p}_{s2} + \tilde{p}_{c2}}_{\tilde{p}} = P + P_{s2}\sin(2\omega t) + P_{c2}\cos(2\omega t) \tag{4.5}$$

$$q = Q + \underbrace{\tilde{q}_{s2} + \tilde{q}_{c2}}_{\tilde{q}} = Q + Q_{s2}\sin(2\omega t) + Q_{c2}\cos(2\omega t) \tag{4.6}$$

where $\tilde{p}$ and $\tilde{q}$ are oscillation terms of the instantaneous active and reactive powers, which are the main focus of this section. Table 4.1 demonstrate the available $\tilde{p}$ and $\tilde{q}$ expressions in the literature. As Table 4.1 states, $\tilde{p}$ and $\tilde{q}$ are zero for IARC and ZSCI strategies. Also, $\tilde{p}$ and $\tilde{q}$ are provided for AARC and PNSC strategies in [43]. However, the obtained expressions in [43] for the BPSC strategy is not correct. Moreover, there is no $\tilde{p}$ expression for ICPS in [44]. It is worthy to be mentioned that the expressions of the maximum values of $\tilde{p}$ and $\tilde{q}$ ($\tilde{p}_{\max}$ and $\tilde{q}_{\max}$) are more important than the expressions of their instantaneous values. $\tilde{p}_{\max}$ and $\tilde{q}_{\max}$ can be written as:

$$\tilde{p}_{\max} = |\tilde{p}| = \sqrt{{P_{s2}}^2 + {P_{c2}}^2} \tag{4.7}$$

$$\tilde{q}_{\max} = |\tilde{q}| = \sqrt{{Q_{s2}}^2 + {Q_{c2}}^2} \tag{4.8}$$

TABLE 4.1. Available expressions for oscillation terms of instantaneous active and reactive powers of UPD-LVRT-RCG strategies

	$\tilde{p}$	$\tilde{q}$
IARC	0	0
AARC	$\left[\frac{2\lvert v^+\rvert\lvert v^-\rvert\cos(2\omega t+\phi^+-\phi^-)}{\lvert v^+\rvert^2+\lvert v^-\rvert^2}\right]P$ [43]	$\left[\frac{2\lvert v^+\rvert\lvert v^-\rvert\cos(2\omega t+\phi^+-\phi^-)}{\lvert v^+\rvert^2+\lvert v^-\rvert^2}\right]Q$ [43]
BPSC	$v^-.i_p$ [43]	$v_\perp^-.i_q$ [43]
ICPS	NA	$\lvert v^-\times i_p^+\rvert$ [44]
PNSC	$v^+.i_q^- + v^-.i_q^+$ [43]	$v_\perp^+.i_p^- + v_\perp^-.i_p^+$ [43]
ZSCI	0	0

Correct and available in literature Not available in literature Incorrect in literature

Hence, this thesis tries to extract and present the useful expressions of $\tilde{p}_{\max}$ and $\tilde{q}_{\max}$. Another effective aspect to be followed is to represent the expressions of $\tilde{p}_{\max}$ and $\tilde{q}_{\max}$ in terms of scalar parameters (like the expressions of $\tilde{p}$ and $\tilde{q}$ for AARC, stated in Table 4.1, which their magnitudes are in terms of $|v^+|$, $|v^-|$, P and Q) rather than vector terms (as for instance, the $\tilde{p}$ and $\tilde{q}$ expressions of PNSC, indicated in Table 4.1, which are in terms voltage and current vectors).

As stated earlier, $\tilde{p}_{\max}$ and $\tilde{q}_{\max}$ are zero in IARC and ZSCI strategies; since their essential objective is to instantaneously control the active and reactive powers. However, for the remaining four strategies in UPD group, the expressions for $\tilde{p}_{\max}$ and $\tilde{q}_{\max}$ are calculated in the following sub-sections.

4.2.1 $\tilde{p}_{\max}$ and $\tilde{q}_{\max}$ Expressions in AARC and PNSC

This thesis frequently uses four important voltage vector terms (i.e. positive- and negative- sequences of original and orthogonal voltage vectors). Neglecting initial voltage angles or assuming that the angle of the original voltage vector is zero, then, these four voltage terms can be written as following expressions:

$$v^+ = \begin{bmatrix} V_p \cos(\omega t) \\ V_p \sin(\omega t) \end{bmatrix} \qquad v^- = \begin{bmatrix} -V_n \cos(\omega t) \\ V_n \sin(\omega t) \end{bmatrix} \tag{4.9}$$

$$v^+_{\perp} = \begin{bmatrix} -V_p \sin(\omega t) \\ V_p \cos(\omega t) \end{bmatrix} \qquad v^-_{\perp} = \begin{bmatrix} -V_n \sin(\omega t) \\ -V_n \cos(\omega t) \end{bmatrix} \tag{4.10}$$

where, V_p is the magnitude of the positive original and orthogonal voltage vectors, i.e. $|v^+|$; and V_n is the magnitude of the negative original and orthogonal voltage vectors, i.e. $|v^-|$. These four terms are frequently used hereinafter to find meaningful results for different expressions.

According to (4.3)-(4.4) and using (3.7), one can rewrite the instantaneous active and reactive powers of the AARC strategy as:

$$p = v.(i_p + i_q) = v.(Gv + Bv_\perp) = Gv^2 + Bv.v_\perp = Gv^2 \quad (4.11)$$
$$0$$

$$q = v_\perp.(i_p + i_q) = v_\perp.(Gv + Bv_\perp) = Gv.v_\perp + Bv_\perp^2 = Bv^2 \quad (4.12)$$
$$0$$

Replacing G, B, and v^2 from (3.5)-(3.6) and applying (4.9)-(4.10):

$$p = Gv^2 = \frac{P}{|v^+|^2 + |v^-|^2}.\left(|v^+|^2 + |v^-|^2 + 2|v^+||v^-|\cos(2\omega t + \phi^+ - \phi^-)\right) \quad (4.13)$$
$$= P + \underbrace{\frac{2|v^+||v^-|.P}{|v^+|^2 + |v^-|^2}\cos(2\omega t + \phi^+ - \phi^-)}_{\tilde{p}}$$

$$q = Bv^2 = \frac{Q}{|v^+|^2 + |v^-|^2}.\left(|v^+|^2 + |v^-|^2 + 2|v^+||v^-|\cos(2\omega t + \phi^+ - \phi^-)\right) \quad (4.14)$$
$$= Q + \underbrace{\frac{2|v^+||v^-|.Q}{|v^+|^2 + |v^-|^2}\cos(2\omega t + \phi^+ - \phi^-)}_{\tilde{q}}$$

So, $\tilde{p}_{\max}$ and $\tilde{q}_{\max}$ of the AARC strategy can be expressed as:

$$\tilde{p}_{\max}^{AARC} = \frac{2|v^+||v^-|.P}{|v^+|^2 + |v^-|^2} \quad (4.15)$$

$$\tilde{q}_{\max}^{AARC} = \frac{2|v^+||v^-|.Q}{|v^+|^2 + |v^-|^2} \quad (4.16)$$

According to (4.3)-(4.4) and using (3.22)-(3.23), one can easily obtain the instantaneous active and reactive powers of the PNSC strategy as (3.20)-(3.21) which are repeated here:

$$p = \underbrace{v^+.i_p^+ + v^-.i_p^-}_{P} + \underbrace{v^+.i_q^- + v^-.i_q^+}_{\tilde{p}_{s2}} = \tag{4.17}$$
$$= P - (v^-{}_{\perp}.v^+)\frac{Q}{|v^+|^2 - |v^-|^2} + (v^-.v^+{}_{\perp})\frac{Q}{|v^+|^2 - |v^-|^2}$$

$$q = \underbrace{v_{\perp}^+.i_q^+ + v_{\perp}^-.i_q^-}_{Q} + \underbrace{v_{\perp}^+.i_p^- + v_{\perp}^-.i_p^+}_{\tilde{q}_{s2}} = \tag{4.18}$$
$$= Q - (v^-.v^+{}_{\perp})\frac{P}{|v^+|^2 - |v^-|^2} + (v^-{}_{\perp}.v^+)\frac{P}{|v^+|^2 - |v^-|^2}$$

applying (4.9)-(4.10) will result:

$$p = P + \underbrace{\frac{2Q|v^+||v^-|}{|v^+|^2 - |v^-|^2}\sin(2\omega t)}_{\tilde{p}} \tag{4.19}$$

$$q = Q - \underbrace{\frac{2P|v^+||v^-|}{|v^+|^2 - |v^-|^2}\sin(2\omega t)}_{\tilde{q}} \tag{4.20}$$

So, $\tilde{p}_{\max}$ and $\tilde{q}_{\max}$ of the PNSC strategy can be presented as:

$$\tilde{p}_{\max}^{PNSC} = \frac{2Q|v^+||v^-|}{|v^+|^2 - |v^-|^2} \tag{4.21}$$

$$\tilde{q}_{\max}^{PNSC} = \frac{2P|v^+||v^-|}{|v^+|^2 - |v^-|^2} \tag{4.22}$$

4.2.2 $\tilde{p}_{\max}$ and $\tilde{q}_{\max}$ Expressions in BPSC and ICPS

According to (4.3)-(4.4) and using (3.10)-(3.11), one can rewrite the instantaneous active and reactive powers of the BPSC strategy as:

$$p = v.(i_p + i_q) = (v^+ + v^-).(G^+v^+ + B^+v^+_\perp) = \\ = G^+ \mid v^+ \mid^2 + \underbrace{B^+v^+.v^+_\perp}_{0} + G^+(v^+.v^-) + B^+(v^-.v^+_\perp) \tag{4.23}$$

$$q = v_\perp.(i_p + i_q) = (v^+_\perp + v^-_\perp).(G^+v^+ + B^+v^+_\perp) = \\ = \underbrace{G^+v^+.v^+_\perp}_{0} + B^+ \mid v^+_\perp \mid^2 + G^+(v^+.v^-_\perp) + B^+(v^-_\perp.v^+_\perp) \tag{4.24}$$

Replacing G^+, B^+, and v^2 from (3.5)-(3.6):

$$p = P \underbrace{- \frac{P \mid v^+ \mid\mid v^- \mid}{\mid v^+ \mid^2} \cos(2\omega t) + \frac{Q \mid v^+ \mid\mid v^- \mid}{\mid v^+ \mid^2} \sin(2\omega t)}_{\tilde{p}} \tag{4.25}$$

$$q = Q \underbrace{- \frac{Q \mid v^+ \mid\mid v^- \mid}{\mid v^+ \mid^2} \cos(2\omega t) - \frac{P \mid v^+ \mid\mid v^- \mid}{\mid v^+ \mid^2} \sin(2\omega t)}_{\tilde{q}} \tag{4.26}$$

So, $\tilde{p}_{\max}$ and $\tilde{q}_{\max}$ of the BPSC strategy are equal and is obtained as:

$$\tilde{p}^{BPSC}_{\max} = \tilde{q}^{BPSC}_{\max} = \frac{\mid v^- \mid}{\mid v^+ \mid}.\sqrt{P^2 + Q^2} \tag{4.27}$$

Finally, (3.17)-(3.18) provides the instantaneous active and reactive powers of the ICPS strategy as:

$$p = v\,.\,i = (v^+ + v^-).(i^+_p + i^+_q) = P + \underbrace{Q\ \frac{v^-.v^+_\perp}{\mid v^+ \mid^2 + v^+.v^-}}_{\tilde{p}} \tag{4.28}$$

$$q = v_\perp\,.\,i = (v^+_\perp + v^-_\perp).(i^+_p + i^+_q) = Q + \underbrace{P\ \frac{v^-_\perp.v^+}{\mid v^+ \mid^2 + v^+.v^-}}_{\tilde{q}} \tag{4.29}$$

applying (4.9)-(4.10) will result:

$$p = P + \frac{Q\,|v^+||v^-|\sin(2\omega t)}{|v^+|^2 - |v^+||v^-|\cos(2\omega t)} \tag{4.30}$$

$$q = Q + \frac{-P\,|v^+||v^-|\sin(2\omega t)}{|v^+|^2 - |v^+||v^-|\cos(2\omega t)} \tag{4.31}$$

So, $\tilde{p}_{\max}$ and $\tilde{q}_{\max}$ of the ICPS strategy can be obtained as:

$$\tilde{p}_{\max}^{ICPS} = \frac{Q\,|v^-|\sqrt{|v^+|^2 - |v^-|^2}}{|v^+|^2 - |v^-|^2} \tag{4.32}$$

$$\tilde{q}_{\max}^{ICPS} = \frac{P\,|v^-|\sqrt{|v^+|^2 - |v^-|^2}}{|v^+|^2 - |v^-|^2} \tag{4.33}$$

4.2.3 Discussions on $\tilde{p}_{\max}$ and $\tilde{q}_{\max}$ Expressions

Table 4.2 summarizes the obtained results of the expressions of $\tilde{p}_{\max}$ and $\tilde{q}_{\max}$ for all six UPD-LVRT-RCG strategies. Table 4.2 reveals numerous facts, as for instances:

- $\tilde{p}_{\max}$ and $\tilde{q}_{\max}$ in the AARC strategy depend on their corresponding power components (i.e. $\tilde{p}_{\max}$ depends on the average value of the active power; while, $\tilde{q}_{\max}$ depends on the average reactive power).
- $\tilde{p}_{\max}$ and $\tilde{q}_{\max}$ in both ICPS and PNSC strategies depend on their anti-corresponding power components (i.e. $\tilde{p}_{\max}$ depends on the average reactive power; while, $\tilde{q}_{\max}$ depends on the average active power).
- $\tilde{p}_{\max}$ and $\tilde{q}_{\max}$ are equal for the BPSC strategy.

TABLE 4.2. Obtained expressions for oscillation terms of instantaneous active and reactive powers of UPD-LVRT-RCG strategies

	$\tilde{p}_{\max}$	$\tilde{q}_{\max}$
IARC	0	0
AARC	$\frac{2\lvert v^+\rvert\lvert v^-\rvert.P}{\lvert v^+\rvert^2+\lvert v^-\rvert^2}$	$\frac{2\lvert v^+\rvert\lvert v^-\rvert.Q}{\lvert v^+\rvert^2+\lvert v^-\rvert^2}$
BPSC	$\frac{\lvert v^-\rvert}{\lvert v^+\rvert}.\sqrt{P^2+Q^2}$	$\frac{\lvert v^-\rvert}{\lvert v^+\rvert}.\sqrt{P^2+Q^2}$
ICPS	$\frac{Q\lvert v^-\rvert\sqrt{\lvert v^+\rvert^2-\lvert v^-\rvert^2}}{\lvert v^+\rvert^2-\lvert v^-\rvert^2}$	$\frac{P\lvert v^-\rvert\sqrt{\lvert v^+\rvert^2-\lvert v^-\rvert^2}}{\lvert v^+\rvert^2-\lvert v^-\rvert^2}$
PNSC	$\frac{2Q\lvert v^+\rvert\lvert v^-\rvert}{\lvert v^+\rvert^2-\lvert v^-\rvert^2}$	$\frac{2P\lvert v^+\rvert\lvert v^-\rvert}{\lvert v^+\rvert^2-\lvert v^-\rvert^2}$
ZSCI	0	0

Due to the near-unity power factor operation of DERs [90], the reactive power is normally much smaller than the active power. Another point to be mentioned is the importance of the $\tilde{p}_{\max}$ for DER owners [23], [152]; since it severely affects the regulation of the DC voltage in the DC-side of the power converter. Knowing these two facts and based on the expressions of Table 4.2, several conclusions can be made on the practicality and effectiveness of the strategies in terms of the active power oscillation and the DC voltage regulation:

- IARC and ZSCI are obviously best options for having instantaneously controlled powers with zero oscillation components.
- In the second and third places, the ICPS and PNSC strategies have, respectively, less oscillations on the active power (compared to AARC and BPSC strategies), since $\tilde{p}_{\max}$ in ICPS and PNSC depends on Q which is normally much smaller than P. Furthermore, since,

$$0 \le \frac{\sqrt{\lvert v^+\rvert^2-\lvert v^-\rvert^2}}{2\lvert v^+\rvert} < 0.5$$

$\tilde{p}_{\max}$ of the ICPS strategy is less than half of $\tilde{p}_{\max}$ value in the PNSC strategy.

- In the fourth and fifth places, the AARC and BPSC are located and their comparison depends on voltage sag characteristics (i.e. $|v^+|$ and $|v^-|$ values) and power components (i.e. P and Q). The relationship between $\tilde{p}_{\max}^{AARC}$ and $\tilde{p}_{\max}^{BPSC}$ can be conducted as:

$$\frac{\tilde{p}_{\max}^{AARC}}{\tilde{p}_{\max}^{BPSC}} = \frac{2|v^+|^2}{|v^+|^2 - |v^-|^2} \cdot \frac{P}{S}$$

where in most cases, not always, the above ratio is greater than 1. Thus, one can stochastically state that the AARC strategy is the worst option in terms of the active power oscillations and DC voltage regulation.

Furthermore, for an advantageous summary of some concrete facts it is valuable to consider Bars 4.1 and 4.2 which indicate the performance of all six strategies in terms of $\tilde{p}_{\max}$ and $\tilde{q}_{\max}$ under 5 different fault cases. It is also useful to generally rank the strategies in terms of maximum oscillations on active and reactive powers, according to Table 4.2, conducted conclusions, and Bars 4.1 and 4.2:

- First, IARC and ZSCI strategies have least oscillations on their respective active and reactive powers, comparing all UPD-LVRT-RCG strategies under the same fault and system conditions. Therefore, these two strategies have the least problem with their DC-voltage regulations.
- In the second place, ICPS and BPSC strategies stand which their oscillations on active and reactive power are reasonable according to Bars 4.1 and 4.2.
- The AARC and PNSC strategies has the third and fourth ranks in terms of oscillations on active and reactive power. Although AARC has the worst oscillations on the reactive power, PNSC is the worst strategy in terms of power oscillations since the importance of the oscillations on the active power is much more than that of the reactive power.

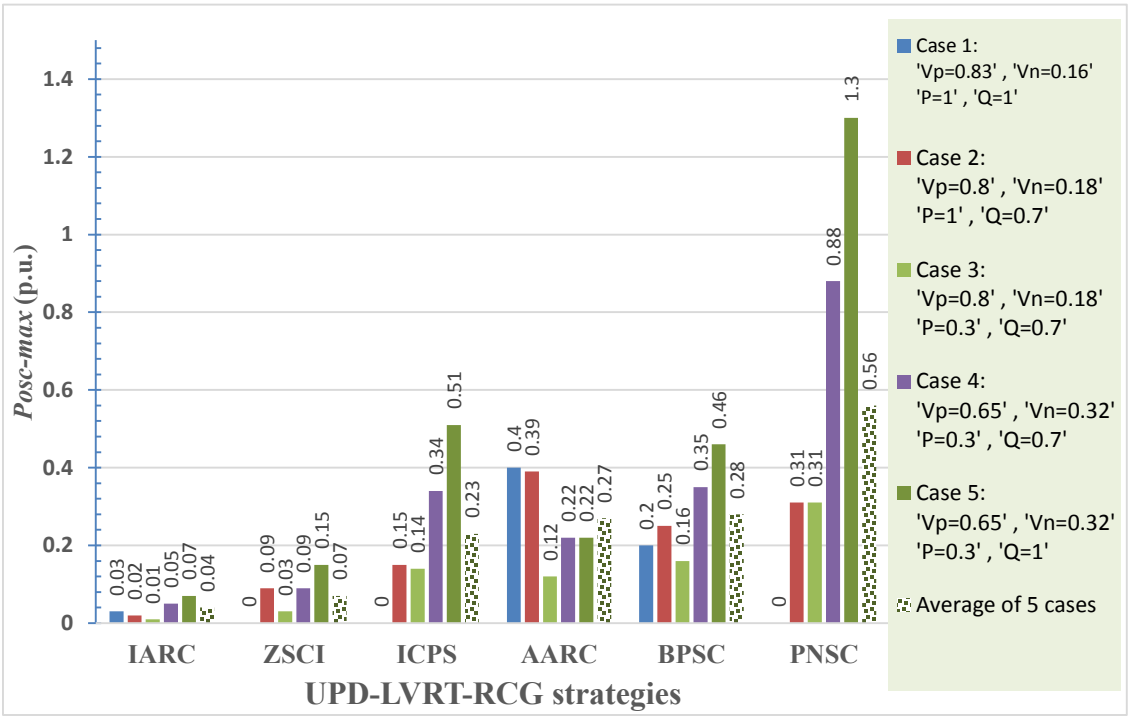

Bar 4.1. $\tilde{p}_{\max}$ values of six strategies under five different conditions (all values are in p.u.).

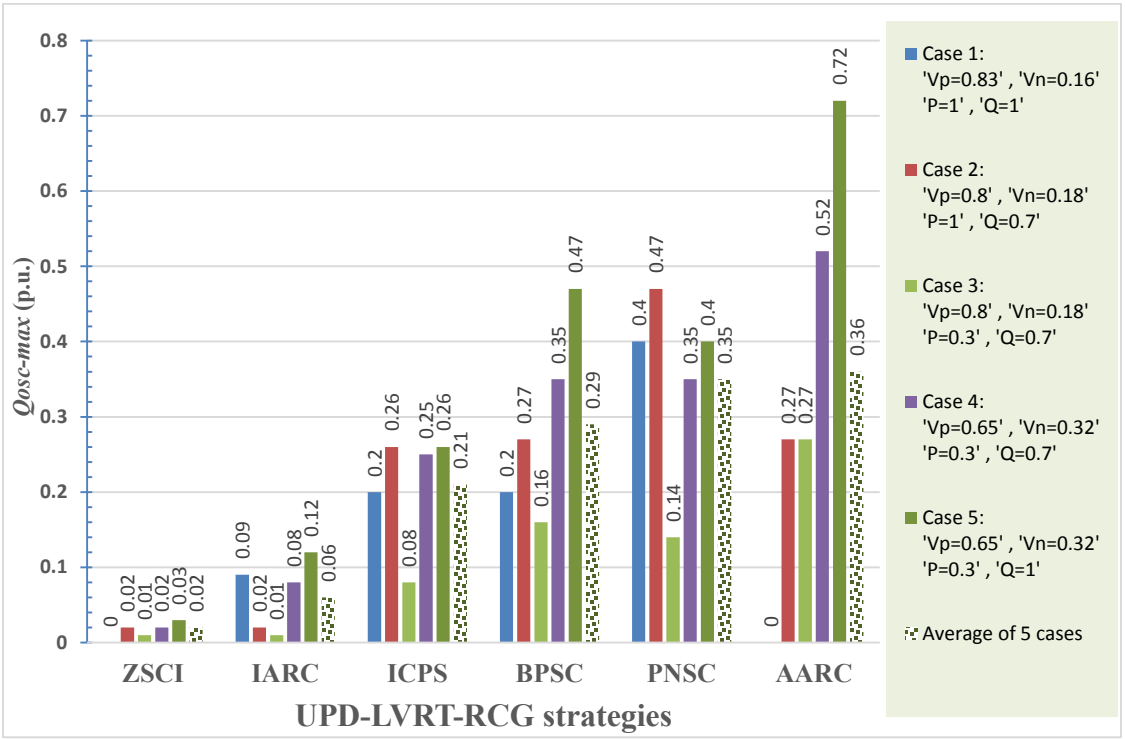

Bar 4.2. $\tilde{q}_{\max}$ values of six strategies under five different conditions (all values are in p.u.).

4.3 Mathematical Expressions of Maximum Instantaneous Phase Currents

Along with four mentioned voltage terms in (4.9)-(4.10), it is very helpful, for the calculation of the I_{max} equations, to represent the PCC voltage vector and its respective orthogonal form in αβ reference frame and in simple forms as:

$$v=\begin{bmatrix} v_\alpha \\ v_\beta \end{bmatrix} = \begin{bmatrix} V_1\cos(\omega t) \\ V_2\sin(\omega t) \end{bmatrix} \quad \text{and} \quad v_\perp = \begin{bmatrix} v_{\perp\alpha} \\ v_{\perp\beta} \end{bmatrix} = \begin{bmatrix} -v_\beta \\ v_\alpha \end{bmatrix} = \begin{bmatrix} -V_2\sin(\omega t) \\ V_1\cos(\omega t) \end{bmatrix}$$

$$where \quad \begin{cases} V_1 = V_p - V_n \\ V_2 = V_p + V_n \end{cases} \tag{4.34}$$

In a balanced operation, the magnitudes of α and β voltage components (i.e. V_1 and V_2) are equal; while in an unbalanced condition, they are varied. Also, as stated earlier the general form of the reference current can be written as:

$$i^* = i_p^* + i_q^* = g\,.\,v + b\,.\,v_\perp \tag{4.35}$$

Therefore, the general form of the injected current under the fault can be written based on (4.34)-(4.35) in the αβ reference frame:

$$i=\begin{bmatrix} i_\alpha \\ i_\beta \end{bmatrix} = \begin{bmatrix} gV_1\cos(\omega t) - bV_2\sin(\omega t) \\ gV_2\sin(\omega t) + bV_1\cos(\omega t) \end{bmatrix} \tag{4.36}$$

To transform the αβ currents of (4.36) into the abc current, a useful transformation matrix is used in this paper which is based on the ideas presented in [43]:

$$\begin{bmatrix} i_a \\ i_b \\ i_c \end{bmatrix} = \begin{bmatrix} 1 & 0 \\ -1/2 & \sqrt{3}/2 \\ -1/2 & -\sqrt{3}/2 \end{bmatrix} \cdot \begin{bmatrix} i_\alpha \\ i_\beta \end{bmatrix} \tag{4.37}$$

Applying (4.37) to (4.36) will result in the general equation of (4.38) which gives the maximum instantaneous current values in each of abc phases under different situations:

$$\begin{bmatrix} I^2_{\max-a} \\ I^2_{\max-b} \\ I^2_{\max-c} \end{bmatrix} = \begin{bmatrix} (gV_1)^2 + (bV_2)^2 \\ (-\frac{1}{2}gV_1 + \frac{\sqrt{3}}{2}bV_1)^2 + (\frac{1}{2}bV_2 + \frac{\sqrt{3}}{2}gV_2)^2 \\ (-\frac{1}{2}gV_1 - \frac{\sqrt{3}}{2}bV_1)^2 + (\frac{1}{2}bV_2 - \frac{\sqrt{3}}{2}gV_2)^2 \end{bmatrix} \tag{4.38}$$

Then, Imax is simply:

$$I_{\max} = \max\left(I_{\max-a}, I_{\max-b}, I_{\max-c}\right) \tag{4.39}$$

4.3.1 I_{max} Expressions in IARC and ICPS

Using (4.38) in both IARC and ICPS strategies and substituting g and b values, respectively, from (3.2)-(3.3) and (3.16) will result in:

$$I^2_{\max-\text{IARC}} = \frac{P^2 + Q^2}{V_p^{\,2} + V_n^{\,2} - 2V_pV_n} \tag{4.40}$$

$$I^2_{\max-\text{ICPS}} = \frac{V_p^{\,2}.(P^2 + Q^2)}{(V_p^{\,2} - V_pV_n)^2} \tag{4.41}$$

Although the reference currents generated by both IARC and ICPS strategies are unbalanced and non-sinusoidal (which are discussed in details in Chapter 3), the equations of (4.40)-(4.41) are still valid to calculate the maximum instantaneous currents.

However, due to the non-sinusoidal currents in these two strategies, it is impossible to find the I_{max} expressions for each specific phase with this general approach.

4.3.2 I_{max} Expressions in AARC, BPSC, and PNSC

Applying (4.38) in AARC, BPSC and PNSC strategies and using g and b values presented, respectively, in (3.6), (3.10)-(3.11) and (3.22)-(3.23) will result in:

$$\begin{bmatrix} I^2_{\max-a-AARC} \\ I^2_{\max-b-AARC} \\ I^2_{\max-c-AARC} \end{bmatrix} = 4\times \begin{bmatrix} \dfrac{P^2V_1^2+Q^2V_2^2}{(V_1^2+V_2^2)^2} \\ \dfrac{(-\frac{1}{2}PV_1+\frac{\sqrt{3}}{2}QV_1)^2+(\frac{1}{2}QV_2+\frac{\sqrt{3}}{2}PV_2)^2}{(V_1^2+V_2^2)^2} \\ \dfrac{(-\frac{1}{2}PV_1-\frac{\sqrt{3}}{2}QV_1)^2+(\frac{1}{2}QV_2-\frac{\sqrt{3}}{2}PV_2)^2}{(V_1^2+V_2^2)^2} \end{bmatrix} \tag{4.42}$$

$$I^2_{\max-a-\text{BPSC}} = I^2_{\max-b-\text{BPSC}} = I^2_{\max-c-\text{BPSC}} = \frac{P^2+Q^2}{V_p^{\,2}} \tag{4.43}$$

$$\begin{bmatrix} I^2_{\max-a-PNSC} \\ I^2_{\max-b-PNSC} \\ I^2_{\max-c-PNSC} \end{bmatrix} = \begin{bmatrix} \dfrac{P^2(V_2)^2+Q^2(V_1)^2}{(V_p^{\,2}-V_n^{\,2})^2} \\ \dfrac{(V_2)^2\left[\frac{1}{2}P+\frac{\sqrt{3}}{2}Q\right]^2+(V_1)^2\left[\frac{1}{2}Q+\frac{\sqrt{3}}{2}P\right]^2}{(V_p^{\,2}-V_n^{\,2})^2} \\ \dfrac{(V_2)^2\left[\frac{1}{2}P-\frac{\sqrt{3}}{2}Q\right]^2+(V_1)^2\left[\frac{1}{2}Q-\frac{\sqrt{3}}{2}P\right]^2}{(V_p^{\,2}-V_n^{\,2})^2} \end{bmatrix} \tag{4.44}$$

Since the reference currents generated by AARC, BPSC and PNSC strategies are sinusoidal, the expressions of their maximum instantaneous values can be calculated phase by phase for each strategy using the presented analytical approach and following (4.34) to (4.39).

4.3.3 I_{max} Expression in ZSCI

The analytical calculation of I_{max} formula in ZSCI strategy is complicated; and, its equation is too large due to the inverse operation of a 6×6 matrix in (3.27). However, the analytical equation of I_{max} can be calculated for the simplified-ZSCI strategy using (3.28). Knowing positive-negative-zero sequence currents obtained from (3.28), the current vector in *abc* frame can be calculated by [153]:

$$\begin{bmatrix} \vec{I}_a \\ \vec{I}_b \\ \vec{I}_c \end{bmatrix} = \begin{bmatrix} 1 & 1 & 1 \\ 1 & a^2 & a \\ 1 & a & a^2 \end{bmatrix} \begin{bmatrix} \vec{I}_0 \\ \vec{I}^+ \\ \vec{I}^- \end{bmatrix} = \begin{bmatrix} 1 & 1 & 1 \\ 1 & a^2 & a \\ 1 & a & a^2 \end{bmatrix} \begin{bmatrix} I_0^{\mathrm{Re}} + jI_0^{\mathrm{Im}} \\ I_d^+ + jI_q^+ \\ I_d^- + jI_q^- \end{bmatrix} \tag{4.45}$$

Therefore,

$$\begin{bmatrix} I_a{}^2 \\ I_b{}^2 \\ I_c{}^2 \end{bmatrix} =$$

$$\begin{bmatrix} (I_0^{\mathrm{Re}} + I_d^+ + I_d^-)^2 + (I_0^{\mathrm{Im}} + I_q^+ + I_q^-)^2 \\ \left[I_0^{\mathrm{Re}} - \frac{1}{2}(I_d^+ + I_d^-) + \frac{\sqrt{3}}{2}(I_q^+ - I_q^-) \right]^2 + \left[I_0^{\mathrm{Im}} - \frac{1}{2}(I_q^+ + I_q^-) - \frac{\sqrt{3}}{2}(I_d^+ - I_d^-) \right]^2 \\ \left[I_0^{\mathrm{Re}} - \frac{1}{2}(I_d^+ + I_d^-) - \frac{\sqrt{3}}{2}(I_q^+ - I_q^-) \right]^2 + \left[I_0^{\mathrm{Im}} - \frac{1}{2}(I_q^+ + I_q^-) + \frac{\sqrt{3}}{2}(I_d^+ - I_d^-) \right]^2 \end{bmatrix}$$

and

$$I_{\max-\mathrm{ZSCI}} = \max\left(I_{\mathrm{a}}, I_{\mathrm{b}}, I_c\right) \tag{4.46}$$

In a single-phase-A voltage dip, the instantaneous currents in other two phases are equal and larger than the phase current of the faulted phase. So:

$$I_{\max-ZSCI} = |I_b| = |I_c| \tag{4.47}$$

4.3.4 Discussion and Summary

Table 4.3 summarizes the expressions of I_{max} obtained in this section. According to Table 4.3, the following facts can be concluded:

- Under the same voltage dip characteristics and equal apparent powers, the IARC and ICPS strategies have the same amount of maximum phase currents.
- The maximum phase current in the BPSC strategy is less than that of either IARC and ICPS; since,

$$V_1^2 = (V_p - V_n)^2 \le V_p{}^2$$

- The ZSCI strategy has the greatest I_{max} value due to the zero-sequence current injection, which is the most notable problem of this strategy.
- Mathematical evaluation on I_{max} expressions of AARC and PNSC strategies indicates that for the case that Q is zero, the maximum phase current in the AARC strategy is less than that of the PNSC strategy, since:

$$when\ \ Q = 0 \qquad \Rightarrow \qquad \frac{I_{\max}^{AARC}}{I_{\max}^{PNSC}} = \frac{(V_p^2 + V_n^2 + V_p V_n).(V_p^2 - V_n^2)^2}{(V_p^2 + V_n^2 + 2V_p V_n).(V_p^2 + V_n^2)^2} \le 1$$

Also,

$$when\ \ P = 0 \qquad \Rightarrow \qquad \frac{I_{\max}^{AARC}}{I_{\max}^{PNSC}} = \frac{(V_p^2 + V_n^2 + 2V_p V_n).(V_p^2 - V_n^2)^2}{(V_p^2 + V_n^2 + V_p V_n).(V_p^2 + V_n^2)^2} \equiv AP$$

The AP ratio is less than 1, when $n = (V_n/V_p)$ is greater than 0.2 and AP is greater than one when n is less than 0.2. Therefore, when P is considerably less than Q, I_{max} of the PNSC can be either greater or less than I_{max} of the AARC depending on the voltage dip characteristics (i.e. n).

Bar 4.3 shows I_{max} values of six strategies under five different conditions, i.e. different active and reactive commands and altered voltage dip characteristics as indicated in the right hand side of the bar graph. It is noteworthy to check the above conducted

TABLE 4.3. Obtained expressions for the maximum instantaneous phase currents of UPD-LVRT-RCG strategies

	I_{max} expressions in the literature	I_{max} expressions obtained in this thesis
IARC	NA	$\frac{P^2+Q^2}{V_p^{\,2}+V_n^{\,2}-2V_pV_n}=\frac{P^2+Q^2}{V_1^2}$
AARC	NA	$4\times\left[\begin{array}{c}\frac{P^2V_1^2+Q^2V_2^2}{(V_1^2+V_2^2)^2}\\ \frac{(-\frac{1}{2}PV_1+\frac{\sqrt{3}}{2}QV_1)^2+(\frac{1}{2}QV_2+\frac{\sqrt{3}}{2}PV_2)^2}{(V_1^2+V_2^2)^2}\\ \frac{(-\frac{1}{2}PV_1-\frac{\sqrt{3}}{2}QV_1)^2+(\frac{1}{2}QV_2-\frac{\sqrt{3}}{2}PV_2)^2}{(V_1^2+V_2^2)^2}\end{array}\right]$
BPSC	NA	$\frac{P^2+Q^2}{V_p^{\,2}}$
ICPS	NA	$\frac{V_p^{\,2}.(P^2+Q^2)}{(V_p^{\,2}-V_pV_n)^2}=\frac{P^2+Q^2}{V_1^2}$
PNSC	NA	$\left[\begin{array}{c}\frac{P^2(V_2)^2+Q^2(V_1)^2}{(V_p^{\,2}-V_n^{\,2})^2}\\ \frac{(V_2)^2\left[\frac{1}{2}P+\frac{\sqrt{3}}{2}Q\right]^2+(V_1)^2\left[\frac{1}{2}Q+\frac{\sqrt{3}}{2}P\right]^2}{(V_p^{\,2}-V_n^{\,2})^2}\\ \frac{(V_2)^2\left[\frac{1}{2}P-\frac{\sqrt{3}}{2}Q\right]^2+(V_1)^2\left[\frac{1}{2}Q-\frac{\sqrt{3}}{2}P\right]^2}{(V_p^{\,2}-V_n^{\,2})^2}\end{array}\right]$
ZSCI	NA	$\left[\begin{array}{l}(I_0^{\mathrm{Re}}+I_d^+ +I_d^-)^2+(I_0^{\mathrm{Im}}+I_q^+ +I_q^-)^2\\ \left[I_0^{\mathrm{Re}}-\frac{1}{2}(I_d^+ +I_d^-)+\frac{\sqrt{3}}{2}(I_q^+ -I_q^-)\right]^2+\ldots\\ \quad\ldots+\left[I_0^{\mathrm{Im}}-\frac{1}{2}(I_q^+ +I_q^-)-\frac{\sqrt{3}}{2}(I_d^+ -I_d^-)\right]^2\\ \left[I_0^{\mathrm{Re}}-\frac{1}{2}(I_d^+ +I_d^-)-\frac{\sqrt{3}}{2}(I_q^+ -I_q^-)\right]^2+\ldots\\ \quad\ldots+\left[I_0^{\mathrm{Im}}-\frac{1}{2}(I_q^+ +I_q^-)+\frac{\sqrt{3}}{2}(I_d^+ -I_d^-)\right]^2\end{array}\right]$

conclusions with the results presented in the bar graph. Also, it is very useful to compare the values of I_{max} of six strategies together under different conditions; in order to evaluate and rank them in terms of maximum phase currents needed to be injected with each strategy. It is worthy to be mentioned that the strategies with high maximum phase currents such as ZSCI and IARC has less capability in supporting the grid voltage with reactive power injection compared to the strategies occupying lower I_{max}s like BPSC and AARC. The detailed study on the capability of each strategy to inject the maximum allowable reactive power will be carried out in Section 4.4.

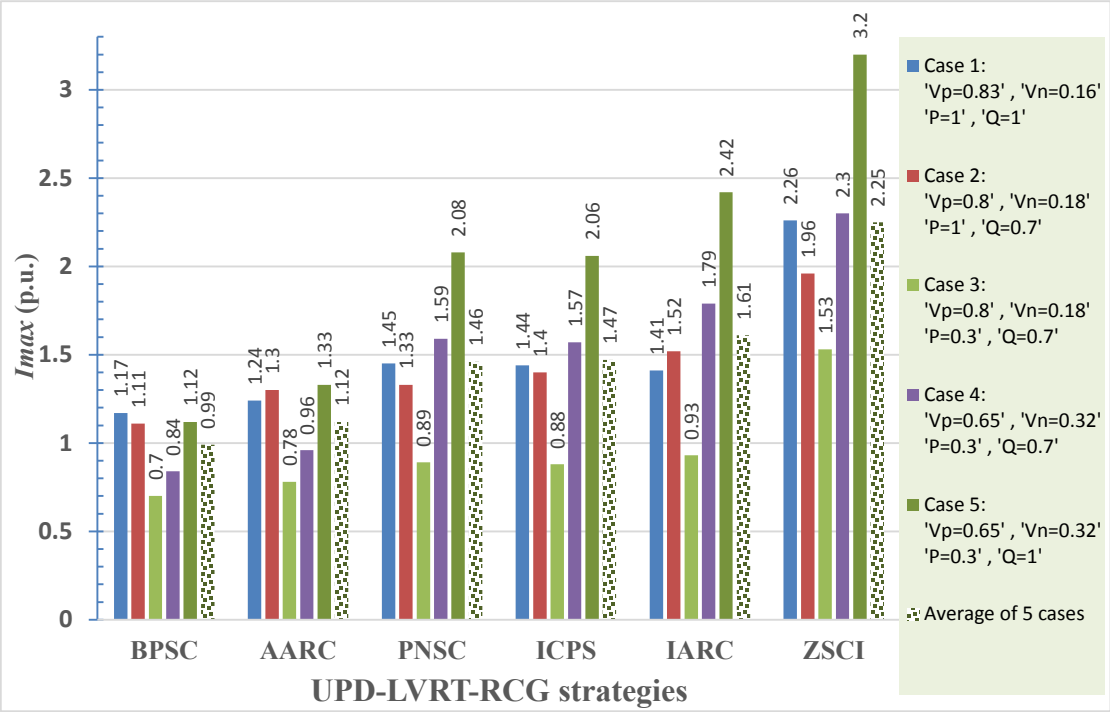

Bar 4.3. I_{max} values of six strategies under five different conditions (all values are in p.u.).

To wrap up the studies in this section, it is beneficial to summarize some concrete facts by generally ranking the strategies in terms of maximum phase currents, according to Table 4.3, conducted conclusions, and Bar 4.3:

- First, BPSC and AARC strategies have least needed maximum phase currents among the UPD-LVRT-RCG strategies under the same fault and system conditions. Therefore, these two strategies have the greatest capability

between UPD-LVRT-RCG strategies in order to support the grid voltage with reactive power injection which will be discussed further in next Section and will be verified by simulation results in Section 4.5.2.

- The PNSC and ICPS strategies has the second and third rank in terms of current under generic fault conditions according to Bar 4.3. Although both PNSC and ICPS occupies almost the same amount of current under different voltage disturbances, ICPS is placed in the third rank since its currents contain harmonic and they are not sinusoidal which is a great drawback of this strategy.
- In the fourth place, the IARC strategy stands since its required currents under the fault are greater than those of heretofore mentioned strategies, i.e. BPSC, AARC, PNSC and ICPS.
- Finally, the ZSCI strategy is the worst in terms of injected currents since it requires very high currents to be injected under voltage disturbances. This high current injection is mainly due to the zero-sequence current required to be injected in order to keep the active and reactive powers constant with sinusoidal currents. Although these features are notably appropriate in terms of non-oscillatory powers and non-harmonic currents simultaneously, high currents injection is the most notable drawback of the ZSCI strategy. Therefore, the ZSCI strategy has the least capability between UPD-LVRT-RCG strategies in order to support the grid voltage with reactive power injection which will be discussed further in Section 4.4.2 and will be verified by simulation results in Section 4.5.2.

4.4 Calculation of the Maximum allowable Reactive Powers; MARPD Equations

In this chapter, the maximum allowable reactive power (Q_{max}) delivery (MARPD) is proposed which is the main contribution of this chapter. Applying the MARPD method

in each of the traditional LVRT-RCG methods provides the best support, to ride through any fault and to assist the disturbed voltage, under an existing very important constraint (the maximum phase currents limitation). Therefore, this section intends to obtain all required equations of Q_{max} for each of the six UPD-LVRT-RCG strategies based on the calculated I_{max} expressions in Section 4.3.

4.4.1 Q_{max} Expressions in IARC, BPSC and ICPS

According to Chapter 3, IARC and ICPS strategies have non-sinusoidal phase currents (harmonically distorted); and finding concrete and accurate I_{max} expressions for each phase in these strategies is impossible, stated in Section 4.3. Therefore, for each of these two strategies, one expression was found, in Section 4.3, which indicates the maximum of the magnitudes of three phases instead of finding specific expressions for all phases. Therefore, obtaining Q_{max} expressions is easy for these two strategies. Knowing (4.40) and substituting the I_{max} with the maximum allowable phase current limitation imposed by DER owners (named as I_{limit}), the following equation for the Q_{max} in the IARC strategy can be easily obtained:

$$Q_{\max}^{IARC} = \sqrt{I_{limit}^2.(V_p{}^2 + V_n{}^2 - 2V_pV_n) - P^2} \tag{4.48}$$

Also, using (4.41), the equation of the Q_{max} in the ICPS strategy can be calculated as:

$$Q_{\max}^{ICPS} = \sqrt{I_{limit}^2(V_p - V_n)^2 - P^2} \tag{4.49}$$

Furthermore, in the BPSC strategy, phase currents are balanced and they have equal magnitudes, as stated in Chapter 3 and shown analytically in Section 4.3 and (4.43). Thus, like IARC and ICPS, finding the Q_{max} expression in the BPSC strategy is easily obtained using (4.43):

$$Q_{\max}^{BPSC} = \sqrt{I_{limit}^2 V_p{}^2 - P^2} \tag{4.50}$$

4.4.2 Q_{max} Expressions in AARC, PNSC and ZSCI

Since I_{max} expressions of AARC, PNSC and ZSCI found in Section 4.3 are different and specifically assigned for each phase; so, the Q_{max} expressions of these three strategies should be found in a way that none of three phase currents in each strategy overpass the determined I_{limit}. For example, using (4.42), three different values may obtain for the allowable maximum Q as indicated in (4.51):

$$\begin{bmatrix} Q_1^{AARC} \\ Q_2^{AARC} \\ Q_3^{AARC} \end{bmatrix} = \begin{bmatrix} \dfrac{\sqrt{\frac{1}{4} I_{limit}^2 (V_1^2 + V_2^2)^2 - P^2 V_1^2}}{V_2} \\ \dfrac{-b + \sqrt{b^2 - 4ac}}{2a} \\ \dfrac{b + \sqrt{b^2 - 4ac}}{2a} \end{bmatrix} \tag{4.51}$$

$$\text{where} \quad \begin{cases} a = 3V_1^2 + V_2^2 \\ b = 2\sqrt{3}P(V_2^2 - V_1^2) \\ c = P^2(V_1^2 + 3V_2^2) - I_{limit}^2 (V_1^2 + V_2^2)^2 \end{cases}$$

However, just one of the obtained Qs is correct where all of the three phase-currents remain under the pre-specified I_{limit} value. Hence, Q_{max} of the AARC strategy will be given to the inverter controllers according to the following expression:

$$Q_{\max} = \min (Q_1 , Q_2 , Q_3) \tag{4.52}$$

Similarly, using (4.44) gives the expression of Q_{max} in the PNSC strategy as follow:

$$\begin{bmatrix} Q_1^{PNSC} \\ Q_2^{PNSC} \\ Q_3^{PNSC} \end{bmatrix} = \begin{bmatrix} \dfrac{\sqrt{I_{limit}^2 (V_p^2 - V_n^2)^2 - P^2 (V_p^2 + V_n^2)^2}}{(V_p - V_n)} \\ \dfrac{-b + \sqrt{b^2 - 4ac}}{2a} \\ \dfrac{b + \sqrt{b^2 - 4ac}}{2a} \end{bmatrix}$$

where (4.52)

$$\begin{cases} a = 3(V_p + V_n)^2 + (V_p - V_n)^2 \\ b = 2\sqrt{3}P\left[(V_p + V_n)^2 - (V_p - V_n)^2\right] \\ c = P^2\left[(V_p + V_n)^2 + 3(V_p - V_n)^2\right] - I_{limit}^2 (V_p^2 - V_n^2)^2 \end{cases}$$

Finally, using (4.46) and considering the simplified-ZSCI equations of (3.28), the Q_{max} expression for the simplified-ZSCI strategy can be attained as:

$$Q_{limit}^{ZSCI} = \frac{b + \sqrt{b^2 - 4ac}}{2a}$$

$$\begin{cases} a = \dfrac{3(V_d^+ + V_d^-)^2 + (V_d^-)^2}{9\left[(V_d^+)^2 - (V_d^-)^2\right]^2} \\ b = \dfrac{(2I_0^{\mathrm{Re}} - I_d^+ + I_d^-)(V_d^+ + V_d^-) - (I_d^+ + I_d^-)V_d^-}{\sqrt{3}\left[(V_d^+)^2 - (V_d^-)^2\right]} \\ c = (I_0^{\mathrm{Re}} - \frac{1}{2}I_d^+ + \frac{1}{2}I_d^-)^2 + \frac{3}{4}(I_d^+ + I_d^-)^2 - I_{limit}^2 \end{cases} \quad (4.53)$$

4.5 Simulation Results

To verify the mathematical expressions obtained in Sections 4.2, 4.3 and 4.4, two test cases are studied and implemented in this chapter. Fig. 1 illustrates the circuit topology

of a grid-connected 1.3 MVA, 690 V, 60 Hz CI-DER unit. In order to ride through temporary faults, the inverter should withstand during the fault and inject the power into the network. Grid ac voltage source in Fig 4.1 realizes the desired voltage dip presented in Fig 4.2. As it is stated earlier, a dc power supply can be used to emulate the renewable energy resources and storage in the dc link [151] which is widely used through most of the studies related to LVRT methods [43]-[47]. It is also assumed that the type B fault (phase A to ground) [75] occurs with significant voltage dip on phase A as indicated in Fig 4.2. The simulation system parameters are listed in Table 4.4.

4.5.1 Test Case A: Instantaneous Active and Reactive Powers Oscillations and Maximum Phase Currents

This section presents the simulation results of each UPD-LVRT-RCG strategy under grid faults in a HV grid, where a single-phase-to-ground fault is emulated after t_1=0.2s, and the grid voltage, V_{Grid}, becomes deteriorated as indicated in Fig 4.2. V+ and V- are calculated with MCCF-PLL [150]. Between t_1=0.2s and t_5=0.4s, a moderate voltage dip is emulated where $V_g+ = 0.8$ p.u. and $V_g- = 0.18$ p.u. as indicated in Fig 4.2. In addition, for more evaluations, a more severe voltage dip is emulated between t_5=0.4s and t_9=0.6s where $V_g+ = 0.65$ p.u. and $V_g- = 0.32$ p.u. as shown in Fig 4.2. In this test case, P^* is set to be 1 MW until t_3=0.3s and 0.3 MW after t_3. Also, Q^* is set to be 0.7 MVAR until t_7=0.5s and 1 MVAR after t_7.

The proportional resonant (PR) control is used in the αβ reference frame for the converter current regulation [43]. The simulation results of the IARC strategy are shown in Fig 4.3. In Fig 4.3(a), the injected currents of IARC are shown. As it is illustrated in Fig 4.3(a), the currents are non-sinusoidal and unbalanced. The I_{max} shown in Fig 4.3(a) is calculated using (4.40). As Fig 4.3(a) shows, the calculated I_{max} is not completely accurate. There are two reasons for this inaccurate I_{max}: first, the PCC voltage is affected by the injected currents; second, inaccurate current regulation due to the huge harmonics in reference currents. Therefore, if the effect of the injected currents on the PCC voltage

is completely eliminated and the reference currents are considered for comparison with calculated I_{max}; then, the calculated I_{max} will be accurate as it is indicated in Fig 4.4. The instantaneous active/reactive powers in the IARC strategy are depicted in Fig 4.3(c). As stated here, the current controllers fail to perfectly track the reference-currents since the currents are not sinusoidal. Therefore, some small oscillations on the active and reactive powers are realistically unavoidable unless a perfect deadbeat controller is used to regulate the output currents of the inverter. Another negative point worth mentioning is high currents generated by the IARC strategy as Fig 4.3(a) shows which is also claimed by analytical calculations in Section 4.3.4. These high currents may cause over current relays tripping which is undesired and against LVRT requirements.

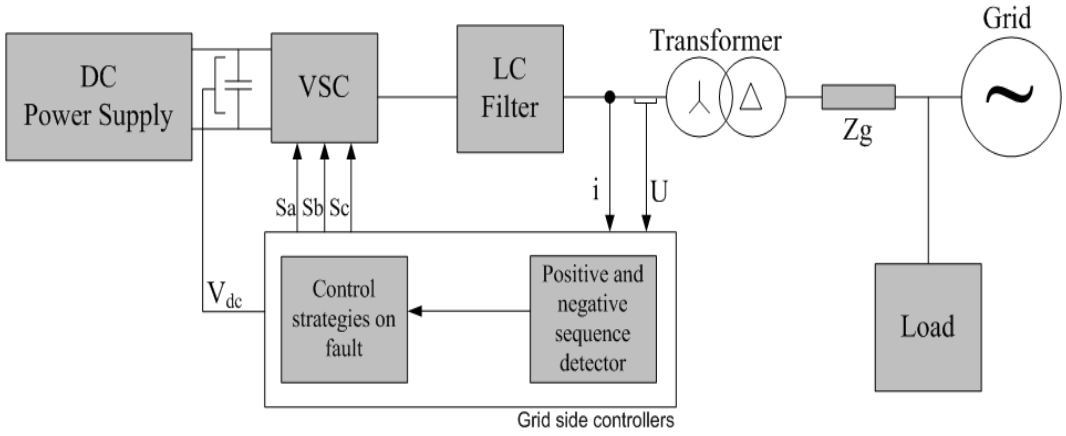

Fig 4.1. Circuit topology of the grid-connected inverter [45].

TABLE 4.4. Specified Active/Reactive Powers Commands and Test System Parameters – Case A

P^* (t_0=0s to t_3=0.3s)	1 MW	Q^* (t_0=0s to t_7=0.5s)	0.7 MVAR
P^* (t_3=0.3s to t_9=0.6s)	0.3 MW	Q^* (t_7=0.5s to t_9=0.6s)	1 MVAR
Z_g (mΩ)	$34.6\angle 78.3^\circ$	V_{DC} (V)	2000
Z_L (mΩ)	$37.8\angle 87^\circ$	$V_{L\text{-}L,\ RMS}$ (V)	690
Z_f (t_1=0.2s to t_5=0.4s)	0.8 mΩ	f (Hz)	60
Z_f (t_5=0.4s to t_{10}=0.65s)	0	S (MVA)	1.3

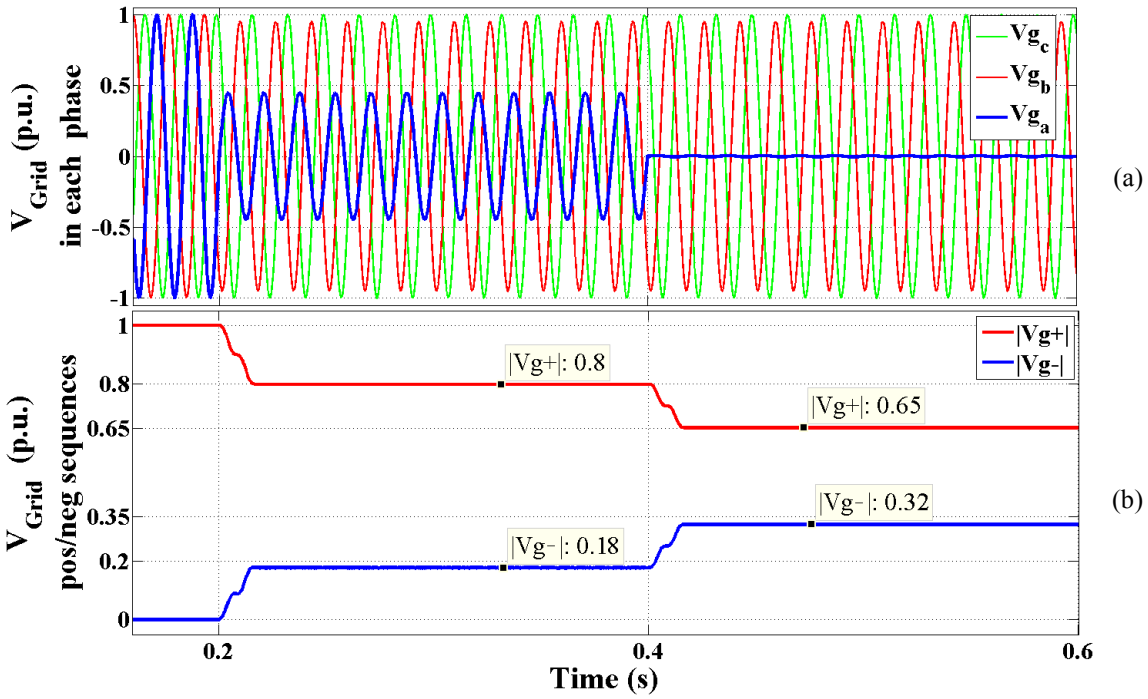

Fig 4.2. Emulated fault: (a) *abc* grid voltages, (b) positive and negative-sequences of the grid voltage.

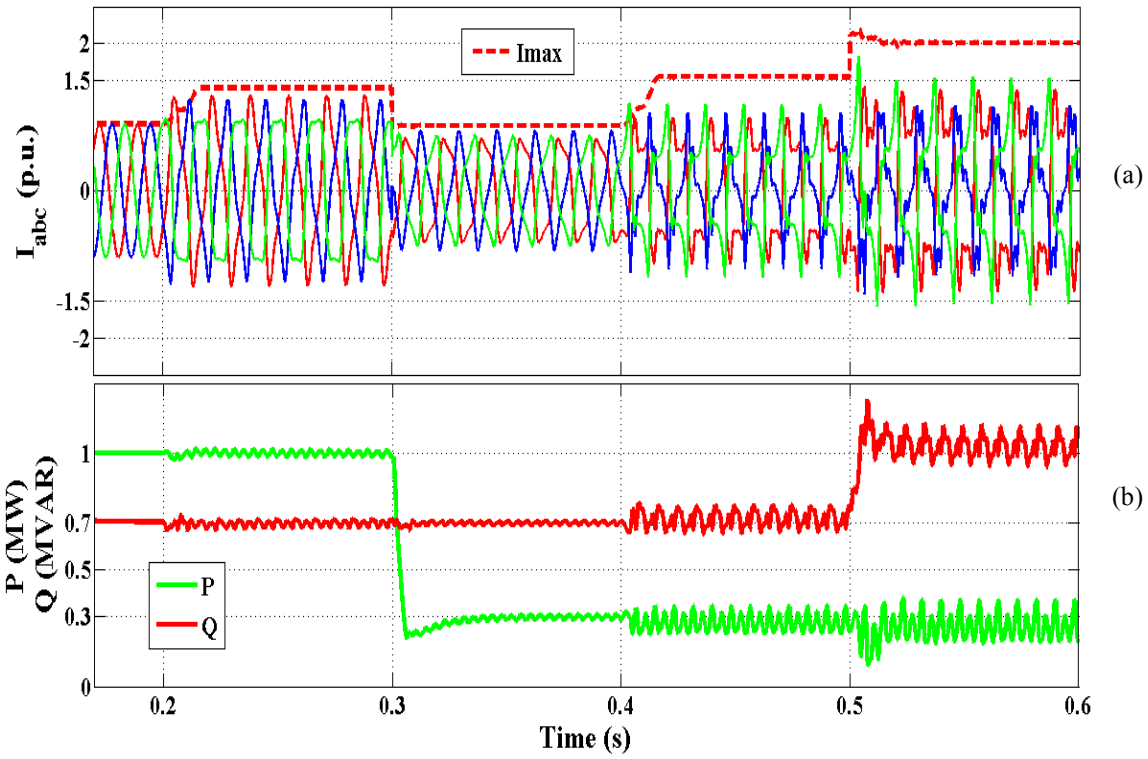

Fig 4.3. Simulation results of IARC: (a) injected currents and maximum instantaneous phase current, and (b) instantaneous active/reactive powers.

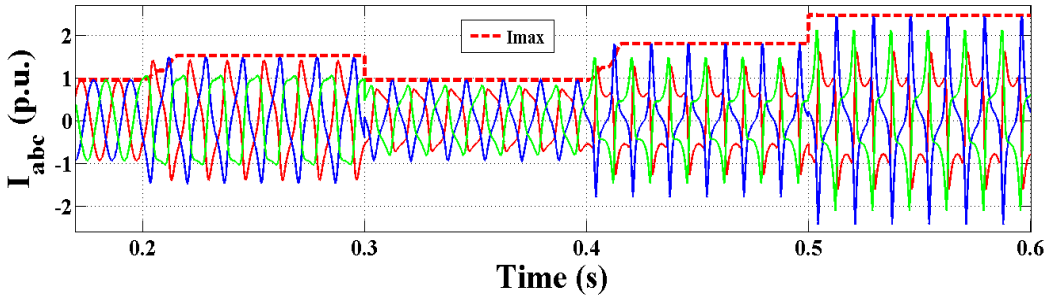

Fig 4.4. Reference currents produced by IARC and calculated maximum instantaneous phase current.

Fig 4.5 illustrates the simulation results of AARC strategy. Using the equations of (4.42), I_{max} in all phases are calculated accurately under different conditions as indicated in Fig 4.5(a). Fig 4.6 and Fig 4.7 illustrate the simulation results of BPSC and ICPS strategies. As it is indicated in Fig 4.7-(a), the I_{max} is inaccurate after t_5=0.4s which is due to the non-sinusoidal reference currents as it is also discussed earlier for the IARC strategy. Relatively lower currents of the BPSC strategy and higher currents of ICPS can be observed from Fig 4.6-(a) and Fig 4.7-(a) in agreement with the conclusions and discussions in Section 4.3.4. Furthermore, the instantaneous active powers in BPSC and ICPS contain more oscillations as illustrated in Fig 4.6-(b) and Fig 4.7-(b) compared to IARC and AARC strategies (see also Fig 4.3-(b) and Fig 4.5-(b)).

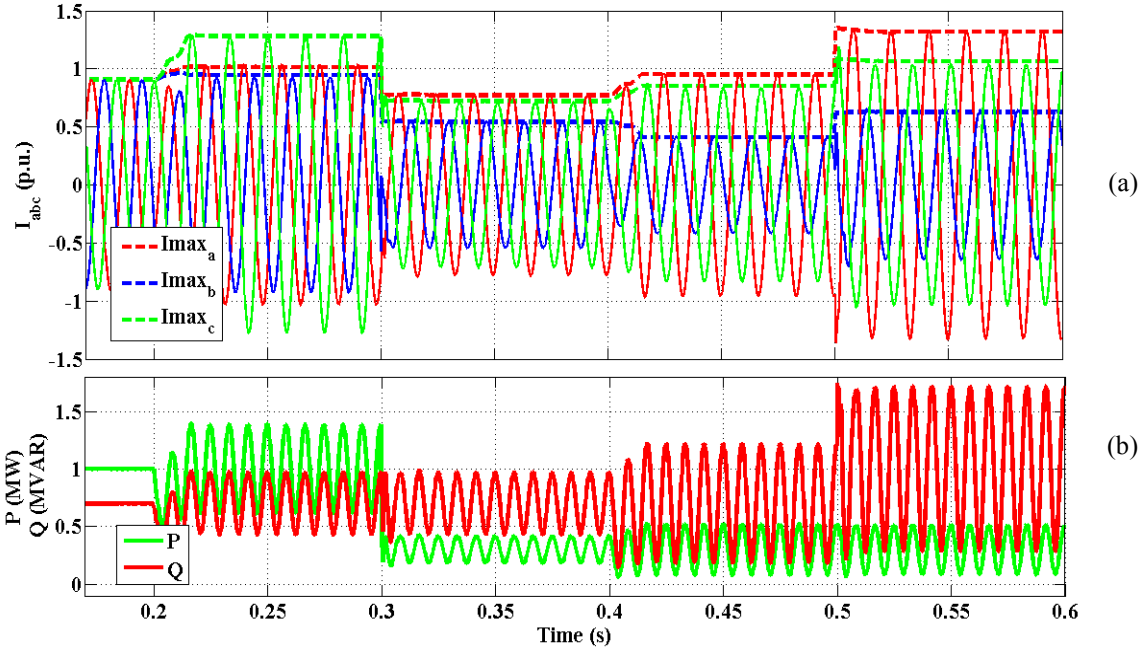

Fig 4.5. Simulation results of AARC: (a) injected currents and maximum instantaneous phase currents, and (b) instantaneous active/reactive powers.

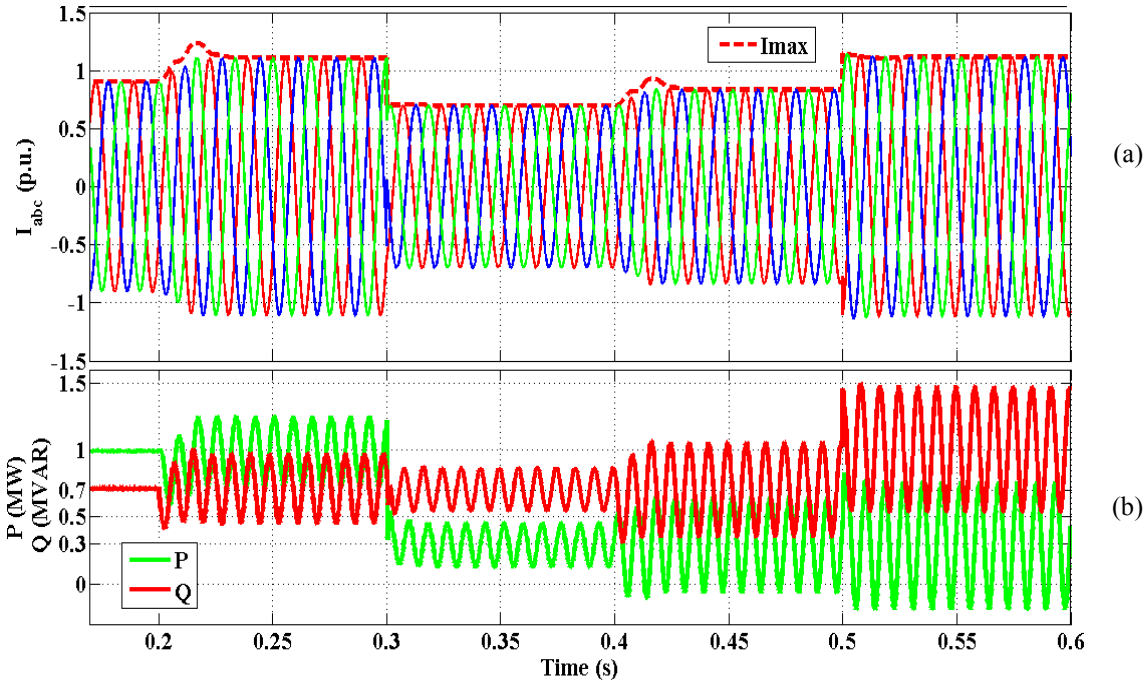

Fig 4.6. Simulation results of BPSC: (a) injected currents and maximum instantaneous phase current, and (b) instantaneous active/reactive powers.

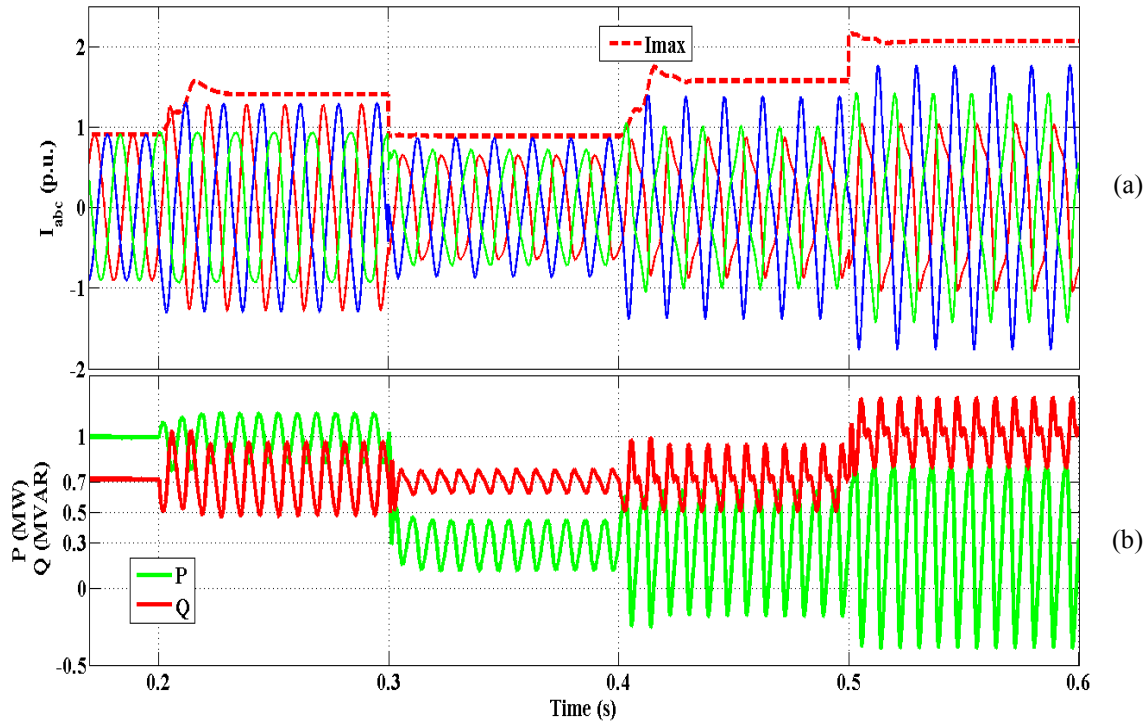

Fig 4.7. Simulation results of ICPS: (a) injected currents and maximum instantaneous phase current, and (b) instantaneous active/reactive powers.

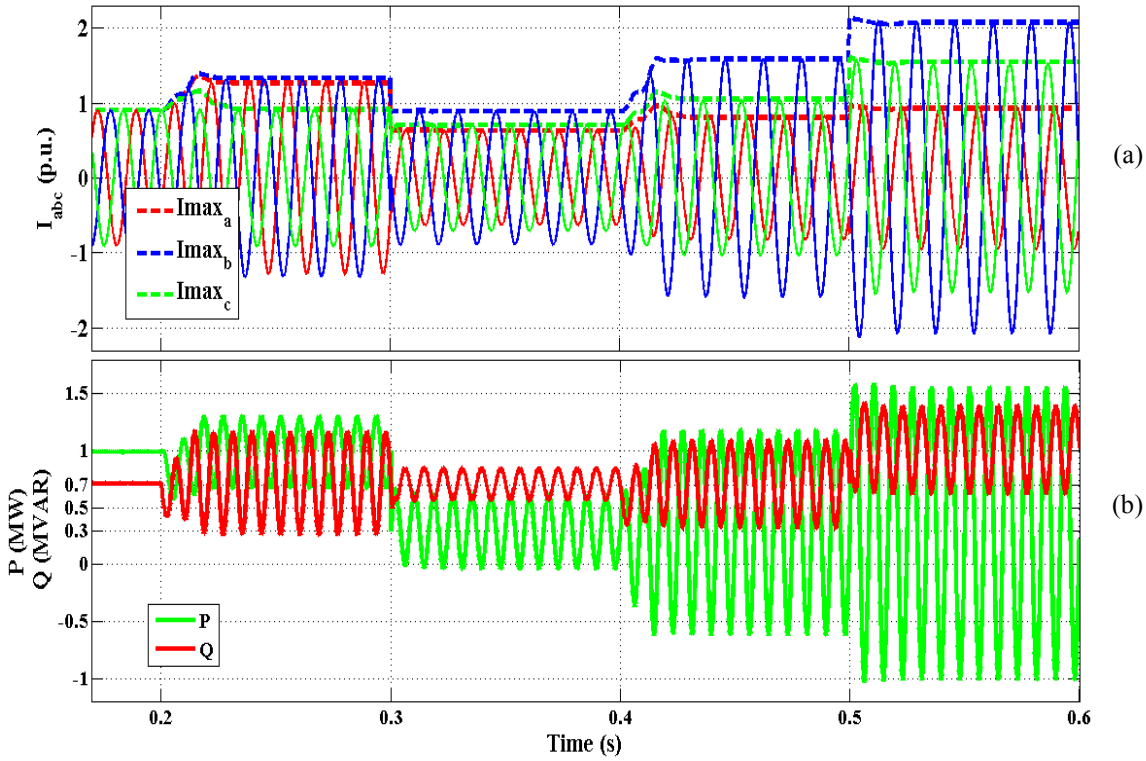

Fig 4.8. Simulation results of PNSC: (a) injected currents and maximum instantaneous phase currents, and (b) instantaneous active/reactive powers.

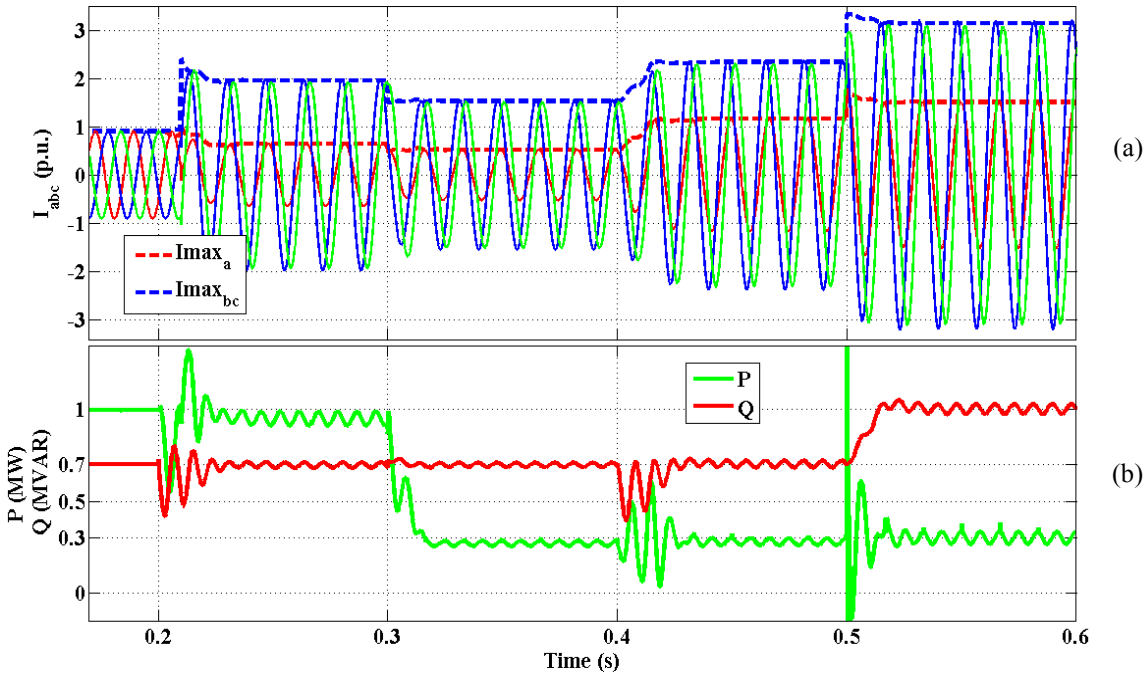

Fig 4.9. Simulation results of ZSCI: (a) injected currents and maximum instantaneous phase currents, and (b) instantaneous active/reactive powers.

Fig 4.8 and Fig 4.9 demonstrate the simulation results of PNSC and ZSCI strategies. Using (4.44) and (4.46), the I_{max} for each phase in PNSC and ZSCI strategies are accurately calculated which are also shown in Fig 4.8-(a) and Fig 4.9-(a). Relatively higher fault currents of both strategies (especially ZSCI) are considerable accordance to the conducted conclusions and results of Section 4.3.4. The instantaneous active power in PNSC contains very high oscillations (i.e. $\tilde{p}_{\max}$ is 1.25 MW after t_7) as shown in Fig 4.8-(b); whereas, oscillations on instantaneous active/reactive powers are negligible in ZSCI as illustrated in Fig 4.9-(b).

4.5.2 Test Case B: Maximum Phase Current Limitation and MARPD Method

This section tests and studies the MARPD method and presents the simulation results of each UPD-LVRT-RCG strategy with MARPD method under different fault conditions in the same HV grid of the test Case A. The grid voltage, V_{Grid}, becomes deteriorated similar to Case A. The only difference is the time of the severe voltage dip which is t_7=0.5s in this test case as it can be seen in Fig 4.10-(a) and time notations i.e. t_1=0.2s, t_2=0.25s, … , t_{11}=0.7s. The values of the deteriorated positive/negative-sequence voltages are similar to the Case A for both slight and severe faults. Moreover, P^* is set to be 1 MW until t_5=0.4s and 0.3 MW after t_5. Also, MARPD is applied in order to support the grid voltage under the fault after t_3=0.3s considering the maximum limit for I_{max} (i.e. I_{limit}) which is taken "3.5 p.u." until t_9=0.6s and "2 p.u." from t_9 to t_{11}=0.7s. Therefore, there are four different fault conditions after applying the MARPD.

TABLE 4.5. Specified Active Power Commands and I_{limit} Commands – Case B

P^* (t_0=0s to t_5=0.4s)	1 *MW*	P^* (t_5=0.4s to t_{11}=0.7s)	0.3 *MW*
I_{limit}^* (t_3=0.3s to t_9=0.6s)	1.5 *p.u.*	I_{limit}^* (t_9=0.6s to t_{11}=0.7s)	2 *p.u.*
Z_f (t_1=0.2s to t_7=0.5s)	0.8 mΩ	Z_f (t_7=0.5s to t_{10}=0.7s)	0

Fig 4.10 shows the simulation results of IARC strategy in test case B. As Fig 4.10-(b) shows, the injected currents are limited to the reference I_{limit} (i.e. I^{*}_{limit}) by calculating the maximum allowable reactive power introduced by (4.48). The currents are even less than the allowable I_{limit} due to the reasons (e.g. high harmonics) mentioned in the previous Case. As it is indicated in Fig 4.10-(c), the maximum allowable reactive power is presented for each of the four fault conditions. For example, the maximum allowable reactive power is 1.3 MVAR between t_5 and t_7 in order to limit the injected currents to the reference I_{limit} which is 1.5 p.u. in this period. In this period, the positive-sequence of the PCC voltage is boosted from 0.8 p.u. to 0.87 p.u.. Furthermore, an increment in the maximum allowable reactive power can be observed at t_9=0.6s from 0.69 MVAR to 0.96 MVAR when the reference I_{limit} increases from 1.5 p.u. to 2 p.u.. This increment in the reactive power delivery results in further boost in the PCC voltage.

Fig 4.11 shows the simulation results of AARC strategy in test case B. As Fig 4.11-(b) depicts, the injected currents are limited to the reference I_{limit} by calculating the maximum allowable reactive power presented in (4.51). The maximum currents are accurately equal to the allowable I_{limit} since the currents are sinusoidal. As it is indicated in Fig 4.11-(c), the maximum allowable reactive power is obtained (which is the average value of the instantaneous reactive power plotted in Fig 4.11-(c)) for each of the four fault conditions where the instantaneous active/reactive powers contain oscillations at twice the fundamental frequency. The positive PCC voltage boost can be observed in Fig 4.11-(a) which is due to the reactive power injection after t_3. This voltage boost is the most (i.e. 0.09 p.u. voltage boost) from t_9 to t_{11} where the specified reference I_{limit} is 2 p.u. and the specified reference active power is only 0.3 MW. Comparing Fig 4.10 and Fig 4.11, one can conclude that the AARC has more capability to support the PCC voltage under the similar fault conditions and the same reference commands (for the active power, P^{*}, and maximum allowable phase currents, I^{*}_{limit}). More capability of AARC strategy in supporting the PCC voltage is at the cost of having more oscillations on the instantaneous active/reactive powers (compare Fig 4.10 and Fig 4.11). In addition to positive voltage

boost, a small reduction in negative PCC voltage is observable in Fig 4.11 (0.3 p.u. negative voltage reduction) which is due to the negative reactive current injection.

Fig 4.12 demonstrates the simulation results of BPSC strategy in test case B. As Fig 4.12-(b) shows, the injected balanced currents are limited to I^*_{limit} by calculating the maximum allowable reactive power obtained in (4.50). The positive PCC voltage boost can be observed in Fig 4.12-(a) which is more than that of the previous strategies. As it is stated in section 4.3.4, the BPSC strategy has the greatest capability among UPD-LVRT-RCG strategies to support the PCC voltage. However, there is no negative voltage reduction in the simulation results of the BPSC strategy shown in Fig 4.12-(a) and according to its objective which is injecting the balanced positive sequence currents. The voltage boost is the most (i.e. 0.13 p.u. voltage boost) from t_9 to t_{11} where I^*_{limit} is 2 p.u. and the reference active power is only 0.3 MW. Furthermore, the value of oscillations on the instantaneous active power in BPSC (i.e. $\tilde{p}_{\max}$ reaches 0.8 MW after t9) is more than that of previous strategies which is a big drawback of this strategy.

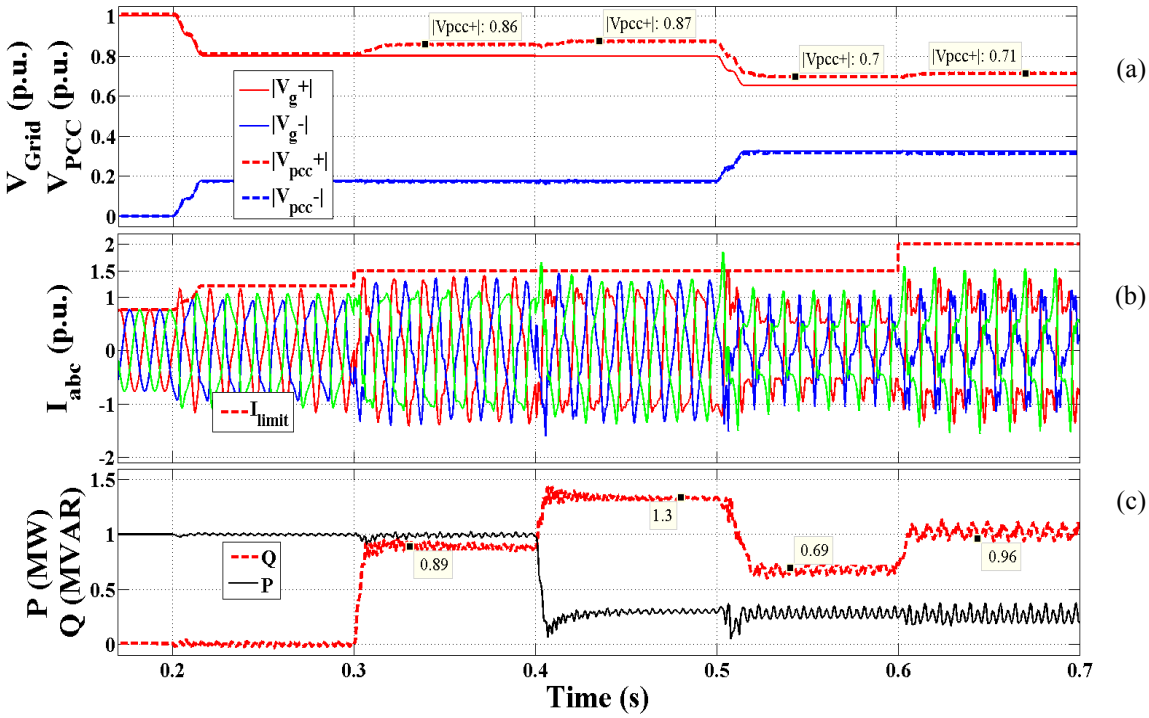

Fig 4.10. Case B – IARC strategy: (a) pos/neg-sequences of grid and PCC voltages, (b) injected currents, (c) instantaneous active/reactive powers

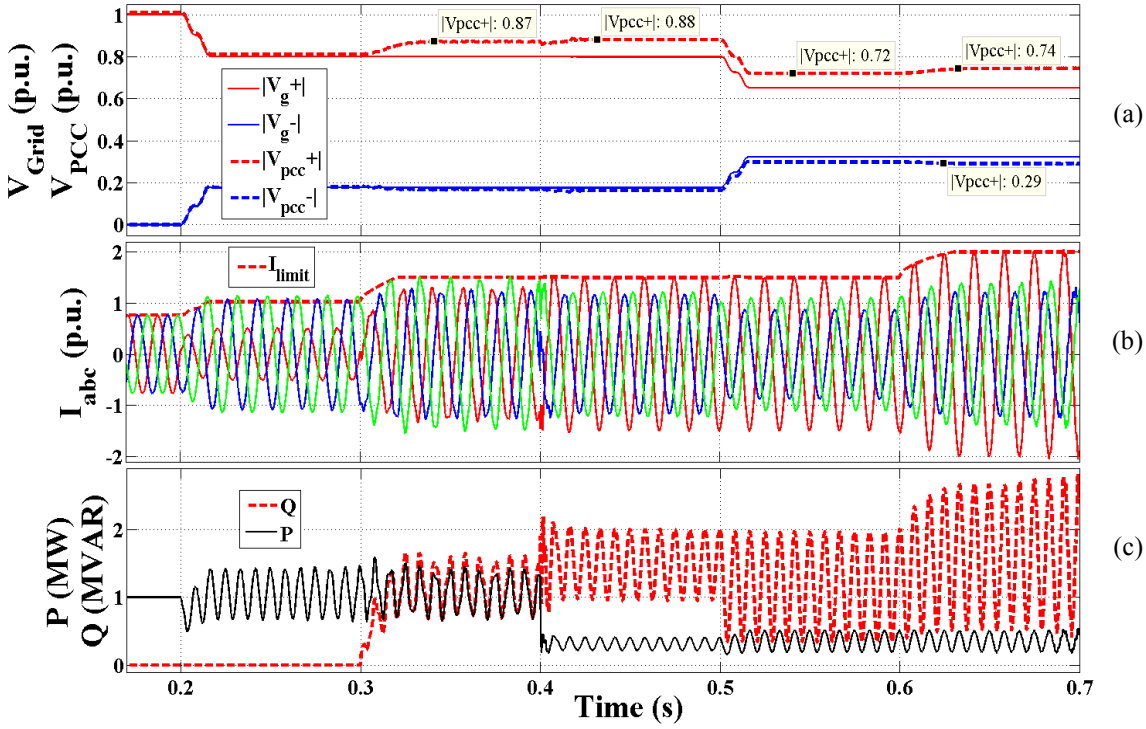

Fig 4.11. Case B – AARC strategy: (a) pos/neg-sequences of grid and PCC voltages, (b) injected currents, (c) instantaneous active/reactive powers

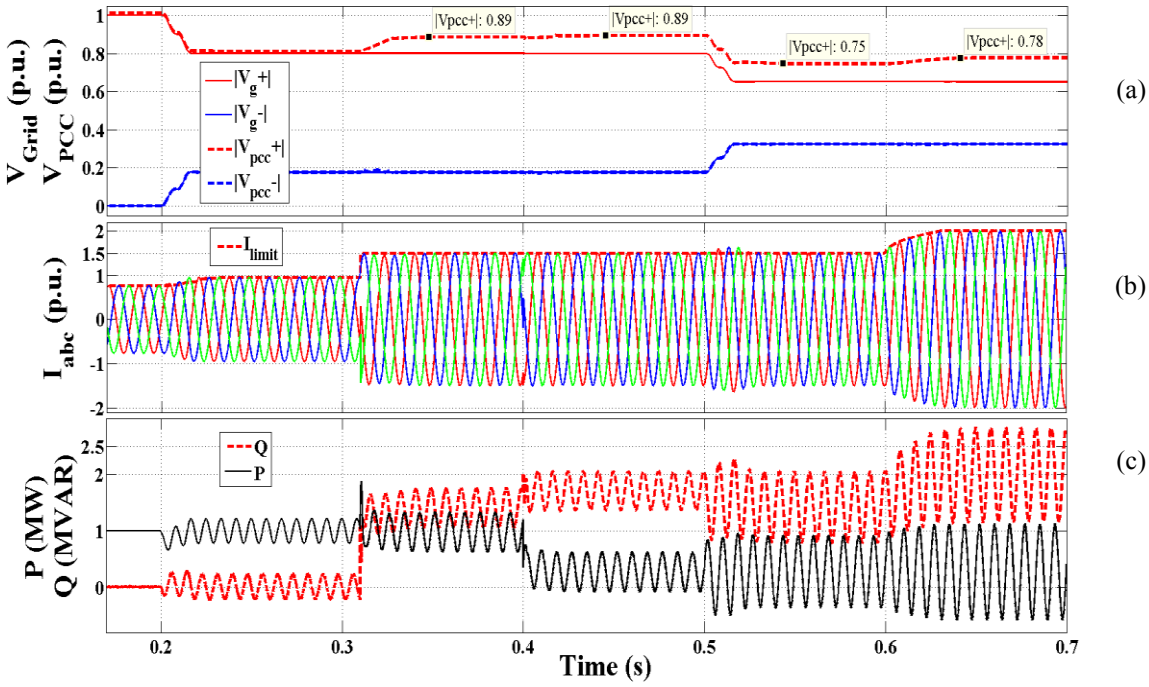

Fig 4.12. Case B – BPSC strategy: (a) pos/neg-sequences of grid and PCC voltages, (b) injected currents, (c) instantaneous active/reactive powers

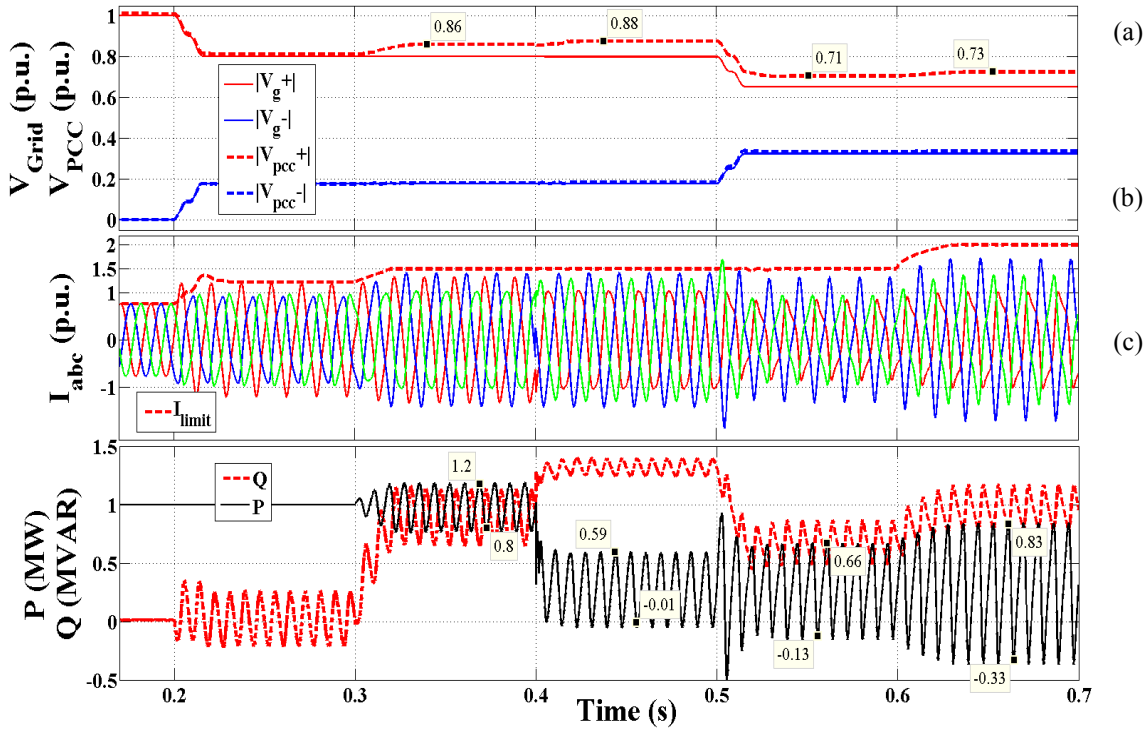

Fig 4.13. Case B – ICPS strategy: (a) pos/neg-sequences of grid and PCC voltages, (b) injected currents, (c) instantaneous active/reactive powers

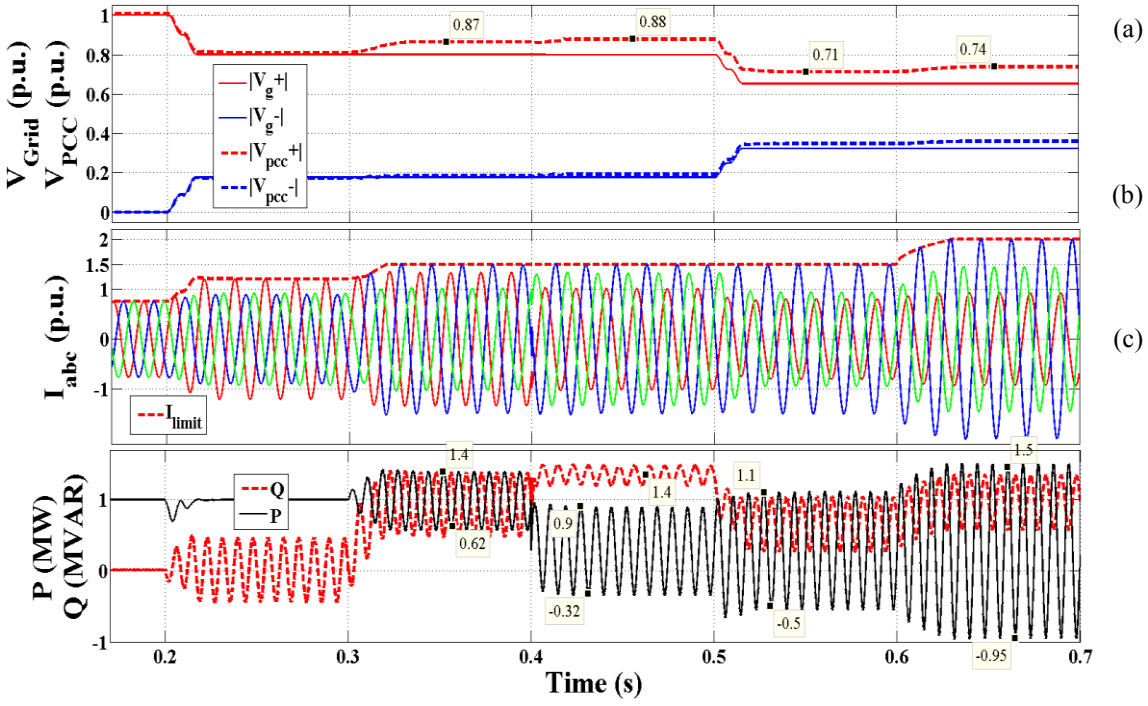

Fig 4.14. Case B – PNSC strategy: (a) pos/neg-sequences of grid and PCC voltages, (b) injected currents, (c) instantaneous active/reactive powers

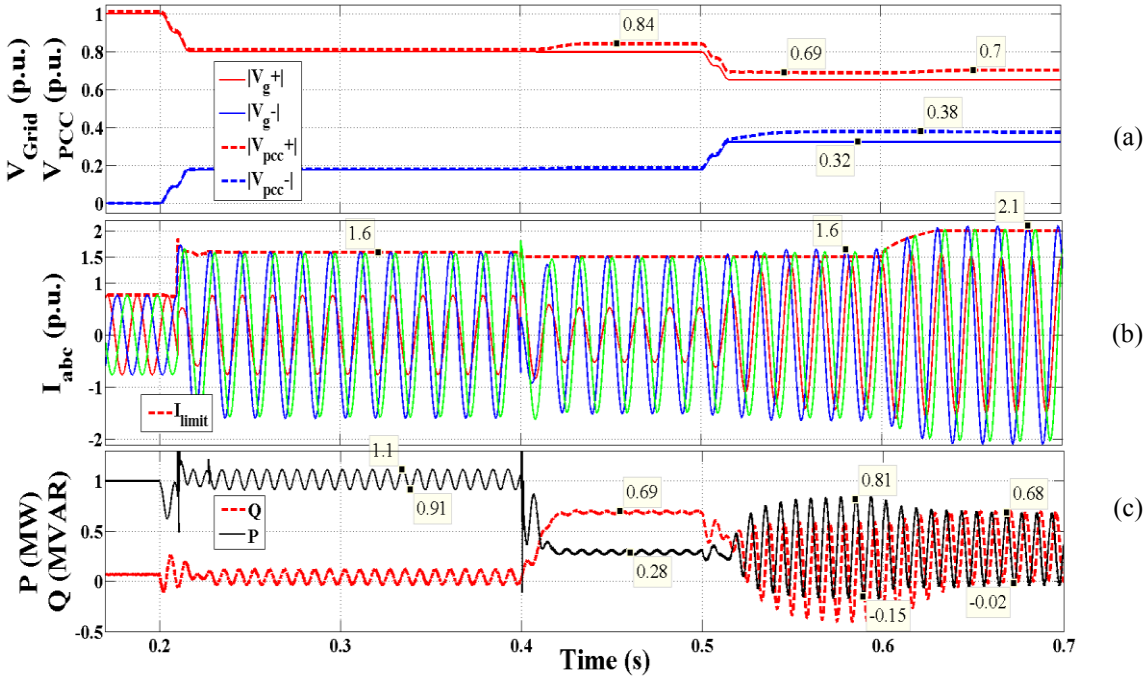

Fig 4.15. Case B – ZSCI strategy: (a) pos/neg-sequences of grid and PCC voltages, (b) injected currents, (c) instantaneous active/reactive powers

Fig 4.13 illustrates the simulation results of ICPS strategy in test case B. As Fig 4.13-(b) shows, the injected non-sinusoidal currents are equal or less than I^*_{limit} by applying the MARPD formula for the ICPS strategy presented in (4.49). As Fig 4.13-(c) illustrates, the maximum allowable reactive power is obtained successfully for each of the four fault conditions. The positive PCC voltage boost can be seen in Fig 4.13-(a) which is less than that of the BPSC strategy under the same fault conditions and same reference values. The voltage boost is 0.08 p.u. from t_5 to t_7 and from t_9 to t_{11}. Furthermore, the values of oscillations on the instantaneous active power in BPSC are depicted in Fig 4.13-(c). For instance, $\tilde{p}_{\max}$ reaches 0.6 MW after t_9).

Fig 4.14 and Fig 4.15 show the simulation results of PNSC and ZSCI strategies in test case B. As Fig 4.14-(b) indicates, the injected unbalanced currents are limited to the I^*_{limit} by applying the MARPD equation for the PNSC strategy presented in (4.52). However, the injected currents of ZSCI strategy depicted in Fig 4.15-(b) are a little greater than I^*_{limit} in some conditions. One of the reasons for this small inaccuracy is the

simplifications made in the ZSCI strategy (i.e. using simplified equations of (3.28) instead of applying the accurate complex equations of (3.27)). Another reason is the inability of the inverter in delivering 0.3 MW active power, riding through the severe fault by ZSCI strategy, and respecting the imposed I^{*}_{limit} simultaneously. Therefore, ZSCI strategy loses its performance and objective (which is delivering non-oscillatory instantaneous active/reactive powers) under the severe voltage dip and in the case of having a limit for injected currents, as it can be seen in Fig 4.15-(b) and Fig 4.15-(c).

4.6 Conclusion

This chapter presented the analytical evaluations and mathematical assessments of all UPD-LVRT-RCG strategies in gird connected converter-based DER units. These strategies aim to provide a proper set of reference-currents in order to have power delivery continuance under different faulty voltage conditions. This chapter introduced and presented three most important parameters of these strategies for a comprehensive evaluation. Oscillation values on instantaneous active/reactive powers and maximum phase currents are three most important terms related to each strategy. Based on the obtained formulas for the maximum phase currents in each strategy, the maximum allowable reactive power delivery, i.e. MARPD method, formulas were proposed specifically for each of the six UPD-LVRT-RCG strategies. The MARPD method aims to provide the best support for the PCC voltage and simultaneously respect the maximum limit for the phase currents (specified by DER owners) under different faults. Simulation results under different fault conditions and altered reference commands were carried out for each strategy. The simulation results showed the accuracy and effectiveness of the proposed formulas of the MARPD method for each strategy.

Chapter 5

Mathematical Assessment, Performance Evaluation, and MARPD Method II: FVS-LVRT-RCG Techniques

5.1 Introduction

Chapter 3 evaluated and studied two groups of LVRT-RCG strategies in grid connected CI-DER units introduced by [43]-[47] which are named as UPD [43]-[45] and FVS [43], [46]-[47] strategies in this thesis. The second group contains three strategies; i.e. FPNSC [43], FBSS [46] and MFBSS [47] which intend to provide a flexible support to the PCC voltage by injecting controlled positive and negative sequences currents. The analytical evaluations, mathematical assessments and performance evaluations of three strategies of the second group are the scope of this chapter.

In Chapter 4, mathematical expressions of $\tilde{p}_{\max}$, $\tilde{q}_{\max}$ and I_{max} of the first group were formulated and their performance comparisons were accomplished under several fault and reference commands conditions. Also, the expressions of the maximum allowable reactive power, Q_{max}, for each of the six strategies of the first group were found. This method is named MARPD and it aims to provide the best support for the PCC voltage (either boost the voltage magnitudes or reduce the voltage imbalances) by injecting the

Q_{max} under a pre-specified and important limitation, I_{limit}. Three FVS strategies are studied, simulated and briefly compared in Chapter 3. However, in terms of their practical applications, their complete analytical evaluations and precise mathematical assessments are exceedingly crucial. This chapter finds the expressions of $\tilde{p}_{\max}$, $\tilde{q}_{\max}$ and I_{max} of these three techniques for their thorough analytical evaluations and reasonable comparisons. Later, the MARPD equations for each of the three FVS strategies are found.

The accurate mathematical equations of $\tilde{p}$ and $\tilde{q}$ for the FBSS strategy, as well as the $\tilde{p}$ expression for the FPNSC strategy are currently available in [46] and [43], respectively, which are reported in Section 5.2. However, the equations of $\tilde{p}$ for FPNSC and the expressions of $\tilde{p}$ and $\tilde{q}$ for FBSS are missing in the literature which are calculated in this chapter based on the instantaneous power theories]311[-]311[, and presented in Sections 5.2.1 and 5.2.3. In addition, the mathematical equation of I_{max} is not available for MFBSS and the I_{max} of the FBSS, presented in [46], is not correct. Therefore, the equations of I_{max} for FBSS and MFBSS strategies are calculated and presented in Sections 5.3.2 and 5.3.3. Using the equations of Section 5.3, it is very useful to obtain the maximum allowable reactive power, Q_{max}, which the converter can deliver to the grid under grid faults without passing the maximum allowable instantaneous phase current limit, I_{limit}, imposed by DG owners. The mathematical equations of Q_{max} under various conditions (i.e. different fault types, various voltage dip characteristics, several system parameters, different operating points, various strategies parameters, etc.) for all three FVS strategies are obtained and presented in Section 5.4. Simulation results for different fault conditions and reference commands values are carried out, in Section 5.5, to verify the accuracy of the calculated expressions and effectiveness of the MARPD formulas.

5.2 Mathematical Equations of Instantaneous Active/Reactive Power Oscillation Terms

In this section, the equations of $\tilde{p}$ and $\tilde{q}$ for three FVS-LVRT-RCG strategies are presented using the instantaneous power theories [133]-[134]. Chapter 4 presented the total reference-current in terms of active/reactive and positive/negative components. Also, the well-known equations of the instantaneous active/reactive powers thoroughly studied in terms of the average components, *P* and *Q*, an oscillation terms, $\tilde{p}$ and $\tilde{q}$. The dot (and cross) product(s) of the voltage and current vectors at the same sequences will result in *P* (and Q). However, their dot (and cross) product(s) in the opposite sequences will give rise to $\tilde{p}$ (and $\tilde{q}$). Also, it is studied in chapter 4 that instantaneous active/reactive powers can be divided into its oscillatory terms one oscillating by $\sin(2\omega t)$ and one oscillating with $\cos(2\omega t)$. Therefore, the general equations for the instantaneous active and reactive power can be summarized as:

$$p = v.i = \underbrace{v^{+}.i^{+} + v^{-}.i^{-}}_{P} + \underbrace{v^{+}.i^{-} + v^{-}.i^{+}}_{\tilde{p}} = P + \underbrace{P_{s2}\sin(2\omega t) + P_{c2}\cos(2\omega t)}_{\tilde{p}} \tag{5.1}$$

$$q = |v \times i| = v_{\perp}.i = \underbrace{v_{\perp}^{+}.i^{+} + v_{\perp}^{-}.i^{-}}_{Q} + \underbrace{v_{\perp}^{+}.i^{-} + v_{\perp}^{-}.i^{+}}_{\tilde{q}} = Q + \underbrace{Q_{s2}\sin(2\omega t) + Q_{c2}\cos(2\omega t)}_{\tilde{q}} \tag{5.2}$$

Table 5.1 demonstrate the available $\tilde{p}$ and $\tilde{q}$ expressions in the literature. As Table 5.1 states, $\tilde{p}$ and $\tilde{q}$ expressions are provided for the FBSS strategy in [46]. Also the $\tilde{p}$ expression of the FPNSC strategy is correctly presented in [43]. It was mentioned earlier, in Chapter 4, that the expressions of $\tilde{p}_{\max}$ and $\tilde{q}_{\max}$ are more useful than the expressions of their instantaneous values, i.e. $\tilde{p}$ and $\tilde{q}$, where:

$$\tilde{p}_{\max} = |\tilde{p}| = \sqrt{{P_{s2}}^2 + {P_{c2}}^2} \tag{5.3}$$

$$\tilde{q}_{\max} = |\tilde{q}| = \sqrt{{Q_{s2}}^2 + {Q_{c2}}^2} \tag{5.4}$$

Hence, this thesis tries to extract and present the useful expressions of $\tilde{p}_{\max}$ and $\tilde{q}_{\max}$. Another point highlighted in the previous chapter is to represent the expressions of $\tilde{p}_{\max}$ and $\tilde{q}_{\max}$ in terms of scalar parameters (specifically in terms of $|v^+|$, $|v^-|$, P and Q) rather than vector terms (as for instance, voltage vector of v_α^- and current vector of i_α^+).

TABLE 5.1. Available expressions for oscillation terms of instantaneous active and reactive powers of FVS-LVRT-RCG strategies

	$\tilde{p}$	$\tilde{q}$
FPNSC	$\left[\frac{k_1 P}{\lvert v^+ \rvert^2} + \frac{(1-k_1)P}{\lvert v^- \rvert^2}\right] v^+ . v^- + \ldots$ $\ldots + \left[\frac{k_2 Q}{\lvert v^+ \rvert^2} - \frac{(1-k_2)Q}{\lvert v^- \rvert^2}\right] v_\perp^+ . v^-$ [43]	NA
FBSS	$\frac{3}{2}(v_\alpha^- i_\alpha^+ + v_\beta^- i_\beta^+ + v_\alpha^+ i_\alpha^- + v_\beta^+ i_\beta^-)$ [46]	$\frac{3}{2}(-v_\alpha^- i_\beta^+ + v_\beta^- i_\alpha^+ - v_\alpha^+ i_\beta^- + v_\beta^+ i_\alpha^-)$ [46]
MFBSS	NA	NA

Available and correct in literature Not available in literature

5.2.1 $\tilde{p}_{\max}$ and $\tilde{q}_{\max}$ of FPNSC

Applying the instantaneous power theories and using (3.29)-(3.31), the instantaneous active and reactive powers can be achieved as:

$$p = \underbrace{k_1\, G^+ v^+ .v^+ + (1-k_1)\, G^- v^- .v^-}_{P} + \ldots$$
$$\ldots + \underbrace{\left[k_1\, G^+ + (1-\mathrm{k}_1)\, G^-\right] v^+ .v^- + \left[k_2\, B^+ - (1-\mathrm{k}_2)\, B^-\right] v_\perp^+ .v^-}_{\tilde{p}} \tag{5.5}$$

$$q = \underbrace{k_2\, B^+ v^+ .v^+ + (1-k_2)\, B^- v^- .v^-}_{Q} + \ldots$$
$$\ldots + \underbrace{\left[k_2\, B^+ + (1-\mathrm{k}_2)\, B^-\right] v^+ .v^- + \left[-k_1\, G^+ + (1-\mathrm{k}_1)\, G^-\right] v_\perp^+ .v^-}_{\tilde{q}} \tag{5.6}$$

Then, substituting v^+, v^- and $v_\perp^+$ from (4.9)-(4.10) and G^+, G^-, B^+, and B^- from (3.31) will result in:

$$\tilde{p} = \underbrace{\left[-k_1 nP - (1-\mathrm{k}_1)\, Pn^{-1}\right]\cos(2\omega \mathrm{t})}_{\tilde{p}_{c2}} + \underbrace{\left[k_2 nQ - (1-\mathrm{k}_2)\, Qn^{-1}\right]\sin(2\omega \mathrm{t})}_{\tilde{p}_{s2}} \tag{5.7}$$

$$\tilde{q} = \underbrace{\left[-k_2 nQ - (1-k_2)\, Qn^{-1}\right]\cos(2\omega \mathrm{t})}_{\tilde{q}_{c2}} + \underbrace{\left[-k_1 nP + (1-k_1)\, Pn^{-1}\right]\sin(2\omega \mathrm{t})}_{\tilde{q}_{s2}} \tag{5.8}$$

So:

$$\tilde{p}_{\max} = \sqrt{P^2\left[-k_1 n - (1-k_1)\, n^{-1}\right]^2 + Q^2\left[k_2 n - (1-k_2)\, n^{-1}\right]^2} \tag{5.9}$$

$$\tilde{q}_{\max} = \sqrt{Q^2\left[-k_2 n - (1-k_2)\, n^{-1}\right]^2 + P^2\left[-k_1 n + (1-k_1)\, n^{-1}\right]^2} \tag{5.10}$$

5.2.2 $\tilde{p}_{\max}$ and $\tilde{q}_{\max}$ of FBSS

According to the instantaneous power theories and taking (3.10) and (3.34)-(3.35) into account, the instantaneous active and reactive powers can be achieved as:

$$p = \underbrace{\frac{3}{2}(v_\alpha^+ i_\alpha^+ + v_\beta^+ i_\beta^+)}_{p^+ = P} + \underbrace{\frac{3}{2}(v_\alpha^- i_\alpha^- + v_\beta^- i_\beta^-)}_{p^- = 0} + \underbrace{\frac{3}{2}(v_\alpha^- i_\alpha^+ + v_\beta^- i_\beta^+ + v_\alpha^+ i_\alpha^- + v_\beta^+ i_\beta^-)}_{\tilde{p} = P_{c2}\cos(2\omega t) + P_{s2}\sin(2\omega t)} \tag{5.11}$$

$$q = \underbrace{\frac{3}{2}(-v_\alpha^+ i_\beta^+ + v_\beta^+ i_\alpha^+)}_{q^+} + \underbrace{\frac{3}{2}(-v_\alpha^- i_\beta^- + v_\beta^- i_\alpha^-)}_{q^-} + \underbrace{\frac{3}{2}(-v_\alpha^- i_\beta^+ + v_\beta^- i_\alpha^+ - v_\alpha^+ i_\beta^- + v_\beta^+ i_\alpha^-)}_{\tilde{q} = Q_{s2}\ sin(2\omega t) + Q_{c2}\ cos(2\omega t)} \tag{5.12}$$

Then, substituting v_α^+, v_β^+, v_α^-, and v_β^- from (4.9)-(4.10) and i_α^+, i_β^+, i_α^-, and i_β^- from (3.10) and (3.34)-(3.35) will result in:

$$\tilde{p} = n\,P\cos(2\omega t) + \frac{2k^+ - 1}{k^+ + n^2 k^-}\,n\,Q\sin(2\omega t) \tag{5.13}$$

$$\tilde{q} = -\,n\,P\,sin(2\omega t) + \frac{1}{k^+ + n^2 k^-}\,n\,Q\,cos(2\omega t) \tag{5.14}$$

$$q^+ = \frac{k^+}{k^+ + n^2 k^-} Q \tag{5.15}$$

$$q^- = \frac{n^2 k^-}{k^+ + n^2 k^-} Q \tag{5.16}$$

So:

$$\tilde{p}_{\max} = n\sqrt{P^2 + Q^2\left[\frac{2k^+ - 1}{k^+ + n^2 k^-}\right]^2} \tag{5.17}$$

$$\tilde{q}_{\max} = n\sqrt{P^2 + Q^2\left[\frac{1}{k^+ + n^2 k^-}\right]^2} \tag{5.18}$$

5.2.3 $\tilde{p}_{\max}$ and $\tilde{q}_{\max}$ of MFBSS

According to (5.11)-(5.12) and substituting v_α^+, v_β^+, v_α^-, and v_β^- from (4.9)-(4.10) and i_α^+, i_β^+, i_α^-, and i_β^- from (3.38) -(3.41) will result in:

$$\begin{aligned} p = P + P\left\{\left(k^+ + \frac{k^- R}{\sqrt{R^2+X^2}}\right)\Big/\left(k^+ + \frac{k^- R}{\sqrt{R^2+X^2}}\, n^2\right)\right\} n \times \cos(2\omega t) \\ + Q\left\{\left(k^+ - \frac{k^- X}{\sqrt{R^2+X^2}}\right)\Big/\left(k^+ + \frac{k^- X}{\sqrt{R^2+X^2}}\, n^2\right)\right\} n \times \sin(2\omega t) \end{aligned} \tag{5.19}$$

$$\begin{aligned} q = Q + Q\left\{\left(k^+ + \frac{k^- X}{\sqrt{R^2+X^2}}\right)\Big/\left(k^+ + \frac{k^- X}{\sqrt{R^2+X^2}}\, n^2\right)\right\} n \times \cos(2\omega t) \\ + P\left\{\left(-k^+ + \frac{k^- R}{\sqrt{R^2+X^2}}\right)\Big/\left(k^+ + \frac{k^- R}{\sqrt{R^2+X^2}}\, n^2\right)\right\} n \times \sin(2\omega t) \end{aligned} \tag{5.20}$$

Then,

$$\tilde{p}_{\max} = \sqrt{{P_{s2}}^2 + {P_{c2}}^2} \quad where \quad \begin{cases} P_{c2} = \dfrac{Pn\left(k^+ + \dfrac{k^- R}{\sqrt{R^2+X^2}}\right)}{k^+ + \dfrac{k^- R}{\sqrt{R^2+X^2}}\, n^2} \\ P_{s2} = \dfrac{Qn\left(k^+ - \dfrac{k^- X}{\sqrt{R^2+X^2}}\right)}{k^+ + \dfrac{k^- X}{\sqrt{R^2+X^2}}\, n^2} \end{cases} \tag{5.21}$$

$$\tilde{q}_{\max}=\sqrt{{Q_{s2}}^2+{Q_{c2}}^2}\quad where\quad \begin{cases} Q_{c2}=\dfrac{Qn\left(k^{+}+\dfrac{k^{-}X}{\sqrt{R^2+X^2}}\right)}{k^{+}+\dfrac{k^{-}X}{\sqrt{R^2+X^2}}n^2} \\ Q_{s2}=\dfrac{Pn\left(-k^{+}+\dfrac{k^{-}R}{\sqrt{R^2+X^2}}\right)}{k^{+}+\dfrac{k^{-}R}{\sqrt{R^2+X^2}}n^2} \end{cases} \tag{5.22}$$

5.3 Mathematical Equations of Maximum Instantaneous Phase Currents

Chapter 4 provided a systematic procedure to find the maximum instantaneous phase currents of any LVRT-RCG strategy. Therefore, the general equation of (4.38) was obtained which is repeated here and gives the maximum instantaneous current values in each of *abc* phases under different situations:

$$\begin{bmatrix} I^2_{\max-a} \\ I^2_{\max-b} \\ I^2_{\max-c} \end{bmatrix}=\begin{bmatrix} (gV_1)^2+(bV_2)^2 \\ (-\frac{1}{2}gV_1+\frac{\sqrt{3}}{2}bV_1)^2+(\frac{1}{2}bV_2+\frac{\sqrt{3}}{2}gV_2)^2 \\ (-\frac{1}{2}gV_1-\frac{\sqrt{3}}{2}bV_1)^2+(\frac{1}{2}bV_2-\frac{\sqrt{3}}{2}gV_2)^2 \end{bmatrix} \tag{5.23}$$

$$where\quad \begin{cases} V_1=V_p-V_n \\ V_2=V_p+V_n \end{cases}$$

also V_p and V_n are voltage magnitudes of the positive and negative sequences voltages, respectively. Moreover, g and b are generic conductance and susceptance, respectively, which can be replaced by specific conductance and susceptance expressions of each LVRT-RCG strategy.

5.3.1 Equations of Maximum Instantaneous Phase Currents in FPNSC

The reference current in FPNSC can be written as:

$$i^{*} = k_1\, g^{+}\, v^{+} + (1-k_1)\, g^{-}\, v^{-} + k_2\, b^{+}\, v_{\perp}^{+} + (1-k_2)\, b^{-}\, v_{\perp}^{-} \tag{5.24}$$

As also stated in section 4.2.1, the voltage under unbalanced condition can be represented as:

$$v^{+} = \begin{bmatrix} v_{\alpha}^{+} \\ v_{\beta}^{+} \end{bmatrix} = \begin{bmatrix} V_p \cos(\omega \mathrm{t}) \\ V_p \sin(\omega \mathrm{t}) \end{bmatrix} \quad v^{-} = \begin{bmatrix} v_{\alpha}^{-} \\ v_{\beta}^{-} \end{bmatrix} = \begin{bmatrix} -V_n \cos(\omega \mathrm{t}) \\ V_n \sin(\omega \mathrm{t}) \end{bmatrix} \tag{5.25}$$

$$v^{+}{}_{\perp} = \begin{bmatrix} v_{\perp\alpha}^{+} \\ v_{\perp\beta}^{+} \end{bmatrix} = \begin{bmatrix} -V_p \sin(\omega \mathrm{t}) \\ V_p \cos(\omega \mathrm{t}) \end{bmatrix} \quad v^{-}{}_{\perp} = \begin{bmatrix} v_{\perp\alpha}^{-} \\ v_{\perp\beta}^{-} \end{bmatrix} = \begin{bmatrix} -V_n \sin(\omega \mathrm{t}) \\ -V_n \cos(\omega \mathrm{t}) \end{bmatrix} \tag{5.26}$$

Therefore, the injected current under the fault can be rewritten in $\alpha\beta$ reference frame using (5.24)-(5.26):

$$\begin{bmatrix} i_{\alpha} \\ i_{\beta} \end{bmatrix} = \begin{bmatrix} \left\{k_1 g^{+} V_p - (1-k_1) g^{-} V_n\right\} \cos(\omega t) \;\cdots \\ \qquad \cdots \;\; -\left\{k_2 b^{+} V_p + (1-k_2) b^{-} V_n\right\} \sin(\omega t) \\ \left\{k_1 g^{+} V_p + (1-k_1) g^{-} V_n\right\} \sin(\omega t) \;\cdots \\ \qquad \cdots \;\; +\left\{k_2 b^{+} V_p - (1-k_2) b^{-} V_n\right\} \cos(\omega t) \end{bmatrix} \tag{5.27}$$

To transform the $\alpha\beta$ currents of (5.27) into the *abc* current, the transformation matrix of (4.37) is used, and the maximum phase currents will be obtained as:

$$\begin{bmatrix} I^2_{\text{max-a-FPNSC}} \\ I^2_{\text{max-b-FPNSC}} \\ I^2_{\text{max-c-FPNSC}} \end{bmatrix} = \begin{bmatrix} (K_1)^2 + (K_2)^2 \\ (-\frac{1}{2}K_1 + \frac{\sqrt{3}}{2}K_4)^2 + (\frac{1}{2}K_2 + \frac{\sqrt{3}}{2}K_3)^2 \\ (-\frac{1}{2}K_1 - \frac{\sqrt{3}}{2}K_4)^2 + (\frac{1}{2}K_2 - \frac{\sqrt{3}}{2}K_3)^2 \end{bmatrix} \tag{5.28}$$

where,

$$\begin{cases} K_1 = k_1 g^+ V_p - (1-k_1) g^- V_n \\ K_2 = k_2 b^+ V_p + (1-k_2) b^- V_n \\ K_3 = k_1 g^+ V_p + (1-k_1) g^- V_n \\ K_4 = k_2 b^+ V_p - (1-k_2) b^- V_n \end{cases} \tag{5.29}$$

5.3.2 Equations of Maximum Instantaneous Phase Currents in FBSS

In the FBSS strategy, the total reference current is:

$$i^* = g\, v^+ + k\, b\, v_\perp^+ + (1-k)\, b\, v_\perp^- \tag{5.30}$$

Then based on (5.25)-(5.26), injected *αβ* currents under the fault can be rewritten as:

$$\begin{bmatrix} i_\alpha \\ i_\beta \end{bmatrix} = \begin{bmatrix} \{gV_p\}\cos(\omega t) - \{kbV_p + (1-k)bV_n\}\sin(\omega t) \\ \{gV_p\}\sin(\omega t) + \{kbV_p - (1-k)bV_n\}\cos(\omega t) \end{bmatrix} \tag{5.31}$$

To transform these *αβ* currents into the *abc* phase currents, the transformation matrix of (4.37) is applied, and the maximum phase currents can be calculated as:

$$\begin{bmatrix} I^2_{\text{max-a-FBSS}} \\ I^2_{\text{max-b-FBSS}} \\ I^2_{\text{max-c-FBSS}} \end{bmatrix} = \begin{bmatrix} (K_1')^2 + (K_2')^2 \\ (-\frac{1}{2}K_1' + \frac{\sqrt{3}}{2}K_4')^2 + (\frac{1}{2}K_2' + \frac{\sqrt{3}}{2}K_3')^2 \\ (-\frac{1}{2}K_1' - \frac{\sqrt{3}}{2}K_4')^2 + (\frac{1}{2}K_2' - \frac{\sqrt{3}}{2}K_3')^2 \end{bmatrix} \tag{5.32}$$

where,

$$\begin{cases} K_1' = K_3' = gV_p \\ K_2' = kbV_p + (1-k)bV_n \\ K_4' = kbV_p - (1-k)bV_n \end{cases} \tag{5.33}$$

5.3.3 Equations of Maximum Instantaneous Phase Currents in MFBSS

The total reference current and its form in $\alpha\beta$ reference frame in the MFBSS strategy are as follows:

$$\begin{cases} i^* = g\,k\,v^+ + g\,R'(1-k)\,v^- + b\,k\,v_\perp^+ + b\,X'(1-k)\,v_\perp^- \\ R' = R\Big/\sqrt{R^2+X^2} \quad , \quad X' = X\Big/\sqrt{R^2+X^2} \end{cases} \tag{5.34}$$

$$\begin{bmatrix} i_\alpha \\ i_\beta \end{bmatrix} = \begin{bmatrix} \left\{ g\,kV_p - g(1-k)R'V_n \right\} \cos(\omega t) \;\cdots \\ \qquad \cdots \; - \left\{ b\,kV_p + b(1-k)X'V_n \right\} \sin(\omega t) \\ \left\{ g\,kV_p + g(1-k)R'V_n \right\} \sin(\omega t) \;\cdots \\ \qquad \cdots \; + \left\{ b\,kV_p - b(1-k)X'V_n \right\} \cos(\omega t) \end{bmatrix} \tag{5.35}$$

The *abc* phase currents are easily obtained similar to the previous strategies, using the transformation matrix of (3.37). Therefore, the maximum phase currents are achieved as:

$$\begin{bmatrix} I^2_{\text{max-a-MFBSS}} \\ I^2_{\text{max-b-MFBSS}} \\ I^2_{\text{max-c-MFBSS}} \end{bmatrix} = \begin{bmatrix} (K_1'')^2 + (K_2'')^2 \\ (-\frac{1}{2}K_1'' + \frac{\sqrt{3}}{2}K_4'')^2 + (\frac{1}{2}K_2'' + \frac{\sqrt{3}}{2}K_3'')^2 \\ (-\frac{1}{2}K_1'' - \frac{\sqrt{3}}{2}K_4'')^2 + (\frac{1}{2}K_2'' - \frac{\sqrt{3}}{2}K_3'')^2 \end{bmatrix} \tag{5.36}$$

where,

$$\begin{cases} K_1'' = g\,kV_p - g(1-k)R'V_n \\ K_2'' = b\,kV_p + b(1-k)X'V_n \\ K_3'' = g\,kV_p + g(1-k)R'V_n \\ K_4'' = b\,kV_p - b(1-k)X'V_n \end{cases} \tag{5.37}$$

TABLE 5.2 Available and obtained expressions of I_{max} of FVS-LVRT-RCG strategies

	I_{max} expressions in the literature	I_{max} s obtained in this thesis*
FPNSC	$\sqrt{a\,P^2 + b\,Q^2 - c\,P\,Q}$ where: $a = \frac{k_1^2}{\lvert v^+ \rvert^2} + \frac{(1-k_1)^2}{\lvert v^- \rvert^2} + \frac{2k_1(1-k_1).\cos 2\gamma}{\lvert v^+ \rvert.\lvert v^- \rvert}$, $b = \frac{k_2^2}{\lvert v^+ \rvert^2} + \frac{(1-k_2)^2}{\lvert v^- \rvert^2} + \frac{-2k_2(1-k_2).\cos 2\gamma}{\lvert v^+ \rvert.\lvert v^- \rvert}$, $c = \frac{(2k_1 + 2k_2 - 4k_1k_2)^2.\sin 2\gamma}{\lvert v^+ \rvert.\lvert v^- \rvert}$	$\begin{cases} K_1 = k_1\frac{P}{V_p} - (1-k_1)\frac{P}{V_n} \\ K_2 = k_2\frac{Q}{V_p} + (1-k_2)\frac{Q}{V_n} \\ K_3 = k_1\frac{P}{V_p} + (1-k_1)\frac{P}{V_n} \\ K_4 = k_2\frac{Q}{V_p} - (1-k_2)\frac{Q}{V_n} \end{cases}$
FBSS	$I_a = \sqrt{(x\,P)^2 + (y\,Q)^2}$ $I_b = \frac{1}{2}\sqrt{(-xP + \sqrt{3}zQ)^2 + (-yQ + \sqrt{3}xP)^2}$ $I_c = \frac{1}{2}\sqrt{(-xP - \sqrt{3}zQ)^2 + (-yQ - \sqrt{3}xP)^2}$ where: $x = \frac{2}{3}\frac{1}{\lvert v^+ \rvert}$, $y = \frac{2}{3}\frac{k.\lvert v^+ \rvert - (1-k).\lvert v^- \rvert}{k.\lvert v^+ \rvert^2 + (1-k).\lvert v^- \rvert^2}$ $z = \frac{2}{3}\frac{-k.\lvert v^+ \rvert - (1-k).\lvert v^- \rvert}{k.\lvert v^+ \rvert^2 + (1-k).\lvert v^- \rvert^2}$	$\begin{cases} K_1' = K_3' = \frac{P}{V_p} \\ K_2' = \frac{kV_p + (1-k)V_n}{kV_p^2 + (1-k)V_n^2}Q \\ K_4' = \frac{kV_p - (1-k)V_n}{kV_p^2 + (1-k)V_n^2}Q \end{cases}$
MFBSS	NA	$\begin{cases} K_1'' = \frac{kV_p - (1-k)\frac{R}{\sqrt{R^2+X^2}}V_n}{kV_p^2 + \frac{R}{\sqrt{R^2+X^2}}(1-k)V_n^2}P \\ K_2'' = \frac{kV_p + (1-k)\frac{X}{\sqrt{R^2+X^2}}V_n}{kV_p^2 + \frac{X}{\sqrt{R^2+X^2}}(1-k)V_n^2}Q \\ K_3'' = \frac{kV_p + (1-k)\frac{R}{\sqrt{R^2+X^2}}V_n}{kV_p^2 + \frac{R}{\sqrt{R^2+X^2}}(1-k)V_n^2}P \\ K_4'' = \frac{kV_p - (1-k)\frac{X}{\sqrt{R^2+X^2}}V_n}{kV_p^2 + \frac{X}{\sqrt{R^2+X^2}}(1-k)V_n^2}Q \end{cases}$

Correct and available in literature Not available in literature Incorrect in literature

* All I_{max} expressions of FVS strategies are in the similar form of (5.28), (5.32), or (5.36); and it is just needed to replace the specific K_1, K_2, K_3 and K_4 values for each of the three strategies from the Table.

5.4 Calculation of the Maximum Allowable Reactive Powers; MARPD Equations

In this section, the maximum allowable reactive power expressions (Q_{max}) or MARPD equations are proposed and calculated for each of the three FVS-LVRT-RCG strategies based on the aforementioned I_{max} equations in the previous sections.

Using (5.28)-(5.29), the equation of Q_{max} in the FPNSC strategy is calculated as:

$$\begin{bmatrix} Q_1^{FPNSC} \\ Q_2^{FPNSC} \\ Q_3^{FPNSC} \end{bmatrix} = \begin{bmatrix} \dfrac{V_p V_n \sqrt{I_{\max}^2 - K_1^2}}{k_2 V_n + (1-k_2)V_p} \\ \dfrac{-b + \sqrt{b^2 - 4ac}}{2a} \\ \dfrac{b + \sqrt{b^2 - 4ac}}{2a} \end{bmatrix} \tag{5.38}$$

$$\begin{cases} a = 3(\dfrac{k_2}{V_p} - \dfrac{1-k_2}{V_n})^2 + (\dfrac{k_2}{V_p} + \dfrac{1-k_2}{V_n})^2 \\ b = 2\sqrt{3}\left[K_3(\dfrac{k_2}{V_p} + \dfrac{1-k_2}{V_n}) - K_1(\dfrac{k_2}{V_p} - \dfrac{1-k_2}{V_n}) \right] \\ c = K_1^2 + 3K_3^2 - 4I_{\max}^2 \end{cases} \tag{5.39}$$

However, just one of the obtained Qs is correct where all of the three phase-currents remain under the pre-specified I_{limit} value. Hence, Q_{max} of the AARC strategy will be given to the inverter controllers according to the following expression:

$$Q_{\max} = \min(Q_1, Q_2, Q_3) \tag{5.40}$$

Using (5.32)-(5.33), the equation of Q_{max} in the FBSS strategy can be expanded as:

$$\begin{bmatrix} Q_1^{FBSS} \\ Q_2^{FBSS} \\ Q_3^{FBSS} \end{bmatrix} = \begin{bmatrix} \dfrac{(kV_p^2+(1-k)V_n^2)\sqrt{I_{\max}^2-K_1'^2}}{kV_p+(1-k)V_n} \\ \dfrac{-b+\sqrt{b^2-4ac}}{2a} \\ \dfrac{b+\sqrt{b^2-4ac}}{2a} \end{bmatrix} \tag{5.41}$$

$$\begin{cases} a = 3(\dfrac{kV_p-(1-k)V_n}{kV_p^2+(1-k)V_n^2})^2+(\dfrac{kV_p+(1-k)V_n}{kV_p^2+(1-k)V_n^2})^2 \\ b = 2\sqrt{3}\left[K_3'\dfrac{kV_p+(1-k)V_n}{kV_p^2+(1-k)V_n^2}-K_1'\dfrac{kV_p-(1-k)V_n}{kV_p^2+(1-k)V_n^2}\right] \\ c = 4(\dfrac{P^2}{V_p^2}-I_{\max}^2) \end{cases} \tag{5.42}$$

Finally, using (5.36)-(5.37), the equation of Q_{max} in the MFBSS strategy can be similarly calculated as:

$$\begin{bmatrix} Q_1^{MFBSS} \\ Q_2^{MFBSS} \\ Q_3^{MFBSS} \end{bmatrix} = \begin{bmatrix} \dfrac{(kV_p^2+(1-k)X'V_n^2)\sqrt{I_{\max}^2-K_1''^2}}{kV_p+(1-k)X'V_n} \\ \dfrac{-b+\sqrt{b^2-4ac}}{2a} \\ \dfrac{b+\sqrt{b^2-4ac}}{2a} \end{bmatrix} \tag{5.43}$$

$$\begin{cases} a = 3(\dfrac{kV_p-(1-k)X'V_n}{kV_p^2+(1-k)X'V_n^2})^2+(\dfrac{kV_p+(1-k)X'V_n}{kV_p^2+(1-k)X'V_n^2})^2 \\ b = 2\sqrt{3}\dfrac{kV_p(K_3''-K_1'')+(1-k)X'V_n(K_3''+K_1'')}{kV_p^2+(1-k)X'V_n^2} \\ c = K_1''^2+3K_3''^2-4I_{\max}^2) \end{cases} \tag{5.44}$$

5.5 Simulation Results

To verify the mathematical expressions obtained in Sections 5.2, 5.3 and 5.4, two test cases are studied and implemented in the same system of the previous chapter. The desired voltage dip shown in Fig 5.1 is realized using three ac voltage sources of the system presented in Chapter 4.

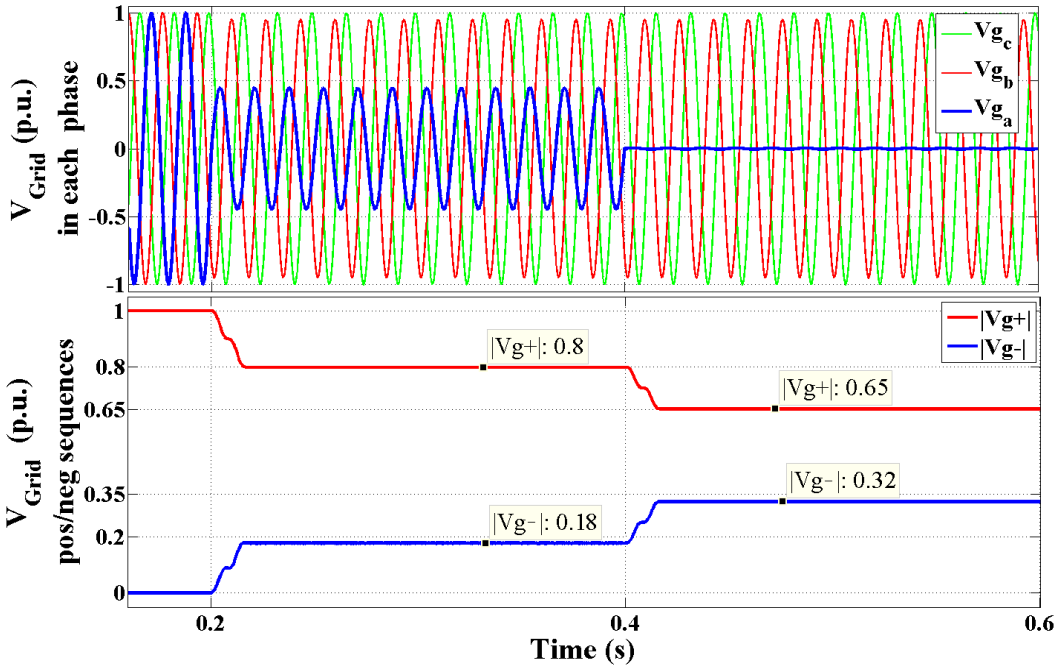

Fig 5.1. Emulated fault: (a) grid voltage in *abc* phases, and (b) positive and negative-sequences of the grid voltage.

5.5.1 Test Case A: Instantaneous Active and Reactive Powers Oscillations and Maximum Phase Currents

This section presents the simulation results of each FVS-LVRT-RCG strategy under grid faults, where a single-phase-to-ground fault is emulated after t_1=0.2s, and the grid voltage, V_{Grid}, becomes deteriorated as indicated in Fig 5.1. Between t_1=0.2s and t_5=0.4s,

a moderate voltage dip is emulated where Vg+=0.8 p.u. and Vg- =0.18 p.u. as indicated in Fig 5.1. In addition, similar to Chapter 4, a more severe voltage dip is emulated between t_5=0.4s and t_{10}=0.65s where Vg+=0.65 p.u. and Vg- =0.32 p.u. as shown in Fig 5.1. In this test case, P^* is set to be 1 MW until t_3=0.3s and 0.3 MW after t_3. Also, Q^* is set to be 0.7 MVAR until t_7=0.5s and 1 MVAR after t_7. The proportional resonant (PR) control is used in the $\alpha\beta$ reference frame for the converter current regulation.

TABLE 5.3. Specified Active/Reactive Powers Commands and Fault Characteristics – Case A

P^* (t_0=0s to t_3=0.3s)	1 MW	P^* (t_3=0.3s to t_{10}=0.65s)	0.3 MW
Q^* (t_0=0s to t_7=0.5s)	0.7 MVAR	Q^* (t_7=0.5s to t_{10}=0.65s)	1 MVAR
Z_f (t_1=0.2s to t_5=0.4s)	0.8 mΩ	Z_f (t_5=0.4s to t_{10}=0.65s)	0

Fig 5.2, Fig 5.3 and Fig 5.4 show the simulation results of FPNSC, FBSS and MFBSS strategies, respectively. In the simulation of the FPNSC strategy, k_1 in (3.29) is set to be "3" until t_2=0.25s, "0.8" from t_2 to t_4=0.15s, and "0.2" from t_4 to t_{10}=0.65s. Also, k_2 in (3.30) is set to be "3" until t_6=0.15s, "0.9" from t_6 to t_8=0.55s, and "0.5" from t_8 to t_{10}. Therefore, there are nine different conditions all in all in the test case of FPNSC as indicated in Fig 5.2. Applying (5.28) and (5.29) gives I_{max} for each phase in all of nine conditions as shown in Fig 5.2-(b). The negative sequence voltage reduction (i.e. imbalance reduction) is obvious after t_8 when k_2 is "0.5", and the inverter intends to inject negative reactive currents. Oscillations on the instantaneous active/reactive powers are high after applying "k_2=0.5" at t_8 as illustrated in Fig 5.2-(c).

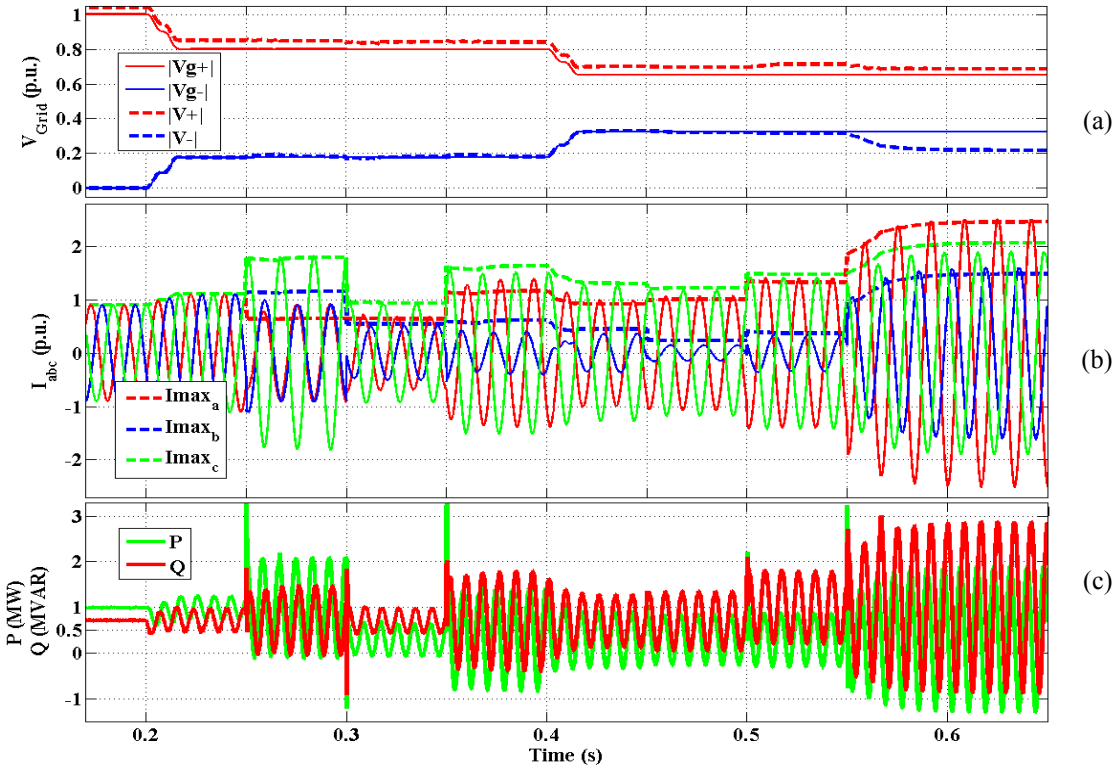

Fig 5.2. Simulation results of FPNSC: (a) positive/negative- sequences of the PCC and grid voltages, (b) injected currents and I_{max}, and (d) instantaneous active/reactive powers.

Since the test system is a HV grid, where the line impedance is mainly inductive, the performance and results of FBSS and MFBSS strategies are similar as shown in Fig 5.3 and Fig 5.4. In the simulation of FBSS and MFBSS strategies, k^+ parameter introduced in (3.34)-(3.35), and (3.38)-(3.41) is set to be "3" until t_6=0.15s, "0.1" from t_6 to t_8=0.55s, and "0.05" from t_8 to t_{10}=0.65s. Therefore, there are seven distinct conditions all in all in the test case of FBSS and MFBSS as illustrated in Fig 5.3 and Fig 5.4. Using (5.32)-(5.33) for FBSS and (5.36)-(5.37) for MFBSS yields I_{max} in all of seven situations as shown in Fig 5.3-(b) and Fig 5.4-(a). The negative sequence voltage reduction or imbalance reduction is obtained by imposing "k^+=0.05" after t_8, where the inverter intends to inject mostly the negative reactive currents to the grid. Oscillations on the instantaneous active/reactive powers in both FBSS and MFBSS strategies are high when injecting the negative reactive currents (i.e. after t_8 when k^+ is 0.05) as demonstrated in Fig 5.3-(c) and Fig 5.4-(b).

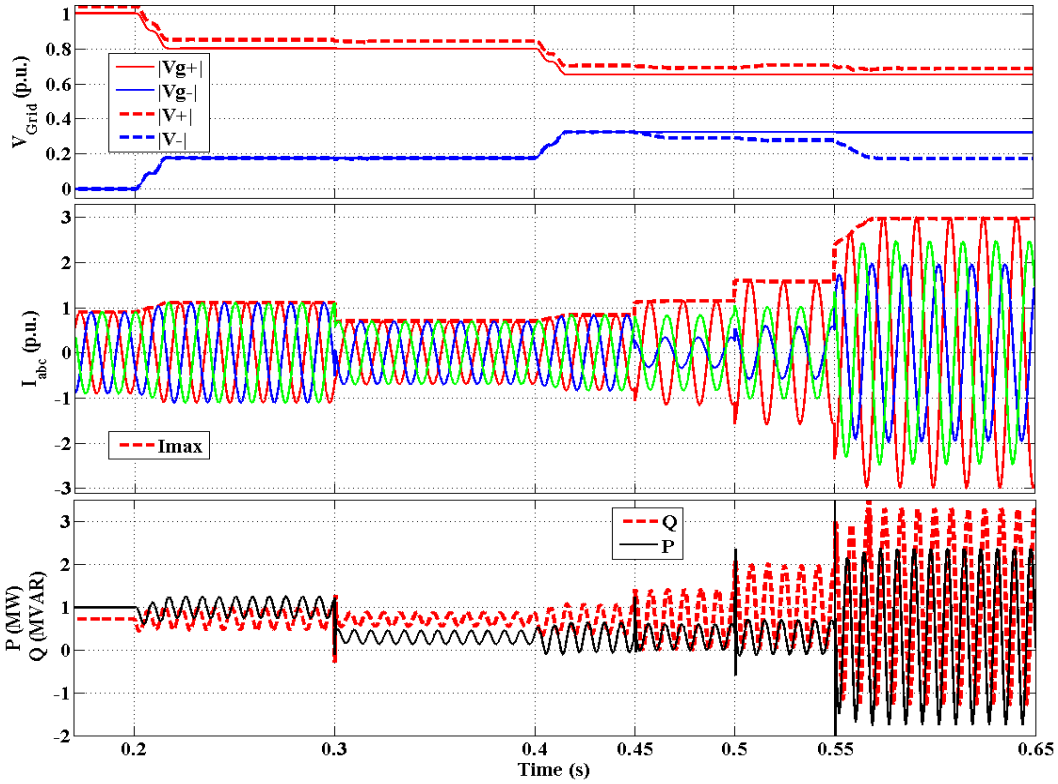

Fig 5.3. Simulation results of FBSS: (a) positive/negative- sequences of the PCC and grid voltages, (b) injected currents and I_{max}, and (d) instantaneous active/reactive powers.

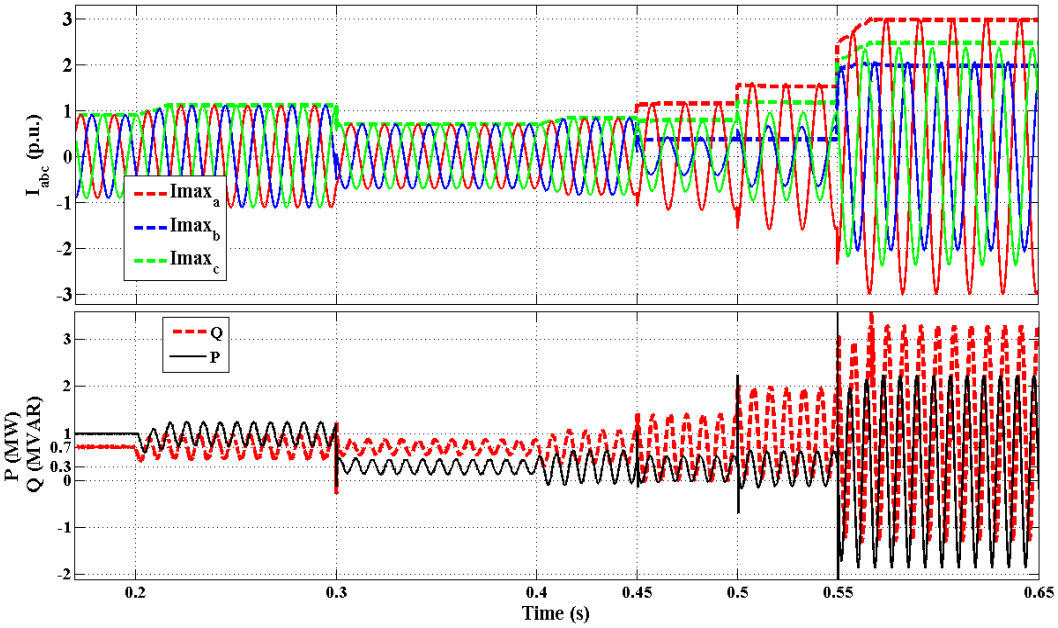

Fig 5.4. Simulation results of MFBSS: (a) injected currents and maximum instantaneous phase currents, and (d) instantaneous active/reactive powers.

5.5.2 Test Case B: Maximum Phase Current Limitation and Maximum Reactive Power Delivery

This section tests and studies the MARPD method and presents the simulation results of each FVS-LVRT-RCG strategy with MARPD method under different fault conditions in the same grid, where the grid voltage becomes deteriorated similar to Case A. The values of the deteriorated positive/negative-sequence voltages are similar to the Case A for both slight and severe faults. The only difference is the time of the severe voltage dip which is t_7=0.5s in this test case as it can be seen in Fig 5.5-(a) and time notations i.e. t_1=0.2s, t_2=0.25s, … , t_{11}=0.7s. Moreover, P^* is set to be 1 MW until t_5=0.4s and 0.3 MW after t_5. Also, MARPD is applied in order to support the grid voltage under the fault after t_3=0.3s as Fig 5.5-(c) shows. The maximum limit for I_{max} (i.e. I_{limit}) which is taken "3.5 p.u." until t_9=0.6s and "2 p.u." from t_9 to t_{11}=0.7s. Therefore, there are four different fault conditions after applying the MARPD as also mentioned in Table 5.4.

Fig 5.5 presents the simulation results of the FPNSC strategy in test case B. k_2 in (3.30) is set to be "3" in the first 50ms of each of the four fault conditions (e.g. from t_3=0.3s to t_4=0.35, or between t_5=0.4s and t_6=0.15s, etc.) and it is "0.5" in the second 50ms of each of the four conditions (e.g. between t_4 and t_5, or between t_6 and t_7=0.5s, etc.). Therefore, there are totally 8 different faulty conditions after applying the MARPD method at t_3. As Fig 5.5-(b) shows, the injected currents, in all eight conditions are limited to I_{limit}^* by applying the MARPD formula presented in (5.38)-(5.40). As Fig 5.5-(c) illustrates, the maximum allowable reactive power is obtained successfully for each of the eight fault conditions. The positive PCC voltage boost and the negative voltage reductions can be seen in Fig 5.5-(a) which shows the flexibility of the FPNSC strategy in order to either

TABLE 5.4. Specified Active Power Commands and I_{limit} Commands – Case B

P^* (t_0=0s to t_5=0.4s)	1 *MW*	P^* (t_5=0.4s to t_{11}=0.7s)	0.3 *MW*
I_{limit}^* (t_3=0.3s to t_9=0.6s)	1.5 *p.u.*	I_{limit}^* (t_9=0.6s to t_{11}=0.7s)	2 *p.u.*
Z_f (t_1=0.2s to t_7=0.5s)	0.8 mΩ	Z_f (t_7=0.5s to t_{11}=0.7s)	0

boost the PCC voltage or reduce the unbalance voltage under the imposed I_{limit}*. For example, the positive voltage boost of 0.09 p.u. is observable between t_3=0.3s and t_4=0.35s when k_2 is equal to "3" and the inverter injects completely-positive reactive currents. On the other hand, a negative voltage reduction of 0.08 p.u. is observable between t_6=0.45s and t_7=0.5s when k_2 is equal to "0.5" and the inverter injects half-positive-half-negative reactive currents. It is predictable that the highest positive voltage boost and negative voltage reduction belong to the period when P* is small (i.e. P*=0.3 MW) and I_{limit}* is high (i.e. I_{limit}*=2 p.u.) which can be seen in Fig 5.5-(a).

Fig 5.6 and Fig 5.7 present the simulation results of FBSS and MFBSS strategies in test case B, where their performances are almost the same; since the test system is a HV grid and line impedance is mainly inductive. k^+ parameter introduced in (3.34), (3.35) and (3.38)-(3.41) is set to be "3" in the first 50ms of each of the four fault conditions and it is "0.05" in the second 50ms of each of the four conditions. Therefore, there are totally 8 different fault conditions after applying the MARPD method at t_3.

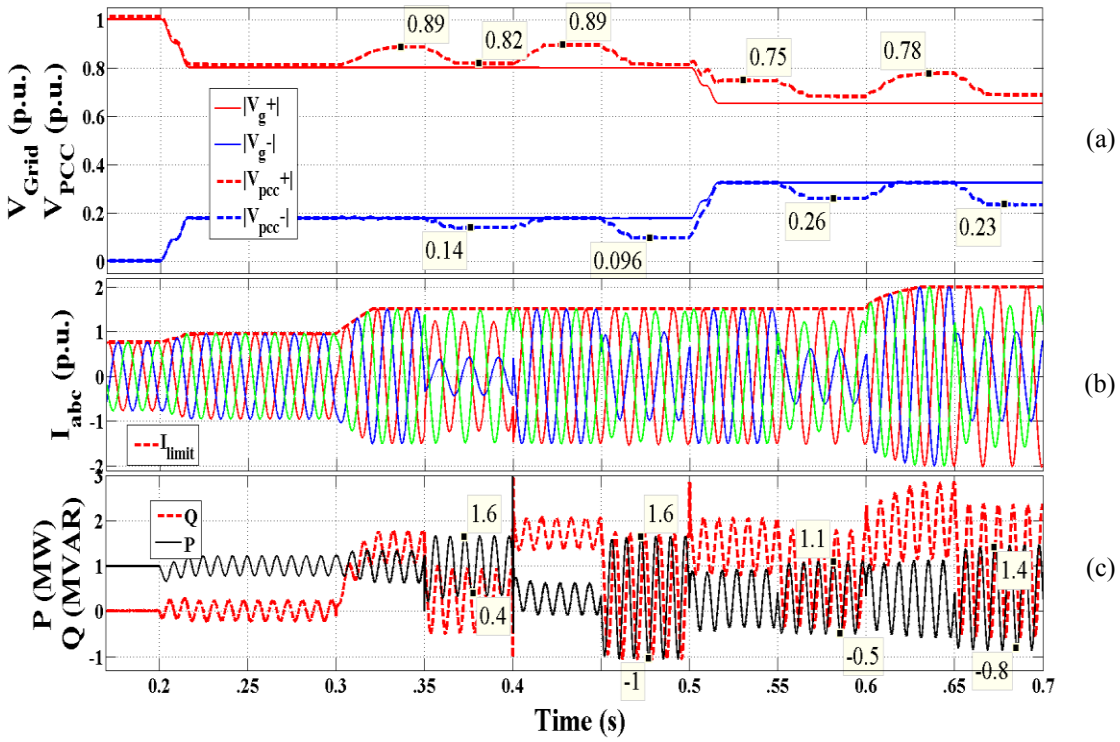

Fig 5.5. Case B – FPNSC strategy: (a) pos/neg-sequences of grid and PCC voltages, (b) injected currents, (c) instantaneous active/reactive powers

As Fig 5.6-(b) and Fig 5.7-(b) show, the injected currents, in all eight conditions are limited to I_{limit}* by applying the MARPD formula presented in (5.41)-(5.42) for FBSS and in (5.43)-(5.44) for MFBSS. As Fig 5.6-(c) and Fig 5.7-(c) illustrate, the maximum allowable reactive powers are obtained successfully for each of the eight fault conditions. The positive PCC voltage boost and the negative voltage reductions can be also seen in Fig 5.6-(a) and Fig 5.7-(a) which shows the flexibility of the FBSS and MFBSS strategies in order to either boost the PCC voltage or reduce the unbalance voltage under the imposed I_{limit}*. For example, the positive voltage boost of 0.09 p.u. is observable between t_5=0.4s and t_6=0.45s when k^+ is equal to "3" and the inverter injects completely-positive currents. On the other hand, a negative voltage reduction of 0.07 p.u. is observable between t_6 and t_7=0.5s when k^+ is equal to "0.05" and the inverter injects high negative-sequence currents. It is similarly predictable that the highest positive voltage boost and negative voltage reduction happen when P* is small and I_{limit}* is high which can also seen in Fig 5.6-(a) and Fig 5.7-(a) after t_9.

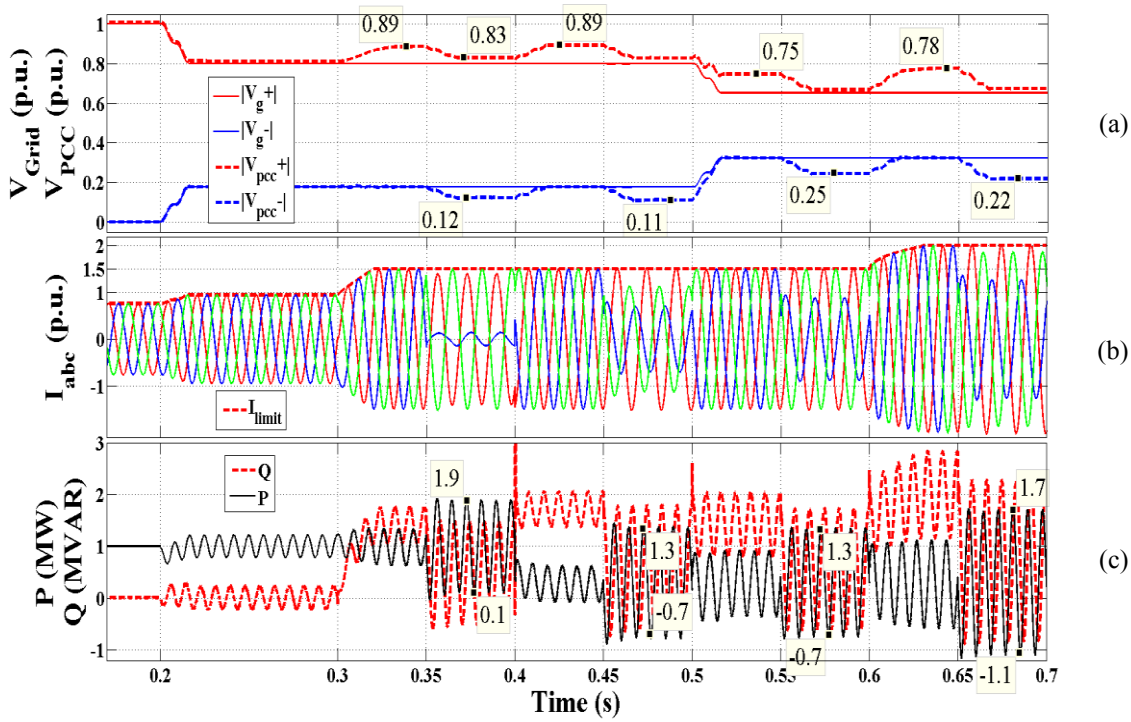

Fig 5.6. Case B – FBSS strategy: (a) pos/neg-sequences of grid and PCC voltages, (b) injected currents, (c) instantaneous active/reactive powers

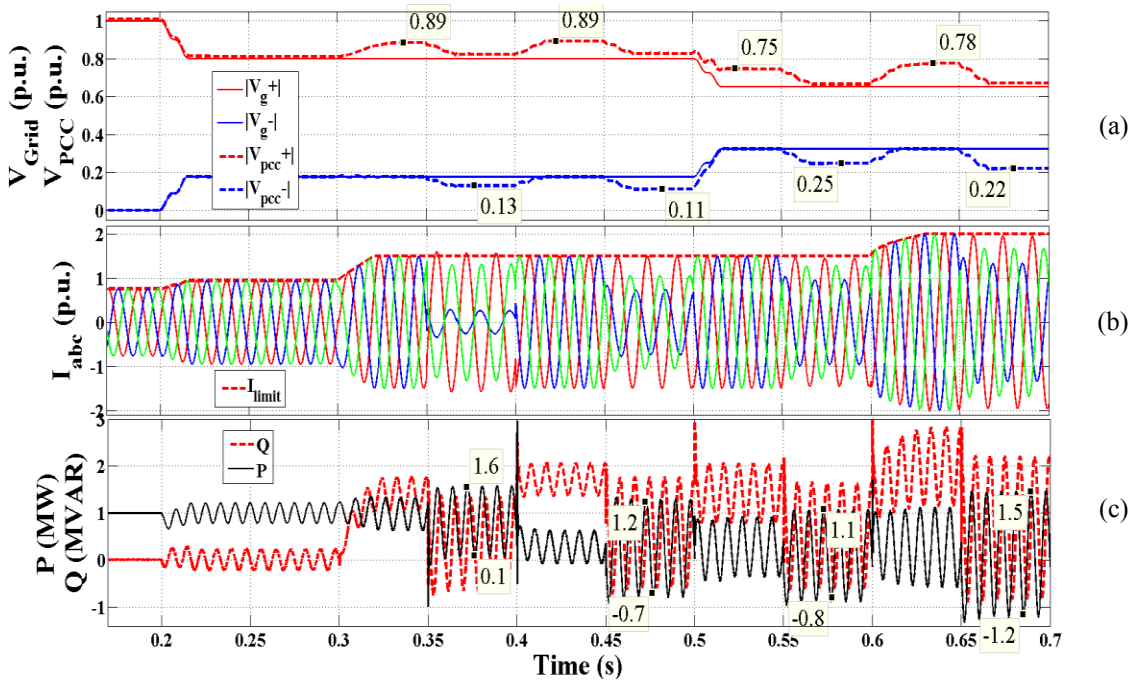

Fig 5.7. Case B – MFBSS strategy: (a) pos/neg-sequences of grid and PCC voltages, (b) injected currents, (c) instantaneous active/reactive powers

5.6 Summary and Discussion

Bar 5.1. summarizes all obtained simulation results of the MARPD method applied in FVS strategies, in test case B, into 4 bar graphs. The first bar graph shows the obtained improvements of the MARPD method in boosting the positive-sequence PCC voltage, *Vp*, in conds. 1, 3, 5, and 7. Similarly, the second bar graph illustrates the negative-sequence voltage reduction or imbalance reductions in conds. 2, 4, 6, and 8, along with the small *Vp* boost in these conditions, as shown in the first bar graph. Bar 5.1-(c) and Bar 5.1-(d) show, for each of the cond. 0 to cond. 8, the maximum oscillation magnitudes in the instantaneous active and reactive powers, respectively. Both Bar 5.1-(c) and Bar 5.1-(d) indicate that the power oscillations are high when the inverter injects some negative currents in conds. 2, 4, 6, and 8, comparing to the conditions where the inverter injects pure positive currents, i.e. conds. 1, 3, 5, and 7. Careful analysis of the obtained

	cond 0	t_3	cond 1	cond 2	t_5	cond 3	Cond 4	Cond 5	Cond 6	Cond 7	Cond 8
Time (s)	0.2-0.3		0.3-0.35	0.35-0.4		0.4-0.45	0.45-0.5	0.5-0.55	0.55-0.6	0.6-0.65	0.65-0.7
$V_{p,Grid}$	0.8 p.u.		0.8 p.u.	0.8 p.u.		0.8 p.u.	0.8 p.u.	0.65 p.u.	0.65 p.u.	0.65 p.u.	0.65 p.u.
$V_{n,Grid}$	0.18 p.u.		0.18 p.u.	0.18 p.u.		0.18 p.u.	0.18 p.u.	0.32 p.u.	0.32 p.u.	0.32 p.u.	0.32 p.u.
P^*	1 MW		1 MW	1 MW		0.3 MW	0.3 MW	0.3 MW	0.3 MW	0.3 MW	0.3 MW
I_{limit}^*			1.5 p.u.	1.5 p.u.		1.5 p.u.	1.5 p.u.	1.5 p.u.	1.5 p.u.	2 p.u.	2 p.u.
k_2			1	0.5		1	0.5	1	0.5	1	0.5
k^+			1	0.05		1	0.05	1	0.05	1	0.05

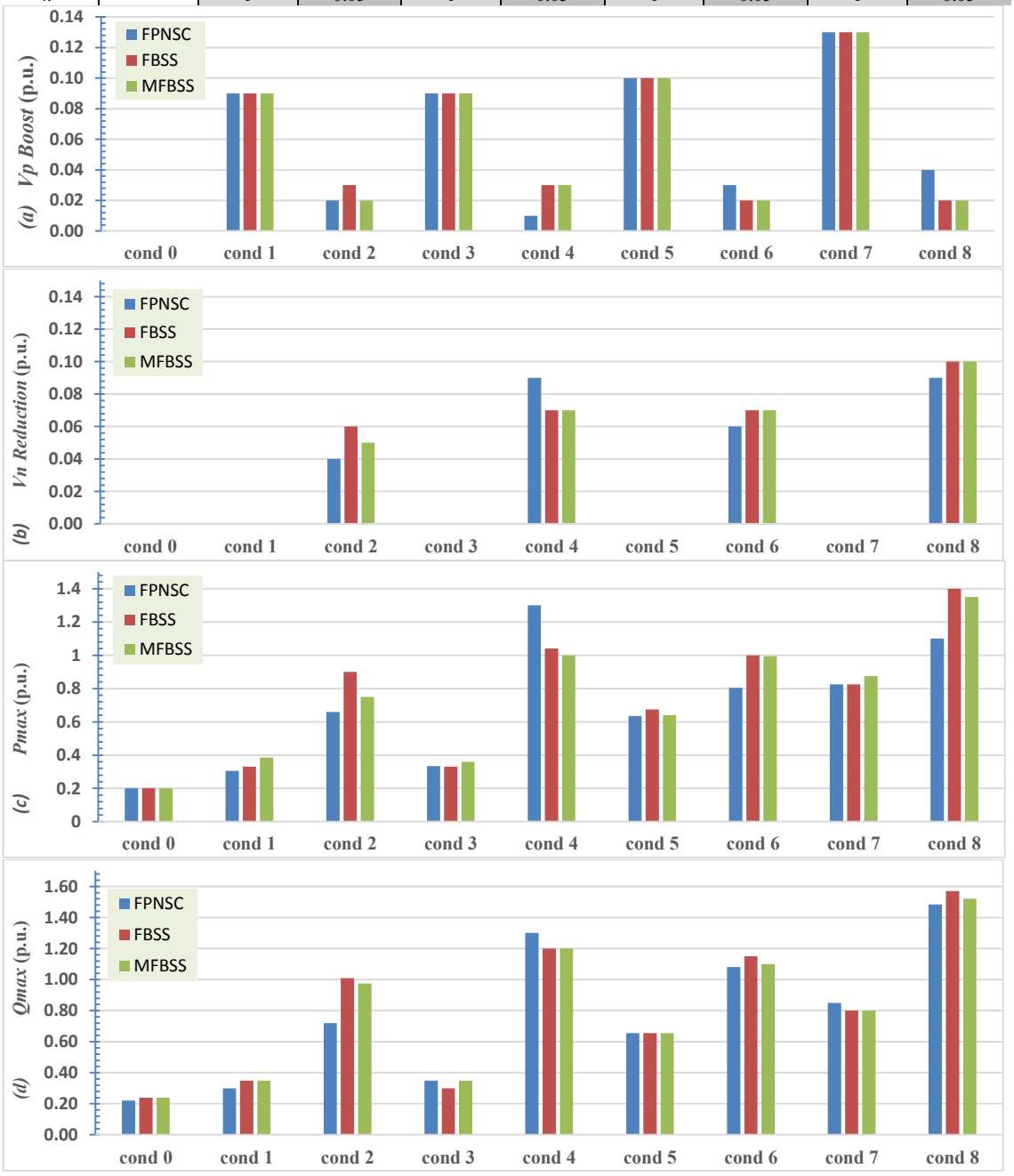

Bar 5.1. Summary of simulation results, Case B, of the MARPD method in FVS strategies: (a) positive sequence PCC voltage boost, (b) negative-sequence PCC voltage reduction, (c) $\tilde{p}_{max}$ and (d) $\tilde{q}_{max}$

results of FVS strategies in Bar 5.1 gives some advantageous conclusions:

- All three FVS strategies show very similar results under the same conditions and there are just limited differences between the results of FPNSC, FBSS and MFBSS. However, FPNSC seems to be more flexible in terms of the range of k parameter control to balance between two objectives of boosting V_p or reducing V_n since it gives appropriate results just by tuning the k parameter to be "0.5". While both FBSS and MFBSS strategies indicate almost the same result with FPNSC by tuning their k^+ parameter to be "0.05".
- According to Bar 5.1-(a) and Bar 5.1-(b), the best improvement, in all three strategies, after applying the MARPD method belongs to cond. 7 and cond. 8, where more capacity for reactive power is provided by increasing the I_{limit}^* from 1.5 p.u. to 2 p.u. at t_9=0.6s.
- According to Bar 5.1-(a), releasing the capacity for reactive power injection, in conds. 3 and 4 by decreasing the active power form 1 MW to 0.3 MW at t_5=0.4s, does not have considerable enhancement or effect on the amount of V_p (compare cond 1 with cond 3 and cond 2 with cond 4 in Bar 5.1-(a)). However, this released capacity for the reactive power enhances the ability of the strategies to reduce V_n more (compare cond 2 with cond 4 in Bar 5.1-(b)).
- According to Bar 5.1-(c) and Bar 5.1-(d), power oscillations during the negative current injections, in conds. 2, 4, 6, and 8, are much higher than the oscillations during the pure positive current injections, in conds. 1, 3, 5, and 7. This issue is one of the most problematic features of these three FVS strategies since DG owners highly need to reduce power fluctuations and their negative effects, specifically reducing the oscillations on the active power.
- According to Bar 5.1-(c) and Bar 5.1-(d), the amount of oscillations on the active and reactive powers are almost the same for each condition.
- According to Bar 5.1, the amount of power oscillations, generally, depend on the amount of improvement in V_p and V_n. In other words, whenever there is a great improvement in either V_p and V_n, there is correspondingly huge fluctuations on active and reactive powers.

5.7 Conclusion

This chapter presented the analytical evaluations and mathematical assessments of all FVS-LVRT-RCG strategies in gird connected converter-based DER units. The expressions of the oscillations on instantaneous active/reactive powers and maximum phase currents are formulated for each strategy. Based on the obtained formulas for the maximum phase currents in each strategy, the maximum allowable reactive power delivery, i.e. MARPD method, formulas were proposed specifically for each of the three FVS strategies. The MARPD method provides the best support for the PCC voltage and simultaneously respects the maximum limit for the phase currents (specified by DER owners) under different faults. Simulation results under different fault conditions, altered reference commands, and different strategy parameters (i.e. k values) were carried out for each strategy. The simulation results showed the accuracy and effectiveness of the proposed formulas of the MARPD method for each strategy.

Chapter 6

Conclusions

6.1 Summary and Conclusions

The main motivations behind this work were:

- To study and evaluate low-voltage-ride-through (LVRT) techniques in grid connected distributed-energy-resource (DER) units.
- To classify these techniques and compare their performances under different distorted voltage conditions.

Therefore, this thesis started with a literature review in Chapter 2. Firstly, the DERs were introduced and discussed with their essential components (i.e. distributed energy storage systems and distributed generation systems). The discussion on DERs was further zoomed into a well-known category with the label of converter-interfaced DERs (CI-DERs). Later in Chapter 2, newly developed grid codes and their tight requirements were categorized and studied from different points of views (such as LVRT requirements in national grid codes, technical standards for DER interconnection, wind energy conversion systems specific codes, etc.). Finally in Chapter 2, two examples of the LVRT technologies were presented in twofold DERs, i.e. directly connected DFIGs and CI-DERs. As the scope of this thesis, the other three chapters focused on LVRT technologies in CI-DERs.

Firstly in Chapter 3, available reference-current-generation (RCG) techniques applied in the grid connected CI-DER units, complying with LVRT requirements imposed by power system operators in high DER-penetrated systems, were presented. These LVRT-RCG strategies were further categorized into two main groups, i.e. uninterrupted power delivery (UPD) and flexible voltage support (FVS) strategies. Later, they were investigated and generally compared in terms of their dominant pros and cons (listed in Tables 3.3 and 3.4).

Chapter 4 presented the analytical evaluations and mathematical assessments of all UPD-LVRT-RCG strategies. These strategies aim to provide a proper set of reference-currents under different distorted voltage conditions in order to continue delivering desired active and reactive powers. This chapter presented three most important parameters of these strategies for a comprehensive evaluation, i.e. oscillation expressions on instantaneous active/reactive powers and maximum phase currents equations. Table 4.2 summarized the obtained results of the expressions of $\tilde{p}_{\max}$ and $\tilde{q}_{\max}$ for all six UPD strategies. Based on the expressions of Table 4.2 and the results of Bars 4.1 and 4.2, several fruitful conclusions were taken and listed. Followings are the most notable conclusions in terms of the power oscillation expressions:

- The IARC and ZSCI are obviously best options for having instantaneously controlled powers with zero oscillation components.

- In the second to fifth places of the power oscillations ranking, the ICPS, BPSC, AARC and PNSC strategies are located, respectively.

Later in Chapter 4, the expressions for maximum phase currents were obtained and listed in Table 4.3. Useful comparable results were also presented in Bar 4.3 for maximum phase currents values of six UPD strategies under different conditions in order to evaluate and rank them in terms of maximum phase currents needed to be injected with each strategy. The general ranking of the strategies in terms of maximum phase currents, according to Table 4.3, and Bar 4.3 is as follow:

- First, BPSC and AARC strategies have least needed maximum phase currents among the UPD strategies under the same fault and system conditions.
- The PNSC, ICPS and IARC strategies have the second to fourth ranks.
- Finally, the ZSCI strategy is the worst in terms of the injected currents since it requires very high currents, due to the zero-sequence currents, to be injected under voltage disturbances.

Finally, in Chapter 4, based on the obtained formulas for the maximum phase currents in each strategy, the maximum allowable reactive power delivery (MARPD) formulas were proposed specifically for each of the six UPD-LVRT-RCG strategies. The MARPD method aims to provide the best support for the PCC voltage and simultaneously respect the maximum limit for the phase currents (specified by DER owners) under different faults.

Chapter 5 presented the analytical evaluations and mathematical assessments of all FVS-LVRT-RCG strategies where the expressions of the oscillations on instantaneous active/reactive powers and maximum phase currents are formulated for each FVS strategy. As for instance, Table 5.2 provided the obtained expressions of the maximum phase currents for three FVS strategies. Based on the obtained formulas for the maximum phase currents, the MARPD formulas were proposed specifically for each of the three FVS strategies. The simulation results not only showed the accuracy and effectiveness of the proposed formulas of the MARPD method for each strategy; but also, they revealed several important facts and some fruitful conclusions, which were presented in Section 5.6. Followings are the most notable highlights extracted from analytical studies and simulation results of Chapter 5:

- All three FVS strategies show very similar results under the same conditions and there are just limited differences between the results of FPNSC, FBSS and MFBSS. However, FPNSC seems to be more flexible in terms of the range of its control parameter, k, to balance between two objectives of boosting positive-sequence voltage or reducing negative-sequence voltage.

- The best improvement in all three strategies after applying the MARPD method, expectedly, belongs to the conditions where more capacity for reactive power is provided by imposing higher I_{limit} and lower active power commands.

- Power oscillations during the negative current injections are much higher than the oscillations during the pure positive current injections. This issue is one of the most problematic features of FVS strategies.

- The amount of power oscillations, generally, depend on the amount of improvement in voltage levels. In other words, whenever there is a great improvement in either positive or negative sequence voltages, there is correspondingly huge fluctuations on active and reactive powers.

6.2 Contributions

As the main contributions of this work, this thesis:

- Highlighted, calculated, evaluated and compared the important analytical expressions (the mathematical equations of maximum oscillations on active/reactive powers and maximum phase currents) of each LVRT-RCG technique under generic grid voltage disturbances and various system parameters.

- Proposed a method which helps each LVRT-RCG technique to provide its best voltage support (either by boosting the positive-sequence voltage or reducing the negative-sequence voltage) under the specific maximum phase current restrictions of that technique where these restrictions values are imposed by DER owners. Therefore, this method applies maximum allowable reactive power delivery (MARPD).

- Analytically calculated the MARPD equations for each of the nine studied LVRT-RCG strategies,

- and verified the calculated equations by simulation results in various conditions, i.e. different voltage sag characteristics, various reference commands imposed by DER owners, and different voltage supporting objectives, etc.

6.3 Future Work

Future work envisioned as a continuance of this thesis comprises:

- Proposing a comprehensive LVRT-RCG strategy which provides a proper set of reference-currents under different distorted voltage conditions and allows the controllability of either boosting the positive-sequence voltage or reducing negative-sequence voltage while, unlike available FVS control strategies, attenuates the oscillations on active power which is very important especially for DC-link voltage regulation.

- Applying the DC-link voltage controller loop in each of the presented LVRT-RCG techniques instead of simplifying the DC-link with a DC voltage source (which is a very common assumption in the existing literature).

References

[1] http://en.wikipedia.org/wiki/Wind_power

[2] http://en.wikipedia.org/wiki/Wind_power_by_country

[3] S. S. Smater, A. D. Domínguez-García, "A Framework for Reliability and Performance Assessment of Wind Energy Conversion Systems", IEEE Trans. on Power Syst., vol. 26, no. 4, November 2011.

[4] http://www.eia.gov/cfapps/ipdbproject/IeDIndex3.cfm?tid=2&eyid=2012&syid=2012&reverseAxes=0&cid=&cid=CA&cid=CH&cid=DA&cid=GM&cid=SP&cid=US&pid=alltypes&aid=12&unit=BKWH&updateB=UPDATE

[5] Gregory Joseph Kish, "Addressing Future Grid Requirements for Distributed Energy Resources", M.Sc. Thesis, University of Toronto, 2011.

[6] A. Moreno-Munoz, J.J.G. de la Rosa, M. A. Lopez, and A. R. Gil de Castro, "Distributed energy resources interconnection: The spanish normative," in 35th Annual Conference of IEEE Industrial Electronics, 2009. IECON '09, Nov. 3–5, 2009, pp. 408 – 412.

[7] L. G. Meegahapola, T. Littler, and Damian Flynn "Decoupled-DFIG Fault Ride-Through Strategy for Enhanced Stability Performance during Grid Faults", *IEEE* TRANSACTIONS ON SUSTAINABLE ENERGY, VOL. 1, NO. 3, OCTOBER 2010.

[8] A. E. Leon, J. M. Mauricio, A. Gómez-Expósito, and J. A. Solsona, "An Improved Control Strategy for Hybrid Wind Farms" IEEE TRANSACTIONS ON SUSTAINABLE ENERGY, VOL. 1, NO. 3, OCTOBER 2010.

[9] M. Jahangir Hossain, Hemanshu R. Pota, Valeri A. Ugrinovskii, and Rodrigo A. Ramos, "Simultaneous STATCOM and Pitch Angle Control for Improved LVRT Capability of Fixed-Speed Wind Turbines" IEEE TRANSACTIONS ON SUSTAINABLE ENERGY, VOL. 1, NO. 3, OCTOBER 2010.

[10] S. Alepuz, S. Busquets-Monge, J. Bordonau, P. Cortes, J. Rodriguez, and R. Vargas, "Predictive current control of grid-connected neutral-pointclamped

converters to meet low voltage ride-through requirements," in IEEE Power Electron. Spec. Conf. (PESC), Jun. 2008, pp. 2423–2428, Rhodes, Greece.

[11] R. Lohde and F.W. Fuchs, "Improved DPC Method of VSC to Fulfill Low Voltage Ride Through Requirements in Wind Power Applications", 14th International Power Electronics and Motion Control Conference (EPE-PEMC), Ohrid, Macedonia, 2010, pp. T12-35 - T12-42.

[12] C. Rahmann, H.-J. Haubrich, A. Moser, R. Palma-Behnke, L. Vargas, and M. B. C. Salles, "Justified fault-ride-through requirements for wind turbines in power systems," IEEE Trans. Power Syst., vol. 26, no. 3, pp. 1555–1563, Aug. 2011.

[13] Alan Mullane, Gordon Lightbody, and R. Yacamini, "Wind-Turbine Fault Ride-Through Enhancement" IEEE TRANSACTIONS ON POWER SYSTEMS, VOL. 20, NO. 4, NOVEMBER 2005.

[14] D. L. Brooks and M. Patel, "Panel: Standards & interconnection requirements for wind and solar generation nerc integrating variable generation task force," in IEEE Power Engineering Society General Meeting, pp. 1 – 3, 2011.

[15] J. Boemer, K. Burges, and T. Kumm, "Compliance with technical codes turns into precondition for support and system services bonus for wind power plants in germany," in IEEE Bucharest PowerTech, 2009, Jun. 28 - Jul. 02 2009, pp. 1 – 8.

[16] IEEE Application Guide for IEEE Std 1547™, IEEE Standard for Interconnecting Distributed Resources with Electric Power Systems IEEE 3 Park Avenue New York, NY 10016-5997, USA 15 April 2009 IEEE Standards Coordinating Committee 21.

[17] THE GRID CODE ISSUE 5 REVISION 9 01 July 2014 © 2013 Copyright owned by National Grid Electricity Transmission plc, all rights reserved.

[18] BDEW MV Guideline 3rd Supplement retrieved in 02/2011

[19] Jump up^ National Grid code retrieved on 9 November 2008

[20] Milad Falahi, Hung-Ming Chou, Mehrdad Ehsani, Le Xie, and Karen L. Butler-Purry, "Potential Power Quality Benefits of Electric Vehicles" IEEE TRANSACTIONS ON SUSTAINABLE ENERGY, VOL. 4, NO. 4, OCTOBER 2013.

[21] Christian Klumpner, and Frede Blaabjerg, “Experimental Evaluation of Ride-Through Capabilities for a Matrix Converter Under Short Power Interruptions”, IEEE TRANSACTIONS ON INDUSTRIAL ELECTRONICS, VOL. 49, NO. 2, APRIL 2002.

[22] Hany M. Hasanien, and S. M. Muyeen, “Design Optimization of Controller Parameters Used in Variable Speed Wind Energy Conversion System by Genetic Algorithms”, IEEE TRANSACTIONS ON SUSTAINABLE ENERGY, VOL. 3, NO. 2, APRIL 2012.

[23] Miteshkumar Popat, Bin Wu, and Navid R. Zargari, “Fault Ride-Through Capability of Cascaded Current-Source Converter-Based Offshore Wind Farm”

[24] Frede Blaabjerg, Marco Liserre, and Ke Ma “Power Electronics Converters for Wind Turbine Systems”, IEEE TRANSACTIONS ON INDUSTRY APPLICATIONS, VOL. 48, NO. 2, MARCH/APRIL 2012.

[25] Ke Ma, Marco Liserre, and Frede Blaabjerg, “Operating and Loading Conditions of a Three-Level Neutral-Point-Clamped Wind Power Converter Under Various Grid Faults”, IEEE TRANSACTIONS ON INDUSTRY APPLICATIONS, VOL. 50, NO. 1, JANUARY/FEBRUARY 2014.

[26] Sebastian S. Smater, and Alejandro D. Domínguez-García, “A Framework for Reliability and Performance Assessment of Wind Energy Conversion Systems”, IEEE TRANSACTIONS ON POWER SYSTEMS, VOL. 26, NO. 4, NOVEMBER 2011.

[27] Ö. Göksu, R. Teodorescu, Claus Leth Bak, Florin Iov, and Philip Carne Kjær, “Instability of Wind Turbine Converters During Current Injection to Low Voltage Grid Faults and PLL Frequency Based Stability Solution”, IEEE TRANSACTIONS ON POWER SYSTEMS.

[28] Surour Alaraifi, Ahmed Moawwad, Mohamed Shawky El Moursi, and Vinod Khadkikar, “Voltage Booster Schemes for Fault Ride-Through Enhancement of Variable Speed Wind Turbines” IEEE TRANSACTIONS ON SUSTAINABLE ENERGY, VOL. 4, NO. 4, OCTOBER 2013.

[29] "A Voltage Detection Method for the Voltage Ride-Through Operation of Renewable Energy Generation Systems Under Grid Voltage Distortion Conditions" IEEE TRANSACTIONS ON SUSTAINABLE ENERGY

[30] Chad Abbey, and Géza Joos, "Supercapacitor Energy Storage for Wind Energy Applications" IEEE TRANSACTIONS ON INDUSTRY APPLICATIONS, VOL. 43, NO. 3, MAY/JUNE 2007.

[31] Xiangwu Yan, Giri Venkataramanan, Patrick S. Flannery, Yang Wang, Qing Dong, and Bo Zhang, "Voltage-Sag Tolerance of DFIG Wind Turbine With a Series Grid Side Passive-Impedance Network" IEEE TRANSACTIONS ON ENERGY CONVERSION, VOL. 25, NO. 4, DECEMBER 2010.

[32] Grazia Todeschini, and Alexander E. Emanuel, "Transient Response of a Wind Energy Conversion System Used as Active Filter", IEEE TRANSACTIONS ON ENERGY CONVERSION, VOL. 26, NO. 2, JUNE 2011.

[33] Shuai Xiao, Hua Geng, Honglin Zhou, Geng Yang, "Analysis of the control limit for rotor-side converter of doubly fed induction generator-based wind energy conversion system under various voltage dips" IET Renewable Power Generation November 2012.

[34] Theodoros D. Vrionis, Xanthi I. Koutiva, and Nicholas. A. Vovos, "A Genetic Algorithm-Based Low Voltage Ride-Through Control Strategy for Grid Connected Doubly Fed Induction Wind Generators" IEEE TRANSACTIONS ON POWER SYSTEMS, VOL. 29, NO. 3, MAY 2014.

[35] Dongliang Xie, Zhao Xu, Lihui Yang, Jacob Østergaard, Yusheng Xue, and Kit Po Wong, "A Comprehensive LVRT Control Strategy for DFIG Wind Turbines With Enhanced Reactive Power Support" IEEE TRANSACTIONS ON POWER SYSTEMS, VOL. 28, NO. 3, AUGUST 2013.

[36] Hua Geng, Cong Liu, and Geng Yang, "LVRT Capability of DFIG-Based WECS Under Asymmetrical Grid Fault Condition", IEEE TRANSACTIONS ON INDUSTRIAL ELECTRONICS, VOL. 60, NO. 6, JUNE 2013.

[37] M. Jahangir Hossain, Tapan Kumar Saha, Nadarajah Mithulananthan, and Hemanshu R. Pota, "Control Strategies for Augmenting LVRT Capability of

DFIGs in Interconnected Power Systems" IEEE TRANSACTIONS ON INDUSTRIAL ELECTRONICS, VOL. 60, NO. 6, JUNE 2013.

[38] Ahmed Moawwad, Mohamed Shawky El Moursi, and Weidong Xiao, "A Novel Transient Control Strategy for VSC-HVDC Connecting Offshore Wind Power Plant" IEEE Transaction on Sustainable Energy

[39] José Matas, Miguel Castilla, Josep M. Guerrero, Luis García de Vicuña, and Jaume Miret "Feedback Linearization Of Direct-Drive Synchronous Wind-Turbines Via a Sliding Mode Approach" IEEE TRANSACTIONS ON POWER ELECTRONICS, VOL. 23, NO. 3, MAY 2008.

[40] Ki-Hong Kim, Yoon-Cheul Jeung, Dong-Choon Lee, and Heung-Geun Kim, "LVRT Scheme of PMSG Wind Power Systems Based on Feedback Linearization" IEEE TRANSACTIONS ON POWER ELECTRONICS, VOL. 27, NO. 5, MAY 2012.

[41] Chia-Tse Lee, Che-Wei Hsu, and Po-Tai Cheng "A Low-Voltage Ride-Through Technique for Grid-Connected Converters of Distributed Energy Resources" IEEE TRANSACTIONS ON INDUSTRY APPLICATIONS, VOL. 47, NO. 4, JULY/AUGUST 2011.

[42] Yongheng Yang, Frede Blaabjerg, and Zhixiang Zou, "Benchmarking of Grid Fault Modes in Single-Phase Grid-Connected Photovoltaic Systems", IEEE TRANSACTIONS ON INDUSTRY APPLICATIONS, VOL. 49, NO. 5, SEPTEMBER/OCTOBER 2013.

[43] R. Teodorescu, et al. "Grid converters for photovoltaic and wind power systems", 2011 John Wiley & Sons, ISBN: 978-0-470-05751-3.

[44] P. Rodriguez, et al. "Flexible active power control of distributed power generation systems during grid faults", IEEE Trans. on Ind. Electron., vol. 54, no. 5, October 2007.

[45] K. Ma, W. Chen, M. Liserre, F. Blaabjerg, "Power controllability of three-phase converter with unbalanced AC source", IEEE Trans. on Power Electron., in press

[46] A. Camacho, et al. “Flexible voltage support control for three-phase distributed generation inverters under grid fault”, IEEE Trans. on Ind. Elect., vol. 60, no. 4, 2013.

[47] X. Guo, et al. “Asymmetrical grid fault ride-through strategy of three-phase grid-connected inverter considering network impedance impact in low-voltage grid”, IEEE Trans. on Power Electron., vol. 29, 2014.

[48] Salvador Alepuz, Alejandro Calle, Sergio Busquets-Monge, Samir Kouro, and Bin Wu, “Use of Stored Energy in PMSG Rotor Inertia for Low-Voltage Ride-Through in Back-to-Back NPC Converter-Based Wind Power Systems” IEEE TRANSACTIONS ON INDUSTRIAL ELECTRONICS, VOL. 60, NO. 5, MAY 2013.

[49] Manuel Reyes, Pedro Rodriguez, Sergio Vazquez, Alvaro Luna, Remus Teodorescu, and Juan Manuel Carrasco, “Enhanced Decoupled Double Synchronous Reference Frame Current Controller for Unbalanced Grid-Voltage Conditions” IEEE TRANSACTIONS ON POWER ELECTRONICS, VOL. 27, NO. 9, SEPTEMBER 2012.

[50] Adrian Timbus, Marco Liserre, Remus Teodorescu, Pedro Rodriguez, and Frede Blaabjerg, “Evaluation of Current Controllers for Distributed Power Generation Systems” IEEE TRANSACTIONS ON POWER ELECTRONICS, VOL. 24, NO. 3, MARCH 2009.

[51] Po-Hsu Huang, Mohamed Shawky El Moursi, Weidong Xiao, and James L. Kirtley, Jr. “Fault Ride-Through Configuration and Transient Management Scheme for Self-Excited Induction Generator-Based Wind Turbine” IEEE Transactions on Sustainable Energy, 2014.

[52] Ion Etxeberria-Otadui, Unai Viscarret, Marcelino Caballero, Alfred Rufer, and Seddik Bacha, “New Optimized PWM VSC Control Structures and Strategies Under Unbalanced Voltage Transients” IEEE TRANSACTIONS ON INDUSTRIAL ELECTRONICS, VOL. 54, NO. 5, OCTOBER 2007.

[53] Salvador Alepuz, Sergio Busquets-Monge, Josep Bordonau, Juan A. Martínez-Velasco, César A. Silva, Jorge Pontt, and José Rodríguez, “Control Strategies

Based on Symmetrical Components for Grid-Connected Converters Under Voltage Dips", IEEE TRANSACTIONS ON INDUSTRIAL ELECTRONICS, VOL. 56, NO. 6, JUNE 2009.

[54] Jaume Miret, Antonio Camacho, Miguel Castilla, Luys Garcya de Vicuna, and Jose Matas, "Control Scheme With Voltage Support Capability for Distributed Generation Inverters Under Voltage Sags" IEEE TRANSACTIONS ON POWER ELECTRONICS, VOL. 28, NO. 11, NOVEMBER 2013.

[55] Pedro Rodryguez, Adrian Timbus, Remus Teodorescu, Marco Liserre, and Frede Blaabjerg, "Letters Reactive Power Control for Improving Wind Turbine System Behavior Under Grid Faults" IEEE TRANSACTIONS ON POWER ELECTRONICS, VOL. 24, NO. 7, JULY 2009.

[56] Antonio Camacho, Miguel Castilla, Jaume Miret, Angel Borrell and Luis Garcıa de Vicuna, "Active and Reactive Power Strategies with Peak Current Limitation for Distributed Generation Inverters During Unbalanced Grid Faults" IEEE TRANSACTIONS ON INDUSTRIAL ELECTRONICS.

[57] Adria Junyent-Ferre, Oriol Gomis-Bellmunt, Tim C. Green, and Diego E. Soto-Sanchez, "Current Control Reference Calculation Issues for the Operation of Renewable Source Grid Interface VSCs Under Unbalanced Voltage Sags" IEEE TRANSACTIONS ON POWER ELECTRONICS, VOL. 26, NO. 12, DECEMBER 2011.

[58] M.F. Akorede, H. Hizam, and E. Pouresmaeil, "Distributed energy resources and benefits to the environment," Renewable and Sustainable Energy Reviews, vol. 14, no. 2, pp. 724 – 734, Feb 2010.

[59] T. Ackermann, G. Andersson, and L. S¨oder, "Distributed generation: a definition," Electric Power Systems Research, vol. 57, no. 3, pp. 195 – 204, Apr. 20, 2001.

[60] Variability of wind power and other renewables. Management options and strategies. IEA, www.iea.org;

[61] Red Eléctrica, "The Spanish Electricity System. Summary 2008," last accessed Feb. 2013.

[Online]. Available: http://www.ree.es/ingles/sistema_electrico/informeSEE-008.asp

[62] Red Eléctrica, “The Spanish Electricity System. Summary 2009,” last accessed Feb. 2013.
[Online]. Available: http://www.ree.es/ingles/sistema_electrico/informeSEE-2009.asp

[63] Red Eléctrica, “The Spanish Electricity System. Summary 2010,” last accessed Feb. 2013.
[Online]. Available: http://www.ree.es/ingles/sistema_electrico/informeSEE-2010.asp

[64] Red Eléctrica, “Press release: Record share of wind energy in demand coverage,” last accessed Feb. 2013. [Online]. Available: http://www.ree.es/ingles/sala_prensa/web/notas_detalle.aspx?id_nota=255

[65] EWEA Large scale integration of wind energy in the European Power Suply; December 2005;

[66] Roberto Cárdenas, Rubén Peña, Salvador Alepuz, and Greg Asher, “Overview of Control Systems for the Operation of DFIGs in Wind Energy Applications” IEEE TRANSACTIONS ON INDUSTRIAL ELECTRONICS, VOL. 60, NO. 7, JULY 2013.

[67] M. Tsili and S. Papathanassiou, “A review of grid code technical requirements for wind farms,” IET Renew. Power Gen., vol. 3, no. 3, pp. 308– 332, Sep. 2009.

[68] Y. A.-R. I. Mohamed, "Mitigation of dynamic, unbalanced and harmonic voltage disturbances using grid-connected inverters with *LCL* filter" *IEEE Transactions on Industrial Electronics*, vol. 58, no. 9, pp. 3914-3924, Sept. 2011.

[69] F. Iov, A. Hansen, P. Soerensen, and N. Cutululis, “Mapping of grid faults and grid codes,” Risoe National Laboratory, Technical University of Denmark, Tech. Rep., Jul 2007. [Online]. Available: http://130.226.56.153/rispubl/reports/ris-r-1617.pdf

[70] A. Kahrobaeian and Y. A.-R. I. Mohamed, “Networked-based hybrid distributed power sharing and control for islanded micro-grid systems,” IEEE Transactions on Power Electronics, vol.30, no.2, pp.603,617, Feb. 2015.

[71] J. Lopez, P. Sanchis, X. Roboam, and L. Marroyo, “Dynamic behavior of the doubly fed induction generator during three-phase voltage dips,” IEEE Trans. Energy Convers., vol. 22, no. 3, pp. 709–717, Sep. 2007.

[72] Grid Code: High and Extra High Voltage, E. ON Netz GmbH, Bayreuth, Germany, 2006.

[73] M. H. J. Bollen – Understanding Power Quality Problems. Voltage sags and interruptions, IEEE Press Series on Power Engineering, 2000, ISBN 0-7803-4713-7;

[74] IEEE Recommended Practice for Monitoring Electric Power Quality, IEEE Std.1159-1995, June 1995.

[75] Giuseppe Saccomando, Jan Svensson, and Ambra Sannino, “Improving Voltage Disturbance Rejection for Variable-Speed Wind Turbines” IEEE TRANSACTIONS ON ENERGY CONVERSION, VOL. 17, NO. 3, SEPTEMBER 2002.

[76] M. Bollen, Understanding Power Quality Problems: Voltage Sags and Interruptions. Piscataway, NJ, USA: IEEE Press, 1999.

[77] M. Bollen and I. Gu, Signal Processing of Power Quality Disturbances. Hoboken, NJ, USA: Wiley, 2006.

[78] EnergiNet – Grid connection of wind turbines to networks with voltages below 100 kV, Regulation TF 3.2.6, May 2004, p. 29;

[79] ESB Networks – Distribution Code, version 1.4, February 2005;

[80] CER – Wind Farm Transmission Grid Code Provisions, July 2004;

[81] National Grid Electricity Transmission plc – The grid code, Issue 3, Revision 17, September 2006;

[82] Going mainstream at the grid face. Examining grid codes for wind, Wind power Monthly, September 2005;

[83] ENEL - – DK 5740 - Criteri di allacciamento di impianti di produzione alla rete MT di ENEL distribuzione, February 2005; 40 Risø-R-1617(EN)

[84] TERNA - Codice di trasmissione, dispacciamento, sviluppo e sicurezza della rete, 2006;

[85] FERC – Interconnection of Wind Energy, 18 CFR Part 35, Docket No. RM05- 4-001; Order No. 661-A December 12, 2005;

[86] Hydro-Québec TransÉnergie – Transmission Provider Technical Requirements for the connection of power plants to the Hydro-Québec Transmission System, March 2006;

[87] Alberta Electric System Operator – Wind Power Facility. Technical Requirements, Revision 0, November 2004.

[88] IEEE Std. 929 - Recommended Practice for Utility Interface of Photovoltaic (PV) Systems, IEEE Std., Jan 2000.

[89] IEEE Std. 1547.2 - Application Guide for IEEE Std 1547, IEEE Standard for Interconnecting Distributed Resources with Electric Power Systems, IEEE Std., 2008.

[90] C22.3 No.9-08 - Interconnection of Distributed Resources and Electricity Supply Systems, CSA Std., Feb 2009.

[91] UL1741 Standard for Safety - Inverters, Converters, Controllers and Interconnection System Equipment for Use With Distributed Energy Resources, Underwriters Laboratories Inc. Std., Jan 2010.

[92] IEEE Std. 519 - Recommended Practices and Requirements for Harmonic Control in Electrical Power Systems, IEEE Std., Apr 1992.

[93] P. Strauss, T. Degner, W. Heckmann, I. Wasiak, P. Gburczyk, Z. Hanzelka, N. Hatziargyriou, T. Romanos, E. Zountouridou, and A. Dimeas, “International white book on the grid integration of static converters,” in 10th International Conference on Electrical Power Quality and Utilisation, 2009. EPQU 2009., Sep. 15–17, 2009, pp. 1 – 6.

[94] V. Van Thong, J. Driesen, and R. Belmans, “Using distributed generation to support and provide ancillary services for the power system,” in International

Conference on Clean Electrical Power, 2007. ICCEP ’07, May 21–23, 2007, pp. 159 – 163.

[95] M. LeBlanc, L. Evans, P. Gardner, and N. Scott, “CanWEA - Canadian Grid Code forWind Development Review and Recommendations,” Garrad Hassan Canada Inc., Tech. Rep., Oct 2005, document no. 11163/OR/01 Issue: B.

[96] I.M. de Alegr´ýa, J. Andreu, J.L. Mart´ýn, P. Iba˜nez, J.L. Villate, and H. Camblong, “Connection requirements for wind farms: A survey on technical requirements and regulation,” Renewable and Sustainable Energy Reviews, vol. 11, no. 8, pp. 1858 – 1872, 2007.

[97] S. Bernard, D. Beaulieu, and G. Trudel, “Hydro-qu´ebec grid code for wind farm interconnection,” in IEEE Power Engineering Society General Meeting, 2005., vol. 2, Jun 2005, pp. 1248 – 1252.

[98] M. Braun, G. Arnold, and H. Laukamp, “Plugging into the zeitgeist,” IEEE Power and Energy Magazine, vol. 7, no. 3, pp. 63 – 76, May-Jun. 2009.

[99] Generating Plants Connected to the Medium-Voltage Network: Guideline for Generating Plants’ Connection to and Parallel Operation with the Medium-Voltage Network, BDEW, Jun 2008. [Online]. Available: http://www.bdew.de/bdew.nsf/id/DE7B6ERDNetzCodesundRichtlinien/$file/BDEW RL EA-am-MS-Netz engl.pdf

[100] A. Notholt, “Germany’s new code for generation plants connected to medium-voltage networks and its repercussion on inverter control,” in International Conference on Renewable Energies and Power Quality (ICREPQ’09), Apr. 15–17, 2009.

[101] NERC, “Special Report: Accommodating High Levels of Variable Generation,” NERC, Tech. Rep., Apr 2009. [Online]. Available: www.nerc.com/filez/ivgtf.html

[102] M. Liserre, R. Cardenas, M. Molinas, and J. Rodriguez, “Overview of multi-MW wind turbines and wind parks,” IEEE Trans. Ind. Electron., vol. 58, no. 4, pp. 1081–1095, Apr. 2011.

[103] N. Goudarzi, W. D. Zhu "A review on the development of wind turbine generators across the world" Int. J. Dynam. Control (2013), © Springer-Verlag Berlin Heidelberg 2013

[104] H. Polinder, F. F. A. van der Pijl, G.-J. de Vilder, and P. J. Tavner, "Comparison of direct-drive and geared generator concepts for wind turbines," IEEE Trans. Energy Convers., vol. 21, no. 3, pp. 725–733, Sep. 2006.

[105] Enercon. (2010). ENERCON wind energy converters Technology & Service, Aurich, Germany. Available: http://www.enercon.de/p/downloads/EN_Eng_TandS_0710.pdf

[106] Vestas, Last Accesed on Sep. 2012. [Online]. Available: http://www. vestas.com/en/wind-power-plants/procurement/turbine-overview. aspx#/vestas-univers

[107] Clipper, Last Accessed on September 2012. [Online]. Available: http:// www.clipperwind.com/productline.html.

[108] Gamesa Elo´ rica, available at: http://www.gamesa.es/gamesa/index.html, accessed September 2006.

[109] M. K. Das, S. Chowdhury, and S. P. Chowdhury, "Protection and voltage control of DFIG wind turbines during grid faults," in Proc. 10th IET Int. Conf. DPSP Manag. Change, 2010, pp. 24–24.

[110] A. Petersson, T. Thiringer, L. Harnefors, and T. Petru, "Modeling and experimental verification of grid interaction of a DFIG wind turbine," IEEE Trans. Energy Convers., vol. 20, no. 4, pp. 878–886, Dec. 2005.

[111] J. Lopez, E. Gubia, P. Sanchis, X. Roboam, and L. Marroyo, "Wind turbines based on doubly fed induction generator under asymmetrical voltage dips, " IEEE Trans. Energy Convers., vol. 23, no. 1, pp. 321–330, Mar. 2008.

[112] M. I. Martinez, G. Tapia, A. Susperregui, and H. Camblong, "DFIG power generation capability and feasibility regions under unbalanced grid voltage conditions," IEEE Trans. Energy Convers., vol. 26, no. 4, pp. 1051–1062, Dec. 2011.

[113] J. Hu and Y. He, "DFIG wind generation systems operating with limited converter rating considered under unbalanced network conditions—analysis and control design," Renew. Energy, vol. 36, no. 2, pp. 829–847, Feb. 2011.

[114] A. H. Kasem, E. F. El-Saadany, H. H. El-Tamaly, and M. A. A. Wahab, "An improved fault ride-through strategy for doubly fed induction generator-based wind turbines," IET Renew. Power Gen., vol. 2, no. 4, pp. 201–214, Dec. 2008.

[115] K. E. Okedu, S. M. Muyeen, R. Takahashi, and J. Tamura, "Participation of facts in stabilizing DFIG with crowbar during grid fault based on grid codes," in Proc. IEEE GCC Conf. Exhib., 2011, pp. 365–368.

[116] J. A. Suul, M. Molinas, and T. Undeland, "STATCOM-based indirect torque control of induction machines during voltage recovery after grid faults," IEEE Trans. Power Electron., vol. 25, no. 5, pp. 1240–1250, May 2010.

[117] W. Qiao, R. G. Harley, and G. K. Venayagamoorthy, "Coordinated reactive power control of a large wind farm and a STATCOM using heuristic dynamic programming," IEEE Trans. Energy Convers., vol. 24, no. 2, pp. 493–503, Jun. 2009.

[118] C. Wessels, F. Gebhardt, and F.W. Fuchs, "Fault ride-through of a DFIG wind turbine using a dynamic voltage restorer during symmetrical and asymmetrical grid faults," IEEE Trans. Power Electron., vol. 26, no. 3, pp. 807–815, Mar. 2011.

[119] T. Kawady, C. Feltes, I. Erlich, and A. I. Taalab, "Protection system behavior of DFIG based wind farms for grid-faults with practical considerations," in Proc. IEEE PES Gen. Meeting, 2010, pp. 1–6.

[120] G. Joos, "Wind turbine generator low voltage ride through requirements and solutions," in Proc. 21st IEEE Power Energy Soc. Gen. Meeting—Convers. Del. Electrical, 2008, pp. 1–7.

[121] I. Erlich, W. Winter, and A. Dittrich, "Advanced grid requirements for the integration of wind turbines into the German transmission system," in Proc. IEEE Power Eng. Soc. Gen. Meeting, 2006, p. 7.

[122] L. Trilla, O. Gomis-Bellmunt, A. Junyent-Ferre, M. Mata, J. Sanchez Navarro, and A. Sudria-Andreu, "Modeling and validation of DFIG 3-MW wind turbine

using field test data of balanced and unbalanced voltage sags," IEEE Trans. Sustain. Energy, vol. 2, no. 4, pp. 509–519, Oct. 2011.

[123] L. Xu and Y. Wang, "Dynamic modeling and control of DFIG-based wind turbines under unbalanced network conditions," IEEE Trans. Power Syst., vol. 22, no. 1, pp. 314–323, Feb. 2007.

[124] X. Dawei, R. Li, P. J. Tavner, and S. Yang, "Control of a doubly fed induction generator in a wind turbine during grid fault ridethrough," IEEE Trans. Energy Convers., vol. 21, no. 3, pp. 652–662, Sep. 2006.

[125] J. Liang, W. Qiao, and R. G. Harley, "Feed-forward transient current control for low-voltage ride-through enhancement of DFIG wind turbines," IEEE Trans. Energy Convers., vol. 25, no. 3, pp. 836–843, Sep. 2010.

[126] J. Lopez, E. Gubia, E. Olea, J. Ruiz, and L. Marroyo, "Ride through of wind turbines with doubly fed induction generator under symmetrical voltage dips," IEEE Trans. Ind. Electron., vol. 56, no. 10, pp. 4246–4254, Oct. 2009.

[127] J. P. da Costa, H. Pinheiro, T. Degner, and G. Arnold, "Robust controller for DFIGs of grid-connected wind turbines," IEEE Trans. Ind. Electron., vol. 58, no. 9, pp. 4023–4038, Sep. 2011.

[128] S. Hu, X. Lin, Y. Kang, and X. Zou, "An improved low-voltage ride through control strategy of doubly fed induction generator during grid faults," IEEE Trans. Power Electron., vol. 26, no. 12, pp. 3653–3665, Dec. 2011.

[129] J. Hu, H. Nian, H. Xu, and Y. He, "Dynamic modeling and improved control of DFIG under distorted grid voltage conditions," IEEE Trans. Energy Convers., vol. 26, no. 1, pp. 163–175, Mar. 2011.

[130] H. Xu, J. Hu, and Y. He, "Operation of wind-turbine-driven DFIG systems under distorted grid voltage conditions: Analysis and experimental validations," IEEE Trans. Power Electron., vol. 27, no. 5, pp. 2354–2366, May 2012.

[131] M. Mohseni, S. Islam, and M. A. S. Masoum, "Fault ride-through capability enhancement of doubly-fed induction wind generators," IET Renew. Power Gen., vol. 5, no. 5, pp. 368–376, Sep. 2011.

[132] M. I. Martinez, G. Tapia, A. Susperregui, and H. Camblong, “Sliding mode control for DFIG rotor- and grid-side converters under unbalanced and harmonically distorted grid voltage,” IEEE Trans. Energy Convers., vol. 27, no. 2, pp. 328–339, Jun. 2012.

[133] Instantaneous Power Theory and Applications to Power Conditioning. By Akagi, Watanabe, & Aredes 41 Copyright © 2007 the Institute of Electrical and Electronics Engineers, Inc.

[134] Maurício Aredes, Hirofumi Akagi, Edson Hirokazu Watanabe, Eumir Vergara Salgado, and Lucas Frizera Encarnação, “Comparisons Between the p--q and p--q--r Theories in Three-Phase Four-Wire Systems” IEEE TRANSACTIONS ON POWER ELECTRONICS, VOL. 24, NO. 4, APRIL 2009.

[135] Arani, M.F.M.; Mohamed, Y.A.-R.I.; El-Saadany, E.F., "Analysis and Mitigation of the Impacts of Asymmetrical Virtual Inertia," Power Systems, IEEE Transactions on , vol.29, no.6, pp.2862,2874, Nov. 2014

[136] Rioual, P., Pouliquen, H. and Louis, J.-P., ‘Regulation of a PWM Rectifier in the Unbalanced Network State Using a Generalized Model’. IEEE Transactions on Power Electronics, 11(3), May 1996, 495–502.

[137] Park, R.H., ‘Tow Reaction Theory of Synchronous Machines. Generalized Method of Analysis Part I’. In Proceedings of Winter Convention of AIEE, 1929, pp. 716–730.

[138] Bo Yin, Oruganti, R., Panda, S. K. and Bhat, A. K. S., ‘An Output-Power-Control Strategy for a Three-Phase PWM Rectifier under Unbalanced Supply Conditions’., IEEE Transactions on Industrial Electronics, 55(5), May 2008, 2140–2151.

[139] Stankovic, A. V. and Lipo, T. A., ‘A Novel Control Method for Input Output Harmonic Elimination of the PWM Boost Type Rectifier under Unbalanced Operating Conditions’. IEEE Transactions on Power Electronics, 16(5), September 2001, 603–611.

[140] Yongsug Suh, Tijeras, V. and Lipo, T. A., ‘Control scheme in hybrid synchronous–stationary frame for PWM AC/DC converter under generalized

unbalanced operating conditions'. IEEE Transactions on. Industry Applications, 42(3), June 2006, 825–835.

[141] Rodriguez, P., Timbus, A. V., Teodeorescu, R., Liserre, M. and Blaabjerg, F., 'Independent PQ Control for Distributed Power Generation Systems under Grid Faults.' In IEEE 32nd Annual Conference on Industrial Electronics, IECON 2006, 6–10 November 2006, pp. 5185–5190.

[142] Hong-Seok Song and Kwanghee Nam, 'Dual Current Control Scheme for PWM Converter under Unbalanced Input Voltage Conditions'. IEEE Transactions on Industrial Electronics, 46(5), October 1999, 953–959,

[143] Teodorescu, R., Blaabjerg, F., Liserre, M. and Loh, P. C., 'Proportional-Resonant Controllers and Filters for Grid-Connected Voltage-Source Converters'. In Electric Power Applications, IEE Proceedings, September 2006, Vol. 153, No. 5, pp. 750–762.

[144] Lascu, C., Asiminoaei, L., Boldea, I. and Blaabjerg, F., 'High Performance Current Controller for Selective Harmonic Compensation in Active Power Filters'. IEEE Transactions on Power Electronics, 22(5), September 2007, 1826–1835.

[145] Serpa, L. A., Round, S. D. and Kolar, J. W., 'A Virtual-Flux Decoupling Hysteresis Current Controller for Mains Connected Inverter Systems'. IEEE Transactions on Power Electronics, 22(5), September 2007, 1766–1777.

[146] Serpa, L.A., Ponnaluri, S., Barbosa, P. M. and Kolar, J.W., 'A Modified Direct Power Control Strategy Allowing the Connection of Three-Phase Inverters to the Grid Through LCL Filters'. IEEE Transactions on Industry Applications, 43(5), September/October 2007, 1388–1400.

[147] Cort´es, P., Rodr´ıguez, J., Antoniewicz, P. and Kazmierkowski, M., Direct Power Control of an AFE Using Predictive Control'. IEEE Transactions on Power Electronics, 23(5), September 2008, 2516–2553.

[148] Cort´es, P., Ortiz, G., Yuz, J. I., Rodr´ıguez, J., Vazquez, S. and Franquelo, L. G., 'Model Predictive Control of an Inverter with Output LC Filter for UPS

Applications'. IEEE Transactions on Industrial Electronics, 56(6), June 2009, 1875–1883.

[149] Zmood, D. N. andHolmes, D. G., 'Stationary Frame Current Regulation of PWM Inverters with Zero Steady-State Error'. IEEE Transactions on Power Electronics, 18(3), May 2003, 814–822. DOI: 10.1109/TPEL.2003.810852.

[150] X. Guo, W. Wu, and Z. Chen, "Multiple-complex coefficient-filter-based phase-locked loop and synchronization technique for three-phase grid interfaced converters in distributed utility networks," IEEE Trans. Ind. Electron., vol. 58, no. 4, pp. 1194–1204, Apr. 2011.

[151] Y. Li and Y. W. Li, "Power management of inverter interfaced autonomous microgrid based on virtual frequency-voltage frame," IEEE Trans. Smart Grid, vol. 2, no. 3, pp. 30–40, Mar, 2011.

[152] Changjin Liu, Dehong Xu, Nan Zhu, Frede Blaabjerg, and Min Chen, "DC-Voltage Fluctuation Elimination Through a DC-Capacitor Current Control for DFIG Converters Under Unbalanced Grid Voltage Conditions" IEEE TRANSACTIONS ON POWER ELECTRONICS, VOL. 28, NO. 7, JULY 2013.

[153] http://en.wikipedia.org/wiki/Symmetrical_components